DEVELOPMENT OF A RAPID LABORATORY PREDICTIVE TEST METHOD USING FLUIDISED BED TECHNIQUES FOR THE DETERMINATION OF OXIDISABILITY OF RESIDUAL CR (III) PRESENT IN SLAGS

BY: Teboho Maidza

Dissertation Presented for the Degree of

MASTER OF SCIENCE IN APPLIED SCIENCE

In the Department of Chemical Engineering

University of Cape Town

Dec 2006

DEDICATION

This one is dedicated to my parents for having to believe in me and let me realize my dreams and all my friends for being there and sharing all the moments.

One love and More fire!!!

SYNOPSIS

Slag arising from smelting in the production of ferrochrome alloys, stainless steel and Platinum group metals (PGM) is known to contain residual chromium in various phases within the slag matrix. Although the bulk of slag ends up on landfills, slag is used in the construction, agriculture and marine industry among others. Applications for slag include as an aggregate in road construction and paving, buttressing, and as a source of lime in agriculture.

Previous studies have shown that about 0.1-1 % of residual Cr(III) in slags with CaO/SiO_2 ratios greater than 2 can be slowly converted to a toxic and water-soluble hexavalent species in the presence of atmospheric oxygen, at ambient temperatures albeit at very slow rates. The produced Cr(VI) is potentially able to leach into underground waterways and terrestrial water bodies, thus posing an environmental hazard.

In a landfill scenario, the oxidation kinetics are likely to be limited by the external diffusion resistance of the bulk of the landfill and the internal diffusion limitations to the reactive phases within individual particles where CaO and Cr_2O_3 phases are in intimate contact. Earlier studies have also shown that the conversion of Cr(III) to Cr(VI) in an ambient atmosphere increases, as the particle size decreases, with an increase in CaO and in the presence of moisture.

Laboratory tests to determine the oxidative stability of Cr(III) bearing slag when exposed to an ambient atmosphere require weeks to months before observing significant Cr(VI) conversions. There thus exists a need to develop a rapid laboratory predictive method to determine the oxidisability of residual Cr(III) in slag. The method should accelerate the oxidation reaction (at ambient temperature), thereby effectively reducing conversion times from weeks/months to hours/days.

It is the aim of this study to investigate the development of a method, which by eliminating the diffusion limitations of atmospheric oxygen through the bulk of slag mass and individual particles will speed up the oxidation of residual Cr(III). Possible means of reducing diffusion resistances in slags at ambient temperature thus need to be identified. Fluidisation techniques are investigated due to their ability to increase gas-solid contact area and enhance mass transfer. However exploratory investigations into the effects of microwave irradiation on slag samples are also presented. The specific aim of this study is to design, construct, commission and evaluate a laboratory scale fluidised bed suitable to fluidise slag particles of Geldart A and Geldart B classification.

A fluidised bed reactor was constructed from Perspex tubing of an internal diameter 65 mm. The design of the column included a 'disengagement zone' before the exhaust gas filters to reduce entrainment of finer particles. Rotameters were used to measure

possibility of introducing moisture into the reactor exists by bubbling a portion of the fluidising air (dry) through water in specially designed humidifier.

The fluidised bed was commissioned using an inert platinum slag. Experimental values of the minimum fluidisation velocity for the selected particle sizes were in close agreement with the values calculated using the Ergun equation.

The experimental design foresaw studying the effect of fluidising narrowly cut size ranges of low carbon ferrochrome slag, with bone-dry air, at ambient temperatures for a maximum time of 72 hrs. Investigative studies were also done with moist air as the fluidising medium at ambient temperatures for periods of up to two weeks. Investigations further included comparative studies on slag samples left to age on laboratory benches exposed to atmospheric oxygen at ambient temperature.

Contrary to expectations, a decrease in Cr(VI) abundance profile with fluidization time has been observed in the finer particles sizes. It is suspected that this is due to possible elutriation of ultrafines from bed. This effect was overcome when fluidizing coarser material, but the Cr(VI) profile generated in these runs presented with no conclusive evidence of the oxidation of residual Cr(III) in the slag. Fluidisation runs with moist air indicated evidence of probable CaO hydration but no indication of accelerated oxidation of residual Cr(III) during fluidization.

Nevertheless, increasing Cr(VI) concentrations with time observed in bench ages indicated that the slag in question is susceptible to atmospheric oxidation. An investigation of the effects of microwave irradiation on slag was not conclusive and the slag seemed not to couple with the microwaves.

As a result of these observations it has been concluded that the rate of oxidation of residual Cr(III) in slag is probably limited by the internal diffusion of oxygen to the reacting phases other than the diffusion resistance of the bulk of the slag.

It has been recommended that the effects of fluidising slag in an oxygen-enriched medium be investigated. The effects of microwaves need to be interrogated further as some scholars mention of possible ionic movements across grain boundaries during irradiation. This might possibly enhance the ionic diffusion of Cr^{3+}ion across the Cr_2O_3-CaO grain boundary.

ACKNOWLEDGEMENTS

Big thanks are extended to the following people:

- Dr Harro von Blottnitz my supervisor for all his inspirational guidance and supervision. Thank you for having the patience and a motivating attitude all the time. God Bless.

- The late Sue Buerger for showing me the ropes around the Old Chemical Engineering Building. Your memories live on.

- Jeniffer Broadhurst for your valuable advice and guidance. Thanks for being such a wonderful friend and sharing all your mineral processing experience.

- The Water Research Commission for funding my research and respect for all the environmental work and efforts all over the country.

- The Rudimentals for all their support and motivation not to lose focus.

- The Levi family for making me feel at home away from home.

- The Green group for all the support and the smiles.

- Kerry McLaren thanks for being the pillar in my life FIRE.

TABLE OF CONTENTS

CHAPTER THREE – EXPERIMENTAL APPROACH AND METHOD

CHAPTER FOUR – RESULTS

CHAPTER FIVE –CONCLUSION

LIST OF FIGURES

LIST OF FIGURES (contd)

LIST OF TABLES

CHAPTER ONE

INTRODUCTION

1.1. Background

Chrome-containing slag is formed as a by-product in the production of ferrochrome (which is needed for the production of stainless steel), and also during the smelting of PGM-bearing concentrates containing chromite. Slag is formed as a result of the reaction between gangue material associated with ores and the fluxes added to alter the activities of mineral oxides, melting temperature, viscosity as well as electrical conductivity during smelting.

Slag is usually disposed to landfill, but may also be used in applications such as road surfacing and agricultural fertiliser, among others. As a result, concern has been raised about the environmental stability of different types of slag.

The mineralogy of a slag is primarily process and additive controlled. Elements such as silicon, manganese, and aluminum are commonly present in ferrochrome slags as compounds of their oxides (Lind *et al.,* 2001). According to Holappa and Xiao (2004), ferrochrome slags are $Al_2O_3 - MgO - SiO_2$ based with minor contents of CaO and Cr_2O_3. Argon Oxygen Decarburization (AOD) slag has been found to have significant levels of residual chromium: samples analyzed by Lind *et al.* (2001) contained about 3% chromium in close agreement with Shen *et al.* (2004) and Pillay (2001), who reported a figure of 3.22% Cr.

This chromium usually occurs in the stable and non-mobile trivalent form, which suggests that the chromium-containing types of slag do not pose an environmental risk. It is the hexavalent form of chromium that is highly toxic and mobile.

It is generally believed that the only naturally occurring oxidant for trivalent chromium is MnO_2. The oxidation to Cr(VI) occurs in aqueous solution and the reaction is pH dependant. In soil systems, oxidation of Cr(III) occurs in the presence of manganese oxides, although workers such as Bartlett and Kimble (1976) have reported that small amounts of Cr(III) have been oxidized by O_2 in soil and water environments.

Studies by Pillay and colleagues in 2003 showed that in some slags, a small portion of Cr (III) (very stable) may gradually oxidise to the mobile and toxic hexavalent form when the slag is exposed to atmospheric oxygen and other weathering conditions. This confirmed earlier work by Petersen (1998), who observed an increase in hexavalent chromium leached from slag in lysimeter columns over a period of 2years.

the leachability of chromium-bearing slags when exposed to simulated acid precipitation.

Kilau and Shah (1984) observed that slags with a CaO/SiO_2 ratio greater than 2 showed maximum chromium leachability. According to Kilau and Shah, the higher the slag basicity the more susceptible the slag to oxidise to the leachable $CaCrO_4$. Thermodynamic calculations indicated the feasibility of the oxidation of chromium oxide in the presence of CaO according to the following reaction:

$$2CaO + Cr_2O_3 + 1.5O_2 \rightarrow 2CaCrO_4 \quad (1)$$

The progressively increasing Cr(VI) profile (with ageing time) from Pillay's bench-aged reagent grade Cr_2O_3-CaO mixtures indicated that oxidation of Cr(III) was feasible, hence under the same experimental conditions, slag with a Cr_2O_3-CaO matrix or mixture was expected to oxidise. Pillay thus sieved samples of such slags into different particle classes namely, <75μm, 75-300μm, 300-1000μm, and then placed 25 g samples from each particle class in weighing boats to age on laboratory benches. Sampling followed by alkali leaching was done at regular intervals to produce a Cr(VI) profile indicating whether the slag does oxidise.

Kilau and Shah's thermodynamic calculations have shown that the reaction is feasible at ambient temperatures but very little is mentioned about the reaction kinetics. It is thus known (from Pillay's experiments on slag) that the oxidation of residual chromium (in slag) in the presence of atmospheric oxygen is possible, but that the reaction is slow. Laboratory experiments of the type that Pillay used to determine the environmental stability of fresh slag are of limited use in industry as they take a long time, with a clear upward trend in Cr(VI) concentrations only emerging after several weeks, and the full extent of oxidisability showing up only after 6-12 months (Pillay, 2002). It is thus important to develop a rapid laboratory test method thereby assisting in making informed decisions in relation to slag disposal.

According to Pillay *et al.* (2003), the key factors influencing the oxidation reaction are:

- The presence of CaO – the reaction extent increased with the amount of CaO
- The particle size – the extent of oxidation was higher in fine particles
- Moisture

Pillay *et al.* (2003) further hypothesised that the oxidation reaction is diffusion controlled, by the rate at which oxygen can migrate to the interfaces between the chromite and calcium oxide phases in the slag particles. Any attempt to speed up the ageing reaction in a laboratory test would thus have to address this diffusion resistance.

Fluidized beds are used in many modern industrial applications such as drying, mixing, gas-solid contacting, coating, heating and cooling among others. The main advantage of coupling processes with fluidisation is to take advantage of the good

1.2. Problem Statement

Industries producing chrome-containing wastes face the challenge of disposing this waste with the confidence and knowledge that it is environmentally safe. Such was an observed situation with Petersen (1998) when a once labelled benign slag produced increasing amounts of Cr(VI) over a period of 2 years. Oxidation experiments carried out on reagent grade chemicals (Cr_2O_3-CaO mixtures) by Pillay *et al.* (2003) showed that the oxidation of Cr(III) progresses slowly under ambient conditions.

Altering the basicity of slag to improve its stability to oxidation as suggested by Kilau and Shah (1984) will not only affect the performance of the slag (dissolving unwanted gangue and mineral elements among other functions) but also the performance and the economics of the smelting process.

Laboratory procedures available for testing whether residual Cr(III) in slag is stable or prone to slow atmospheric oxidation are either inconclusive in terms of disposal decision making or take long time. It is therefore imperative that an onsite rapid predictive methodology be developed to couple with production, thereby ensuring proper and environmentally safe slag-waste disposal decision-making. An onsite rapid predictive method will determine whether the residual Cr(III) will oxidise to Cr(VI) in the long term, thus allowing such slag to be avoided if possible, or properly treated and disposed, avoiding costly slag dump rehabilitation exercises.

1.3. Thesis Objectives

The study reported on in this dissertation aimed to achieve the following:

1. Developing a rapid laboratory method that gives an indication of the environmental stability of slag towards oxidation before disposal. As fluidization is known to enhance mass transfer, and as the atmospheric oxidation of residual Cr(III) is believed to be a diffusion controlled reaction, a fluidized bed was believed to be a suitable apparatus for enhancing the rate of oxidation.
2. Constructing a fluidized bed apparatus capable of putting slag of suitable particle sizes into intensive contact with atmospheric oxygen or oxygen-enriched air for periods of hours, days or weeks.
3. Accelerating the oxidation of residual Cr(III) in slag to Cr(VI) to a matter of hours to days, speeding up the waiting time of weeks to months associated with bench ageing, using fluidization techniques at ambient temperatures.

1.4. Research Approach

In order to achieve the objectives as laid out above, laboratory work had to be undertaken with real slag samples containing residual Cr(III), and likely to be prone to slow atmospheric oxidative ageing.

A slag from UG-2 ore smelting, and a ferrochrome slag were obtained from suitable industrial sources. After particle size classification, the size classes selected for fluidization were acid digested and their Fe, Cr, Mg and Ca composition determined. Milling of the largest size fraction was done where necessary to increase the fractions required for fluidization.

The research objectives also called for the development of new laboratory method, with design and construction of suitable laboratory equipment. A fluidized bed was designed and constructed out of Perspex tubing. The fluidized bed was equipped with relevant instrumentation so as to compare the measured onset of fluidization with the design calculations.

Slag samples were then fluidized for up to 72 hours under different conditions, with regular sampling at predetermined times. The samples were then analyzed for Cr(VI) using Spectrophotometric methods. It should be noted that binary CaO-Cr_2O_3 mixtures as used by Pillay, were not included in the fluidization experiments as the purpose of the method was to eliminate oxygen diffusion resistances to the Cr_2O_3-CaO phases within a slag particle. Pillay's experiments highlight the feasibility of the oxidation of Cr_2O_3 in the presence of CaO and the significance of the key factors r mentioned in the tests.

In a control experiment, representative samples from selected particle sizes were weighed into weighing boats and aged on the laboratory benches with regular sampling to document the evolution of a Cr(VI) profile, over a period of several weeks as described by Pillay (2002).

In a further data-checking step, leach residues were air dried, chemically digested and analyzed for total chrome using Atomic Absorption Spectroscopy.

1.5. Scope and Limitations

The main aim of this study was the designing of a fluidization rig and to successfully fluidize the selected particle size ranges. The study considered the effects of 72 hours of fluidization (with regular sampling) on three particle sizes, 38-63µm, 63-90µm and 90-106µm and aimed at establishing the effects of particle size in diffusion-controlled reactions. The bench tests served as control experiments indicating whether the Cr(III) in the slag had oxidized.

The study was undertaken in fulfillment of the requirements of a degree of MSc in Engineering, with work reported in this dissertation being equivalent to at least one year's full-time research, but not significantly more than that.

1.6. Thesis Structure

Chapter 2 introduces the likely problematic slags by providing a description of the smelting process, and the different furnaces producing the different Chromium Ore Processing Residues (COPR). A concise description of the furnace additives is given, shedding light on the mineralogy of the different slags. The difference in mineralogy of platinum group metals (PGM) and ferrochrome slag is reviewed. A brief review of the chemistry of Cr(III) and Cr(VI) highlights the environmental significance and the toxicity of chromium. The literature review discusses the oxidation of Cr(III) in slag and the leaching characteristics of the COPR. Focus is also given to the respective speed-up-techniques for oxidation, gas-solid and diffusion controlled reactions. The use of microwaves as a reaction speed-up technique is also reviewed. In this context fluidization techniques and their effect on reaction kinetics are emphasized.

Chapter 3 describes the experimental approach and methodology used to test a detailed hypothesis formulated upon completion of the literature review. This chapter describes the experimental methods used to determine the mineralogy, total chrome and Cr(VI), density and particle size. The sampling method is discussed and the fluidized bed design process is also presented. The chapter gives a detailed description of the materials used in the tests.

Chapter 4 presents the results obtained in the study. These include the determination of the minimum fluidization velocity in comparison to theoretical values, the effect of fluidization on the oxidation of residual Cr(III) as measured by leachable Cr(VI), and a discussion of control measurements on particle size and the total chrome content in the sample. Comparative Cr(VI) concentrations obtained in bench tests are also presented. This chapter also includes a brief description of exploratory work on effects of microwaves on slag.

Chapter 4 also discusses the presented results of the study, focusing on the observed trends and the likely causes. The outcomes of the study are compared to previous relevant studies and their implication on the proposed problem statement. The discussions also highlight new observations.

Chapter 5 concludes the thesis by summarizing the findings and whether these met the thesis objectives. The chapter also highlights the shortfalls of the investigations and provides recommendations and future areas of investigation in the light of the previous investigation.

CHAPTER TWO

LITERATURE REVIEW

This chapter will give a description of the processes resulting in chromium containing slag followed by an introduction to the chemistry of Cr(III) and Cr(VI). The importance of chromium as a dietary supplement and its toxicity will be highlighted. The chapter will review literature on the oxidation of reagent grade $Cr_2O_3 - CaO$ mixtures and slag left to age on laboratory benches. The use of microwaves as a possible speed up technique in the oxidation of residual Cr(III) is reviewed. The chapter then proceeds to review fluidisation as well as other techniques to enhance diffusion controlled reactions. The chapter concludes with a summary of important insights and information in the literature, which is fundamental in the research.

2.1. Chromium in Slags

Processing of precious metal ores produces a variety of mineral waste in form of waste rock, floatation tailings and slag. Slag from the ferrochrome industry and the smelting of PGM concentrates are known to contain levels of residual chromium. The mineralogical composition of a slag is process and additive dependant such that in some processes high levels of chrome in the slag is a desired goal. This study will focus on slags from smelting of chromite-containing PGM concentrates and chrome containing ores.

2.1.1. Slags from the Ferrochrome Industry

Approximately one tonne of stainless steel slag is generated for every three tonnes of stainless steel produced (Shen *et al.*, 2004). In the production of stainless steel, a series of furnaces are used to melt the charge, remove gangue minerals, and add value adding as well as performance enhancing additives. The furnaces employed include the Electric Arc Furnace (EAF), Vacuum Oxygen Decarburization (VOD), Argon Oxygen Decarburization (AOD) and the Creusot-Loire-Uddeholm converter (CLU) furnace. The AOD, VOD and CLU furnaces are converters used to achieve low carbon stainless steels. The carbon is reduced by lowering the partial pressure of carbon monoxide in the furnace. In most cases argon gas is used whilst the VOD uses a vacuum to achieve this. Slag from each of these furnaces has different mineralogy and chemistry.

Figure 2-1 illustrates the manufacture of stainless steel the sources of slag and some of the basic additives in this industry.

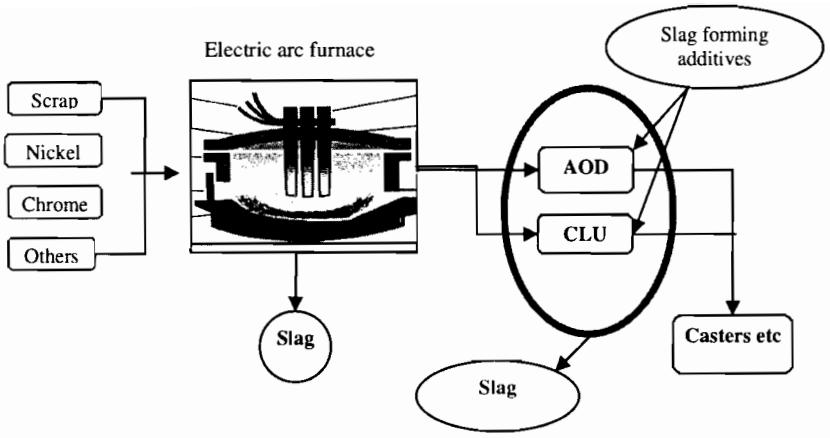

Figure 2-1: The sources of slag in the making of stainless steel

Measured proportions of nickel, ferrochrome, scrap and other slag forming additives are charged into the Electric Arc furnace at the beginning of every smelting cycle, producing an EAF slag and molten metal. The molten metal is transferred to the AOD, VOD or CLU furnaces where further smelting produces AOD/CLU slag and the desired stainless steel alloy. The scrap is usually of a certain size and density to promote rapid melting and simultaneous protection of the furnace walls from electric arc radiation (www.steel.org/learning/howmade/eaf.htm). Ferrochrome is derived in a prior smelting operation from chromium ore, which is a spinel solid solution of Fe_3O_4, $FeO \cdot Cr_2O_3$, $MgO \cdot Cr_2O_3$, $MgO \cdot Al_3O_3$ and $(Cr, Al)_2O_3$ usually charged as chromite ore (Hino *et al.*, 1995).

Typical EAF slags consist mostly of oxides of elements, calcium, chromium, magnesium, aluminum and silicon. Samples of EAF slag studied by Proctor *et al.* (2000), recorded significant levels of hexavalent chromium although the majority of the chromium was in the trivalent state. Ideally the chromium oxide content in slag should be less than 5 %; hence in most cases it is overlooked as an environmental concern. Table 2-1 shows the typical constituents, their source and composition range in an EAF slag:

Table 2-1: Typical constituents of an EAF slag (www.steel.org/learning/howmade/eaf.htm)

Component	Source	Composition Range
CaO	Charged	40 – 60%
SiO_2	Oxidation product	5 – 15%
FeO	Oxidation product	10 – 30%
MgO	Charged as Dolomite	3 – 8%
CaF_2	Charged slag fluidizer	
MnO	Oxidation product	2 – 5%
S	Absorbed from steel	
P	Oxidation product	

In conventional EAF smelting processes, the Cr_2O_3 in slag is normally present as a solid spinel of magnesium ($MgCr_2O_4$) and calcium ($CaCr_2O_4$) phases (Pretorius and Nunnington, 2002). Kilau and Shah (1984) identified the existence of chromium as

abundant magnesium formed picrochromite ($MgO.Cr_2O_3$) spinel, in which trivalent chromium is the major oxidation state. This compound is known to be resistant to oxidation, hence the observed decrease in the leached Cr(VI) in Kilau and Shah's investigations.

Shen *et al.* (2000) characterized slag samples from AOD and EAF furnaces using X-ray diffraction and SEM techniques, identifying Fe-Cr-Ni alloys, Ca-Mg-Al silicates, Fe-Cr oxides and Ca-Mg oxides as the main phases in the two types of slags. Higher percentages of CaO and the subsequent high alkaline water leaches (pH ranges between 10 and 11), were noted from the AOD than the EAF slag during various tests by Shen and colleagues.

The basicity of a slag is defined as the ratio of the sum of the percentage of CaO and MgO to SiO_2 (Pretorius and Nunnington, 2002):

$$Basicity = \frac{CaO + MgO}{SiO_2} \qquad (1)$$

In steel production careful monitoring of factors such as slag fluidity, oxygen activity, % CaO/% Al_2O_3 and slag basicity improves the cleanliness of steel (Yoon *et al.*, 2002). The basicity of a slag has an influence on the slag's leachate generation characteristics (especially pH and Cr(VI) contents) as observed by Kilau and Shah (1984). Elevated levels of CaO (among other factors) during smelting, result in the formation of calcium chromite phases ($CaO \cdot Cr_2O_3$) among other Mg-Si-Al phases. Thermodynamic calculations by Kilau and Shah, showed that the oxidation of chromium oxide (equation 2) in the presence of CaO and oxygen is feasible at ambient temperatures.

$$2CaO + Cr_2O_3 + 1.5O_2 \rightarrow 2CaCrO_4 \qquad (2)$$

The calcium chromate will then release Cr(VI) species in leachate under alkaline and aggressive acid leaching conditions. The possibility of this reaction occurring under ambient conditions was further emphasized by observed increases in Cr(VI) levels from $CaO - Cr_2O_3$ chemical mixtures left to age for weeks on laboratory benches by Pillay (2001).

During smelting itself, slag basicity is also known to have significant effects on the activities of chromium oxides: the higher the slag basicity, the higher the activities of chromium oxides and the lower the divalent chromium fraction. This saturates the slag with CrO_x due to its decreased solubility in high CaO contents promoting better recovery of chromium (Xiao and Holappa, 1993). X can be any value between 1 and 1.5 determined by the operating conditions in the experiment and the possible-stable $CaO\text{-}SiO_2\text{-}CrO_x$.

2.1.2. Slags from the Platinum Group Metals (PGM) Industry

The Bushveld Igneous Complex, a large mineral deposit in the Northen region of South Africa, contains one of the world's largest known deposits of PGMs (Bartie *et al.*, 2003). One of the PGM containing seams, Upper Group 2 (UG-2) is a chromite seam. The high levels of chromium in the concentrates result in the formation of undesired chromite spinels during smelting for PGMs. According to Bartie *et al.*, (2003) the chromite spinels reduce the effective furnace-volume, and increase the liquidus temperature, making tapping difficult.

The slag from PGM smelting differs physically and chemically from ferrochrome and stainless steel slag due to the differences in process conditions and feed contents.

The diagram below is an illustration of the PGM refining process

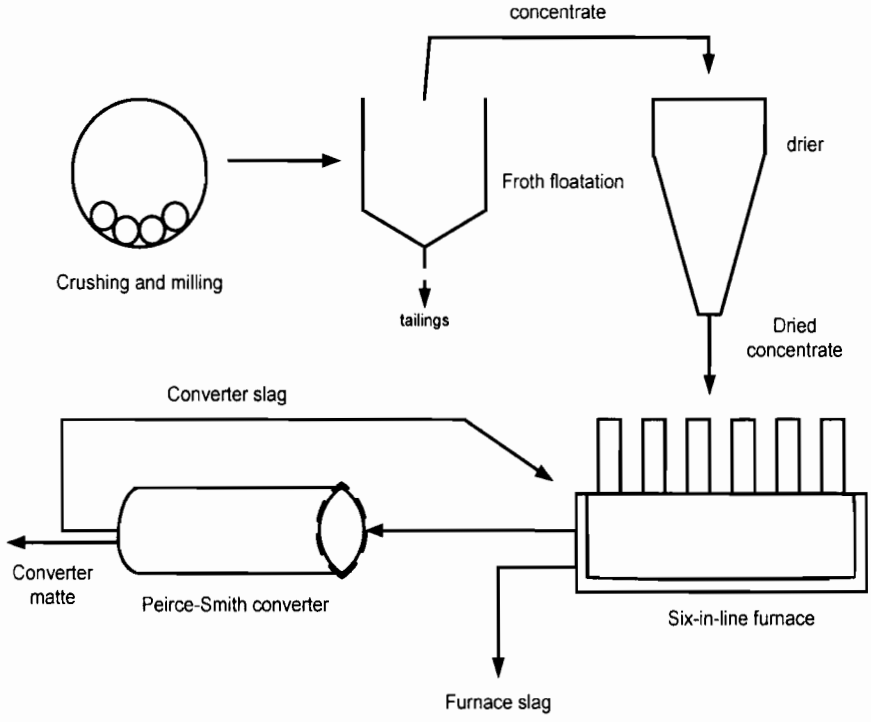

Figure 2-2: Schematic representation of a typical platinum smelting process (Jones, 1999)

With particular reference to the South African smelting process, Jones (1999) mentions that the smelting furnaces are operated at high slag: matte ratio due to the low concentration of valuables in the concentrate. Dried concentrates from the floatation tanks are charged into a six-in-line furnace together with slag forming additives producing a matte and furnace slag. The matte containing nickel, copper, cobalt, iron, sulphur and PGMs is then transferred to the converters for further removal of iron, sulphur and other impurities.

During conversion, air is blown into the matte to oxidize most of the sulphur (the sulphur exits the system as SO_2 which is recaptured for the production of sulphuric acid) and iron which is fluxed out by silica as an iron silicate slag. The converter slag usually requires further treatment due to the entrainment of valuable PGMs as a result of the turbulent nature of the converter furnace; however the presence of chromite ($FeCr_2O_4$) and magnetite ($FeFe_2O_4$) spinels in the slag poses a challenge of increasing the chromium concentration in the furnace (Jones, 1999). Nell (2004) attributes the reluctance by many process engineers to recycle converter slag due to its oxidized nature resulting in a lower solubility of chromium in the smelting furnace.
The matte from the converter is milled first before the last refining stage, which uses sulphuric acid to leach out copper and nickel obtaining a high-grade PGM concentrate (Jones, 1999).

Table 2-2 shows the typical average composition of a slag obtained from UG-2 ore smelting. It is important to note the differences in the SiO_2 and CaO contents between the EAF slag composition (Table2-1) and the UG-2 ore slag.

Table 2-2: Average Industrial Slag Composition from UG-2 Ores (Bartie *et al.*, 2003)

FeO_x	MgO	SiO_2	Al_2O_3	Cr_2O_3	CaO
11.5	21.4	51.4	6.4	1.6	6.3

Basicity calculations using values from Table 2-2 indicate that, the PGM (UG-2) slags are generally acidic (basicity is less than 1.0) and contain relatively small amounts of CaO in comparison to the ferrochrome slags. During PGM smelting, the challenge is to have as little chromium as possible in the matte, avoiding the formation of chromite spinels and the increase of the liquidus temperature (Bartie *et al.*, 2003).

However the smelting conditions in the PGM furnaces are slightly reducing (Nell, 2004) promoting lower oxidation states of chromium, which are soluble in the silicon rich slag. A similar observation was by Frohberg and Richter (as quoted by Xiao and Holappa, 1993) who found the ratio of Cr^{2+}/Cr^{3+} to increase with a decrease in oxygen potential, slag basicity and an increase in temperature. This results in the formation of chromium spinel systems in which divalent chromium is the dominant oxidation state.

$MgCr_2O_4$, $FeCr_2O_4$ spinels rather than Fe_3O_4 (magnetite) at higher temperatures. Higher smelting temperatures result in the partitioning of chromium into the spinel, although the amount of Cr^{+3} substituted for Fe^{+3} (at temperature range 1400-1600°C) depends on the bulk of Cr_2O_3 content and bulk FeO_x/MgO ratio (Bartie *et al.* 2003). Earlier findings by Lee and Nassaralla (1998) mention of the formation of $MgO \cdot Cr_2O_3$, $2CaO \cdot Al_2O_3 \cdot SiO_2$ and $CaO \cdot SiO_2$ phases instead of calcium chromate phase when Al_2O_3 is substituted for SiO_2.

Using the findings from Lee and Nassaralla (1998) and Bartie *et al.* (2003), and considering the PGM smelting conditions, one can infer that the chromium in the PGM slag exists as a 'stable' spinel of either MgO or SiO_2 compared to the oxidisable CaO spinels in some ferrochrome slags.

Figure 2-3 shows the different combinations of compounds that can form for different compositions (Wt %) of CaO, Cr_2O_3, MgO and SiO_2 at defined temperatures and pressure. From the Figure 2-3, it can be seen that at high MgO and SiO_2 compositions the $MgO \cdot Cr_2O_3$ phase can exist. According to Figure 2-3, the $CaO \cdot Cr_2O_3$ phase will exist at high CaO compositions and small amounts of SiO_2 and MgO.

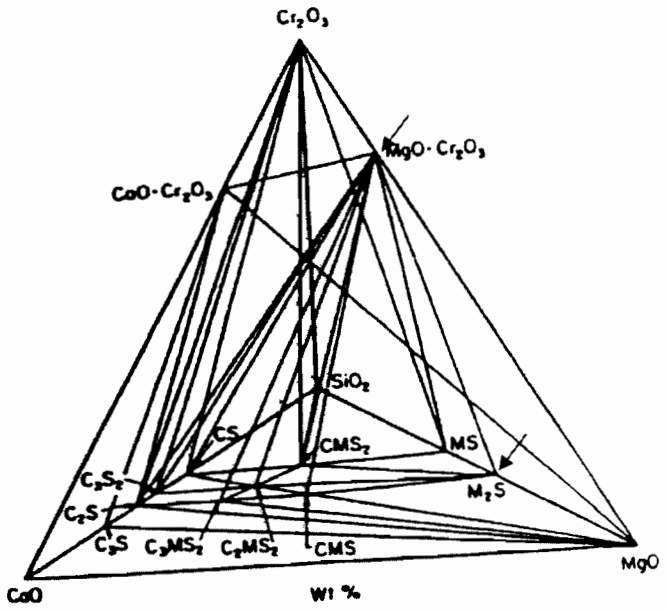

Figure 2-3: System CaO-MgO-Cr_2O_3 –SiO_2 showing subsolidus compatibility relations. C = CaO. M = MgO. S = SiO_2 (according to Berezhnoi and Gul'ko) –Kilau and Shah (1984)

Using the quaternary phase diagram by Berezhnoi and Gul'ko, Kilau and Shah (1984) proposed the existence of the following phases at different $CaO:SiO_2$ ratios:

Table 2-3: Proposed phases at different $CaO:SiO_2$ ratios

$CaO:SiO_2$ Ratio	Phases
0 - 1	1: $SiO_2 - CaO \cdot MgO \cdot SiO_2 - MgO \cdot SiO_2 - Cr_2O_3$ 2: $CaO \cdot SiO_2 - CaO \cdot MgO \cdot 2SiO_2 - SiO_2 - Cr_2O_3$ 3: $CaO \cdot SiO_2 - 2CaO \cdot MgO \cdot 2SiO_2 - CaO \cdot MgO \cdot 2SiO_2 - MgO \cdot Cr_2O_3$
1 – 1.5	1: $3CaO \cdot 2SiO_2 - 2CaO \cdot MgO \cdot 2SiO_2 - CaO \cdot SiO_2 - MgO \cdot Cr_2O_3$ 2: $3CaO2SiO_2 - 3CaOMgO2SiO_2 - 2CaOMgO2SiO_2 - MgOCr_2O_3$ 3: $3CaO \cdot 2SiO_2 - 2CaO \cdot MgO \cdot 2SiO_2 - 2CaO \cdot SiO_2 - MgO \cdot Cr_2O_3$
1.5 – 2.0	1: $2CaO \cdot SiO_2 - 3CaO \cdot MgO \cdot 2SiO_2 - 2CaO \cdot MgO \cdot 2SiO_2 - MgO \cdot Cr_2O_3$ 2: $2CaO \cdot SiO_2 - MgO - 3CaO \cdot MgO \cdot 2SiO_2 - MgO \cdot Cr_2O_3$
2.0 – 3.0	1: $2CaO \cdot SiO_2 - MgO - MgO \cdot Cr_2O_3 - CaO \cdot Cr_2O_3$ 2: $2CaO \cdot SiO_2 - 3CaO \cdot SiO_2 - MgO - CaO \cdot Cr_2O_3$
>3.0	1: $3CaO \cdot SiO_2 - CaO - MgO - CaO \cdot Cr_2O_3$

According to Nell (2004), a good PGM slag should ideally have the following characteristics among others:

1) A low viscosity to allow clean slag-matte separation;
2) A low liquidus temperature to avoid excessive superheating of matte;
3) The ability to dissolve all the chromium present in the concentrate to avoid formation of chromium-bearing spinel and the transfer of chromium to the matte.

In summary, PGM slags have basicity less than 1, contain chromium in spinels of MgO and SiO_2 and should therefore be stable towards acid or alkaline leaches.

2.1.3. Slag Waste Management

Slag is either dumped in landfills or used for various purposes ranging from civil engineering to agricultural industries. Slag stockpiles that form over years of mineral processing remain even after the cessation of the smelting process, creating a variety of environmental issues due to dust generation, leaching of toxic heavy metals, and land usage among others. Modern environmental laws, require assessments to be done on [e.g. US EPA Toxicity characteristic leaching procedure (TCLP)] solid wastes before any environmental application or disposal (Jing *et al*, 2006).

dikes, river bank buttresses and eroded river beds (Motz and Gieseler, 2001). Environmental impact studies on ferrochrome slag in road construction indicated low leaching of elements such as chromium, copper, cobalt, cadmium and nickel from the slag (Lind *et al.*, 2001). Ziemkiewicz (1998) mentions of steel slag's application in the control of acid mine drainage utilizing the high alkaline leach solutions generated by slag. Takahashi and Yabuta (2002) mention slag usage in sand-capping (a marine environment improvement technology), where organic sea-bottom sediments are covered with finely-ground slag to suppress elution of nutrient salts.

However environmental concerns have been raised due to slag's elementary compositions and long-term environmental stability with regards to leachability of heavy metals under different environmental conditions and applications (e.g. acid rains).

2.2. Chemistry of Chromium

Chromium is the 21st most abundant element in the Earth's crust, and occurs mostly in the trivalent oxidation state in combination with iron or other metal oxides (Barnhart, 1997). Chromium is used in the production of chemicals, the making of alloys and other protective functions e.g. wood treatment.
Chromium can occur in several oxidation numbers from 0 to VI, with only Cr(III) and Cr(VI) stable enough to exist in the natural environment. Only two oxidation states, Cr(III) and Cr(VI) will be briefly reviewed. An extensive review on the chemistry of Cr(III) and Cr(VI) can be found in Pillay (2001).

2.2.1. Chromium in Diet

Chromium is an essential trace element in the day-to-day human diet. Chromium supplements have been known to aid weight loss and blood sugar regulation. (Drew, *et al.*, 1992) Chromium deficiency has been associated with impaired glucose tolerance, fasting hyperglycemia, glucosuria, elevated body fat, decreased sperm count, and decreased lean body mass, cardio vascular disease (Drew, *et al.*, 1992) among others. However large doses of chromium can be lethal.

2.2.2. Toxicity of Chromium

The National Academy of Science established that a safe daily intake of chromium for

Of the two oxidation states, Cr(VI) is considered to be highly toxic. When absorbed into the body, Cr(VI) can be rapidly taken up by erythrocytes and reduced to Cr(III) there by oxidising organics therein.
Workers exposed to Cr(VI) vapour have reported nasal mucosa ulceration. It has been reported to be a respiratory tract irritant elevating the risks of lung cancer (Calder, 1998). Inhalation, ingestion and dermal exposure have been known to damage renal tubules although it is excreted via urine. Exposure pathways for Cr(VI) include dermal exposure, breathing contaminated dusts and ingestion

2.2.3. Cr(III) Chemistry

The presence and quantities of the Cr(III) state in any environment is known to depend on a variety of chemical and physical processes such as hydrolysis, complexation, redox reactions and absorption. In soils, Cr(III) forms stable complexes with organic compounds at low pH. Aerated soils containing manganese oxides tend to oxidise Cr(III) to Cr(VI)(Makino *et al.*, 1998). In the natural environments Cr(III) is generally immobile and stable, although strongly aerated solutions show a high oxidising potential in which Cr(VI) can exist from a pH of 2 (Bartlett, 1976).

In aqueous environments in the absence of complexing agents, Cr(III) exist as a hexa-aquachromium and exhibits acidic characteristics (pK ~ 4) (Rai et al., 1988). According to Rai *et al.*, (1987) the most common aqueous species of Cr(III) are Cr^{3+}, $Cr(OH)^{2+}$, $Cr(OH)_3$ and $Cr(OH)^{-}_4$ and these exist at low Eh values. Deltombe *et al.* (1966) mentions the trivalent chromium as a 'hard' Lewis acid as it readily complexes with a variety of ligands, such as hydroxyl, sulphate, ammonium, cyanide and sulphocyanide, flouride and chloride, and other natural and synthetic organic ligands.

Cr(III) shows an increase in its adsorption tendencies towards 'solids' as the pH increases. This behaviour can be attributed to the negative charge formed on the solids' surfaces as the pH changes from acid to base (Richard and Bourg, 1991). Consequently any species with a high charge density will compete with Cr(III) for adsorption sites (Richard and Bourg, 1991).

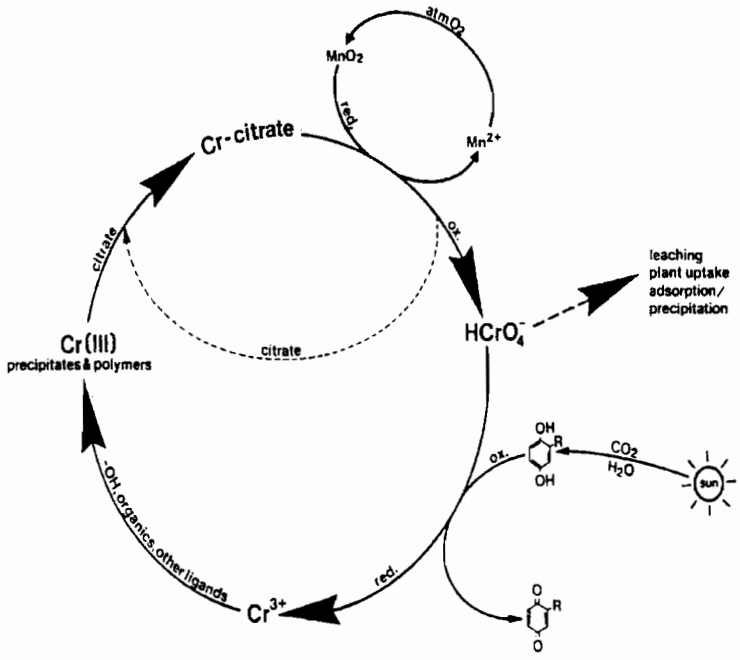

Figure 2-4: The chromium cycle in soils and water (James and Bartlett, 1983b)

The chromium citrate complex and other complexes are known to increase the solubility as well as the mobility, of the trivalent chromium up to a pH of 7. In the absence of these organics at pHs around 5, an immobile hydroxide is formed (James and Bartlett, 1983b)

In any soil, the chromium balance depends on many factors some of which are pH, presence of organic ligands, sorption surfaces, MnO_2 surfaces, amount of aeration, water pathways, temperature, rain and even the soil geometry. More importantly the balance depends on the overall chromium loading of the soil from processes such as waste sludge, etc. and this upset may be equilibrated after a long time as most reactions proceed slowly.

2.2.4. Cr(VI) Chemistry

The environmental toxicity of chromium mostly depends on the Cr (VI) species, and this is culminated by its mobility in the environment. In solution Cr (VI) appears as chromic acid, H_2CrO_4 in equilibrium with its anions. Chromic acid is a very strong acid that exists mainly in solutions at pH < 0.6. In mildly acidic solutions, pH 6.5, the CrO_4^{2-} ion predominates (Richard and Bourg, 1991).

Hexavalent chromium can exist as monomeric ions, H_2CrO_4, $HCrO_4^-$ (bichromate) and CrO_4^{2-}(chromate) or as a dimeric $Cr_2O_7^{2-}$ ion (Richard and Bourg, 1991). The hydrogen chromate dimerises to dichromate at a total Cr(VI) concentration of greater than 0.01M. The dimerisation of the hydrogen chromate in acidic pH is according to

$$HCrO_4^- + HCrO_4^- \rightarrow Cr_2O_7^{2-} + H_2O \qquad k_d \qquad (3)$$

pk_d is -1.54 (Allison *et al.*, 1990). In solution, the relative concentration of these species ($HCrO_4^-$) is dependant on the overall pH Cr (VI) concentrations (Palmer and Puls, 1994).
According to Schroeder and Lee (1975) the presence of electron donors can reduce Cr(VI) to Cr(III) and consequently precipitating or adsorbing on to available species in the water or soil. Schroeder and Lee also observed the reduction of Cr(VI) by industrial organic wastes, and organic sulphides.

Rai *et al.* 1988 proposed the Cr(VI) reduction by Fe(II) ions, in the following way;

$$3FeO + 6H^+ + Cr(VI)_{aq} \rightarrow Cr(III)_{aq} + 3Fe(III)_{aq} + 3H_2O \qquad (4)$$

The overall chromium level in the aquatic environment is subject to many processes. Richard and Bourg (1991) presented the chromium aquatic cycle as below;

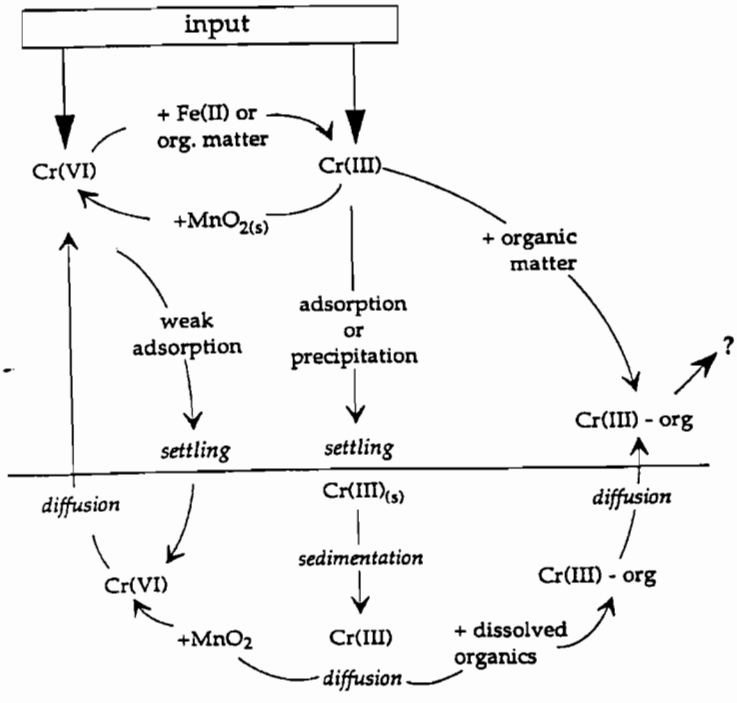

Figure 2-5: Chromium cycling in the aquatic environment (Richard and Bourg, 1991)

Besides the natural existence of Cr(VI) in the environment, most Cr(VI) loading in some environments is as a result of anthropogenic activities such as leather tanning, electroplating, paint and textile industries among many others. With stringent environmental laws, [permissible limit of Cr(VI) in industrial wastewater is 0.1 mg/L

carbon are some of the materials observed to reduce levels of Cr(VI) levels in pregnant solutions (Karthikeyan *et al.,* 2005). One of the common methods used to remove. Cr(VI) from solution uses a reducing agent sodium sulphite (Erdem and Tumen, 2004) to convert Cr(VI) to Cr(III).
The removal of hexavalent chromium in aqueous solutions as a trivalent-chrome precipitate or sludge, provides with a short term solution as the sludge has been found to slowly oxidize in ambient atmospheres generating Cr (VI) (Apte *et al.*, 2005).

2.3. Oxidation of Cr(III) to Cr(VI) in Slags

Chromium containing sludge has been found to readily oxidize to Cr(VI) in the presence of MnO_2. The manganese acts as an electron carrier in the reaction between Cr(III) and the dissolved oxygen (Apte *et al.*, 2005). Kilau and Shah (1984) proposed the leaching of Cr(VI) from a test slag to be as a result of $CaCrO_4$ formed during the slag melting.
Kilau and Shah (1984) proposed the oxidation of chromium oxide in the presence of calcium oxide and oxygen to occur according to the following reaction:

$$2CaO + Cr_2O_3 + 1.5O_2 \rightarrow 2CaCrO_4 \qquad (5)$$

Calculations by Pillay (2001) using data from Hattori *et al.* (1978) [Table 2-3] showed that the reaction was feasible over a temperature range 298.15 K– 1000 K. Petersen (1998) observed a significant increase in Cr(VI) in lysimeter leach solutions from high alkaline slag samples left ageing from weeks to months at ambient temperatures.
In 2003, Pillay and colleagues observed an increasing Cr(VI) profile in mixtures of $Cr_2O_3 - CaO$ reagent grade chemicals left to age in ambient atmosphere. In these tests, the reaction was enhanced by the presence of moisture. An increase in moisture was also observed to increase the rate of oxidation.

Table 2-4: Thermodynamic data from Hattori *et al.*, 1978 for the oxidation of chromium oxide in the presence of CaO (Pillay, June 2001)

Material	Enthalpy of formation ($kJmol^{-1}$) at 298.15 K	Entropy of formation at 298.15 K ($JK^{-1}mol^{-1}$)	Heat capacity (298.15 – 1300 K) ($JK^{-1}mol^{-1}$)
Cr_2O_3	-1141	81.1	$119.4+9.20 \times 10^{-3} T-15.65 \times 10^{5} T^{-2}$
CaO	-635.1	39.7	$49.63+4.52 \times 10^{-3} T-6.95 \times 10^{-5} T^{-2}$
$CaCrO_4$	-1379	134	$160.96+9.333 \times 10^{-3} T-2.80 \times 10^{-6} T^{2}$

The observations by Kilau and Shah (1984), Petersen (1998), Pillay (2001), show that $Cr_2O_3 - CaO$ mixtures and high-lime ferrochrome slag will oxidize in the presence of oxygen at ambient temperatures. In milled slag samples (75μm-1000μm) (as observed by Pillay, 2001) the reaction proceeded very slowly (6-9 months) with only 0.1-1 % of the chromium being oxidized.
It is important to emphasize that slags of high basicity will contain calcium chromite phases, which will slowly oxidize in ambient oxygen to a leachable calcium chromate in landfill situations. In the case of ferrochrome slags, careful control of $CaO:SiO_2$ ratios in slags quantities might make a costly impact on the cleanliness of the matte, but consideration has to be given to the long term impact of tonnes of Cr(VI) generating waste in landfills.

2.4. Chromite Ore Processing Residue (COPR) Leaching Characteristics

The generation and migration of a leachate influences the emergence of mineral toxins in underground waterways and the surrounding soils. Petersen and Petrie (2000) mentioned these processes as affecting the leachate process generation and mobility

1) Bulk transport of the aqueous phase through the deposit
2) Diffusion effects of dissolved species through the matrix
3) Chemical reaction mechanisms

Petersen and Petrie mention the bulk transport of an aqueous phase through a porous matrix as multi-directional, although in packed bed situations preferential flow areas; stagnant zones and areas of trickling flow may exist. The movement of dissolved chemical species in the bulk aqueous phase is also as a result of chemical diffusion besides the overall movement of liquid (Petersen and Petrie, 2000). According to Petersen and Petrie diffusion effects become significant in stagnant zones (these exist when fluid is trapped in dead end pores, within micro pores and in regions of inhomogeneous packing) and micro-pores within particles.
In situations where the release of chemical components into the aqueous phase involves dissolution of solids, the release is governed by the thermodynamic equilibrium and the rate at which the equilibrium is achieved (Petersen and Petrie, 2000).
In conclusion Petersen and Petrie mention dissolution as the most significant release mechanism in waste leaching although desorption of adsorbed species, chemical reaction and complexation are other common mechanisms.

As mentioned earlier, the toxicity and environmental mobility of chromium is determined by its oxidation state. It is of fundamental importance to understand and

In laboratory tests conducted on COPR and pure chemicals (Cr_2O_3+CaO) the leached Cr(VI) was a result of the oxidation of residual Cr(III) in ambient atmosphere (Pillay *et al.,* 2003).

It was observed by Pillay *et al.* (2003) that, of the total chrome, about 1 % will oxidize. It is also interesting to note that a small percentage of this is available as readily leachable Cr(VI). This confirms Petersen's (1998) earlier observations of continuous leaching of small amounts of Cr(VI) followed by increasing amounts of Cr(VI) as a result of oxidation.

This initial slow release of Cr(VI) is attributed to slow dissolution kinetics of Cr(VI) containing species (Farmer *et al.*, 2006). It should be noted that the aqueous concentration of Cr(VI) is influenced by other secondary in-solution processes such as adsorption and reduction by elements such as Fe(II) and organic compounds. Using phase identification techniques such as X-ray powder diffraction (XRPD) and scanning electron microscopy (SEM), Thomas *et al.* 2001 and Hillier *et al* (as quoted by Geelhoed *et al.*, 2002) observed phases containing un-reacted chromite and phases containing Cr(VI). Farmer et al., 2006 divided the mineral phases into three categories; un-reacted chromite ore ($(Mg,Fe)(Cr,Al)_2O_4$); high temperature phases formed during smelting (brownmillerite, $Ca_2(Al,Fe,Cr)_2O_5$; periclase, MgO; and larnite, Ca_2SiO_4) and minerals formed under weathering conditions in landfill situations (brucite, $Mg(OH)_2$; calcite, aragonite, $CaCO_3$; hydrogarnet, $Ca_3(Al,Fe)_2(H_4O_4)_3$; hydrocalumite, $Ca_4(Al,Fe)_2(OH)_{12}(OH)_2 \cdot 6H_2O$; and ettringite $Ca_6Al_2(OH)_{12}(SO_4)_3 \cdot 26H_2O$. Cr (VI) was found in hydrocalumite and hydrogarnet phases. Hillier *et al.*, 2003 (as quoted by Farmer *et al.,* 2005) included ettringite in the Cr(VI) containing phases when he conducted tests on COPR. This confirms Perkins and Palmer's earlier suggestions that due to the similarities in both structure and comparable thermochemical radii of CrO_4^{2-} and SO_4^{2-}, the CrO_4^{2-} should readily substitute the SO_4^{2-} in the ettringite compound. Interestingly the hydrogarnet phase is reported by Hillier *et al.* (2003) to be present as small crystals of a magnitude in the order of 2µm in diameter and ettringite as needle-like crystals of 50µm. Such seems synonymous with observations noted, of the high Cr(VI) content in the ultrafines.

Calculations conducted using modeling software by Meeussen in 2003 indicated that the most probable solubility-controlling phases at pH range 9.5 - 11 are a Cr(VI)-substituted hydrogarnet $(Ca_3Al_2(H_4O_4,CrO_4)_3)$ and Cr(VI) –hydrocaluminate $(Ca_4Al_2(OH)_{12}CrO_4 \cdot \text{^}6H_2O)$ although the model's Cr(VI) concentration predictions were more accurate after the inclusion of Cr(VI)-ettringite $(Ca_6Al_2(OH)_{12}(CrO_4)_3 \cdot 26H_2O)$.

Well known is the significance of pH in mineral solubility but also to consider are the buffering effects of the phases within a mineral compound as these influence the resultant pH of the leach solutions. Due to the large buffering capacity of COPR, the leach solutions are always at a high pH (Farmer *et al.*, 2006). Such a buffering capacity has effects on the extraction procedures one selects for potential

consume excessive amounts of weak acid used to maintain a constant pH in the TCLP method, raising the overall leaching pH to above 7 (Kilau and Shah, 1984).
The leaching behavior of COPR is a complex process, not only is it governed by the leaching conditions but also by the mineralogy of the slag. Hence careful consideration should be taken when interpreting leach data from slag or selecting a leach method.

2.5. Speed up Techniques for Chemical Reactions

2.5.1. The Use of Microwaves

In the environment, the fate of residual Cr(III) in slag is affected by the post disposal reactions occurring in the bulk of the landfill. As observed in various studies (Petersen, 1998; Pillay, 2001) oxidation of Cr_2O_3 in the presence of oxygen and CaO is one of the reactions that 'decides' the fate of residual Cr(III) in a landfill. Due to the slow nature of the kinetics of this reaction (as shown on Petersen's tests) diagnostic tests are cumbersome and take a long time, hence the need to extensively interrogate literature on available techniques to enhance the oxidation reactions on laboratory scale at ambient temperatures.
However the enhancement of the reaction kinetics should not affect the thermodynamics of the reaction in question, hence the consideration of microwave techniques and fluidized bed reactors.

The use of microwaves in chemical reactions has been under investigations for sometime. The use of microwaves is very common in organic synthesis and related bio-systems.
The preparation of oxides of metals such as vanadium, tungsten and molybdenum oxide bronzes has been improved by the use of microwave technology. According to Rao *et al.* (1999), the reaction temperatures used were remarkably lower than those employed for conventional synthetic techniques and the reactions proceeded at extremely fast rates.
According to Freeman, as quoted by Rao, the rapidity of microwave reaction compared to the conventional reactions can be understood by the fact that ionic diffusion is greatly enhanced in the presence of a microwave field. (Besides the obvious heating effects)
Berlan, (1995) mentions the fact that irradiation results in reaction rate enhancements, higher yields and improved selectivity. Kinetic control versus thermodynamic control poses a classical problem in the use of microwaves. In the study of the speed up techniques, the main objective is to find a method that avoids altering the thermodynamics of the reaction in question (the oxidation of residual Cr(III) in slag) but at the same time increasing the reaction kinetics.
Berlan, (1995) observed that the heating effects of microwaves differ from conventional methods of heating in that during microwave heating the heat is

occurs from the treated medium to the outside and due to this mass heating, faster temperature increases can be obtained.
Although many scholars suggest that microwave heating will only cause a thermodynamic effect, Raner *et al.* (1993) suggested that the effect of microwaves to organic solvents is dipolar heating. This involves the alignment of the dipoles of molecules with the electric field component of the radiation as shown in figure 2-5 below:

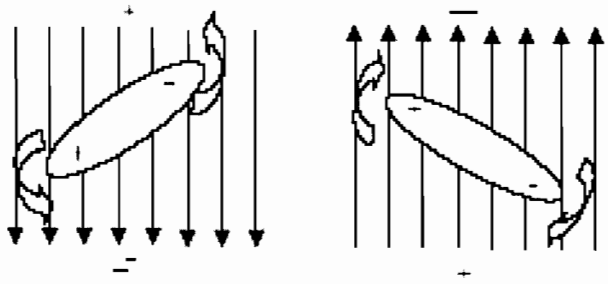

Figure 2-6: Realignment of a dipole in an electromagnetic field (Al-Harahsheh and Kingman, 2004)

Metaxas, (1983) as quoted by Raner *et al.* (1993) mentions that the developed polarization vector lags behind the electric field vector and this causes heating. In his arguments, Raner suggests that the radiation does not directly excite the molecules to higher vibrational or rotational energy levels but the internal energy will increase. It is this energy that will either be partitioned between transitional, vibrational, and rotational energy (these happens regardless of the method of heating).
Fini *et al.* (1999) mentions the effects of microwaves on different materials, with some materials such as metals reflecting microwaves, and dielectrics interacting with microwaves to different extents, hence materials that absorb microwaves can display different heating patterns. This is also influenced by their composition and if solids, by the dimension of their particles.
The microwave energy is lower than ionisation energy, hydrogen bonds or even van de Waals interactions and hence most effects on reaction rate enhancement can only be explained by thermal effects (Fini *et al.*, 1999). Experiments conducted by Freeman, Booske and Copper (as quoted by Rybakov *et al.*, 1997) to test solid-state ionic diffusion showed no increase in the bulk diffusion coefficient although they observed quasistationary ionic currents to flow in an irradiated crystal.
Contradicting the statements that microwave effects can only be explained by thermal effects, Freeman *et al.* (1998) mentions 'this previously unrecognised phenomena' as a "ponderomotive force" (pmf) which non-thermally enhances solid state ionic mass transport. In a solid ionic mass with discontinuities, microwave-excited ionic currents, at the interface become locally rectified giving rise to an additional driving force for mass transport across the boundaries (Freeman *et al.*, 1998). Booske *et al,* (1997) makes mention of this force (observed in halide salt ceramics) arising at any abrupt non-uniformity in the medium transport properties, such as grain boundaries or free surfaces.

distributions or deterministic, time averaged drift motion of matter or both [Booske *et al.*, 1997]) are more pronounced in some solid state reactions than thermal (interactions resulting in increased random motion of particles where kinetic energy statistics of such fluctuations are represented by a single thermodynamic equilibrium distribution such as Maxwell-Boltzmann [Booske *et al.*, 1997]) effects.

2.5.2. The Use of Fluidised Bed Techniques

Fluidisation techniques are used extensively in industrial applications where intimate contact between solids and either a gas or liquid stream is required. Fluidisation is known to enhance heat and mass transfer properties in a system making fluidisation suitable for circumstances where careful monitoring of parameters such as temperature is required.

Exposing iron to high temperatures in a normal atmosphere produces wustite (FeO) in areas adjacent to the surface then a layer of magnetite (Fe_3O_4) (Bodas *et al.*, 1996). Workers quoted by Bodas, found that in such reaction conditions, the proportion of the wanted product, haematite (Fe_2O_3) is not more than 5% by weight of the total quantity of oxides. This was irrespective of temperature, time of exposure and composition of the oxidizing environment (which had 100% O_2). Bodas explained this to be as a result of the high diffusion rate (at high temperatures) of iron from the core to the outer oxidized layer diluting the haematite to lower oxidation states

$$Fe_2O_3 \rightarrow Fe_3O_4 \qquad (6)$$

To achieve maximum conversions after reasonable reaction times, the iron powder was fluidized using compressed air at temperatures ranging between 500 °C – 900 °C. The cold model fluidized bed reactor is shown in Figure 2-7. Bodas found that fluidizing iron particles of size 90μm, at temperature range 750 °C – 900 °C, for 4 hours gave a 95 % yield of Iron Oxide. Fluidization provided adequate passage of oxygen into the powder resulting in efficient oxidation as well as an even heat transfer through the reacting particle (Bodas *et al.*, 1996).

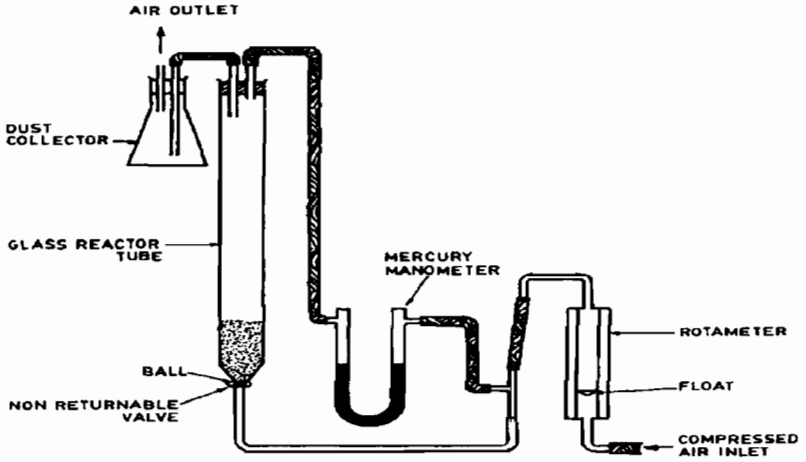

2.6. Techniques to Enhance Diffusion Controlled Reactions

This study aims to speed up the oxidation of Cr(III) in slag as a way of determining the slag's oxidisability using fluidized bed techniques. Pillay *et al.* (2003) proposed that the ageing kinetics of Chromium (III)-bearing slag are diffusion controlled. It is therefore important to study gas-solid diffusion controlled reactions to get an understanding of the rate limiting factors and how to accelerate the reactions.

The square of the particle size is an important factor in diffusion controlled reactions despite imperfections within pores of the solid reacting with the gas (Bhattacharya *et al.*, 2003). Studies by Bhattacharya and colleagues of the oxidation of graphite particles of different physico-chemical properties having different particle sizes, gave indications of the importance of particle characteristics and the atmosphere employed (during oxidation) on the rate of the oxidation reaction.
Further studies conducted on the oxidation of coal at low temperatures can be used to explain some of the mechanisms of oxidation of Cr (III) in slags. The studies showed that the oxidation occurs both at the external surface of the coal particles and internal surface of coal pores (Wang *et al.*, 2003).
Wang proposed four steps for the oxidation reaction:

1) Oxygen transport to the surface of coal particles (convective mass transfer from bulk of film surrounding a particle followed by the diffusive mass transfer in the film)
2) Pore diffusion (oxygen diffusing within the coal pores)
3) Chemical interaction between coal and oxygen
4) Release of heat and emission of gaseous products

The process can be illustrated diagrammatically as shown in Figure 2-8.

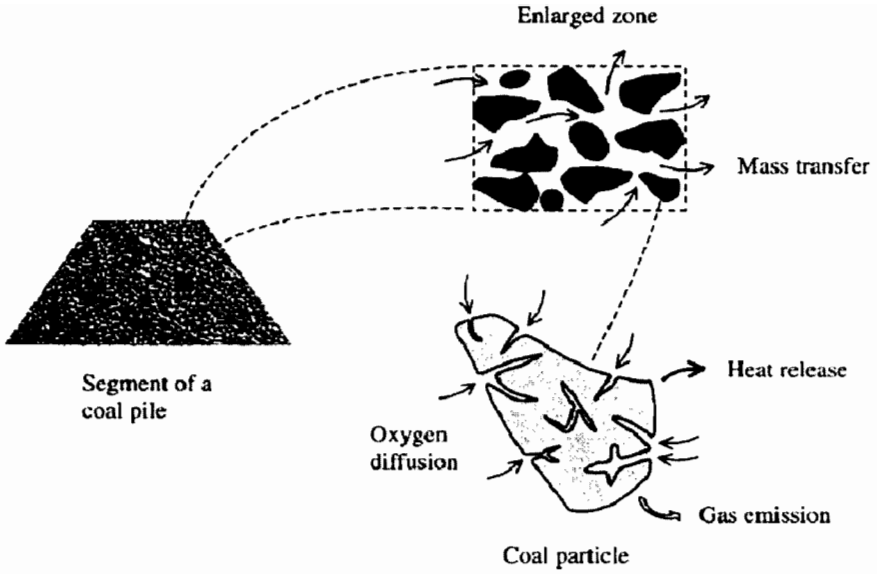

Figure 2-8: An illustration of the fundamental phenomena occurring in the coal oxidation process (Wang et al., 2003)

Of significance to this study are the first two processes as this study aims to enhance the pore diffusion of oxygen in slags to facilitate the Cr(III) oxidation.

Wang *et al.* (2003) mentions the significance of external variables such as temperature, partial pressure of oxygen and the moisture content in the gas medium, on the rate of oxidation.

Although the effect of moisture in the oxidation of coal differs to that in the oxidation of Cr(III) in slag, it will be considered in this study. In the oxidation of coal, as mentioned by Wang (2003), the moisture absorbed from the gas medium will result in heat release due to condensation (enthalpy of condensation) and the wetting of coal by liquid water.

Wang's experimental results showed an increase in the rate of oxidation as the particle size decreased. As quoted by Wang *et al.* (2003), Bouwman and Freriks mention of two types of oxidation occurring as a result of the particle size; Macropore and Micropore oxidation.

Macropore oxidation is when the transport of oxygen is the rate limiting step in the oxidation process. This type of oxidation is affected by the particle size or external surface of the particles.

In micro pore oxidation the particle has no diffusion limitations and this is not the rate-limiting step. This process is dominant in small particles.

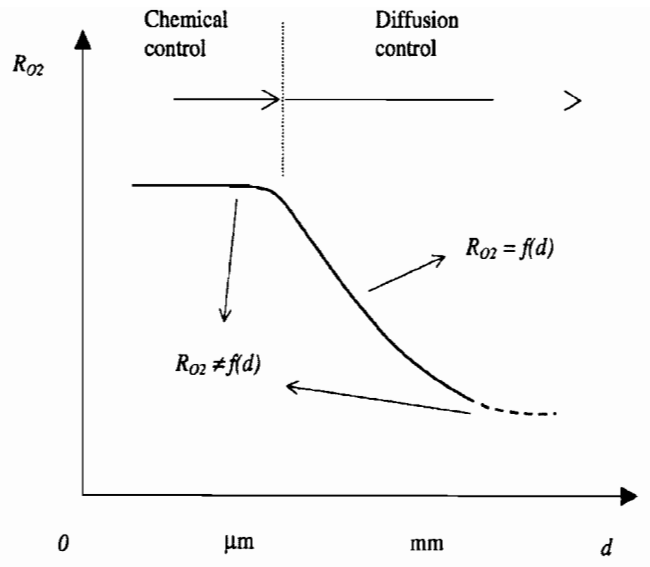

Figure 2-9: A typical trend illustrating the effect of particle size on the rate of oxygen consumption (Wang et al., 2003)

This dependence of the rate on the particle size (as confirmed by Bhattacharya, 2003) can be linked to the diameter of the particle size or the external surface area of coal particles i.e. there is an increase in surface area as the particle size decreases at the same time the diffusion path is decreased as the mean diameter of the particle is decreased. Although temperature variations will obviously affect the oxidation rate, Wang observed that at varying oxygen concentrations, the oxygen consumption can be expressed as a power of partial pressure of oxygen in the medium. Oxygen concentrations of below 2 % were observed to significantly reduce the rate of reaction to very low levels. Similar observations were noted by Pillay (2001) on experiments done on slag in a nitrogen atmosphere.

However the effect of moisture on the oxidation of Cr(VI) remains a debatable issue. Pillay (2003) mentions the hydration of CaO to $Ca(OH)_2$ to provide extra oxygen centres for the Cr(III) during the oxidation reaction.

2.7. Techniques for Gas-solid Reactions

Bab and Mendoza-Zelis (2004), mention reactions occurring at an appreciable rate and at much lower temperatures (than normally required) when milling is conducted in a reactive atmosphere, for solid-gas reactions. The mechanical processing plays a similar role played by other forms of energy commonly employed to induce chemical reactions. It also generates clean surfaces for gas adsorption as well as reducing the gas diffusion path to the reaction site as the particles get smaller. (Bab and Mendoza-Zelis., 2003)

Bade *et al.* (1996) confirms these findings in the reaction of metallurgical grade silicon with gaseous hydrogen chloride in a vibration mill. The chemical reaction taking place in the vibrating mill is the hydrochlorination of metallurgical grade silicon resulting in the formation of chlorinated silanes of the form SiH_xCl_{4-x}. Trichlorosilane $SiHCl_3$ and silicon tetrachloride $SiCl_4$ are the main products. Conventionally the comminution and chemical reaction are carried out in two separate apparata, a mill and a fluidized bed reactor. The reaction is conducted in a heatable vibration mill capable of withstanding temperatures and pressures of 450°C and 2MPa respectively and very high accelerations (up to 65g) and high amplitudes (7mm).

These workers noticed that high amplitudes and fast accelerations reduced the silicon size fraction from charge size 800 – 1000μm to < 40μm (yield of 95 %) in 40 minutes (after 4 minutes the fraction < 40μm had reached 15 %).
They also observed a reduction in reaction induction time in the case of simultaneous comminution and reaction compared to the reaction without comminution. Figure 2-10 below illustrates this observation

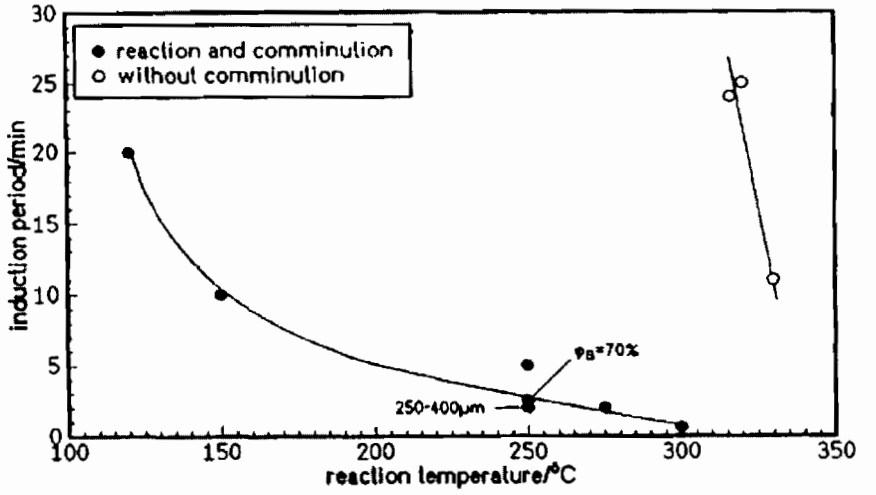

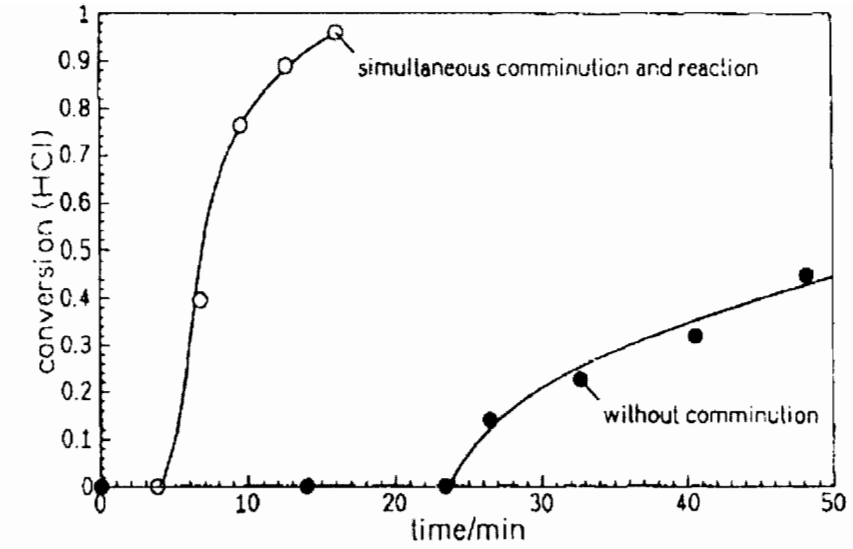

Figure 2-11: Conversion of hydrogenchloride with MG silicon (800 – 1000 μm) in the reaction mill at 320°C with and without comminution (Bade et al., 1996)

Bade *et al.* (1996) explains the increase in reaction rate for reactions with simultaneous comminution and chemical reaction to be as a result of the enlargement of specific area (due to size reduction of particles) and the formation of fresh non-passivated surface area due to mechanical abrasion. The mechanical agitation also lowers the activation energy allowing the reaction to start at lower temperatures (Figure 2-10).

2.8. Fluidization Theories and the Advantages of Fluidized Beds in Enhancing Chemical Reactions

Fluidization is the operation by which solid particles are transformed into a fluid like state through suspension in a gas or liquid. A fixed bed is when the fluid flows at slow flow rate and merely percolates through the void spaces between stationery particles.
An increase in the flow rate results in particles moving apart and some vibrating in restricted regions. Such a bed is called an expanded bed. At a certain fluid velocity, the frictional force between fluid and particle counterbalances the weight of the particles, and the vertical component of the compressive force between adjacent particles disappears. At this point the pressure drop through the bed equals the weight of the fluid and particles. The bed is said to be at minimum fluidization (Kunii and Levenspiel, 1991).
In gas solid systems, an increase in the gas flow rate beyond minimum fluidization results in large instabilities in the bed such that bubbling and gas channeling can be

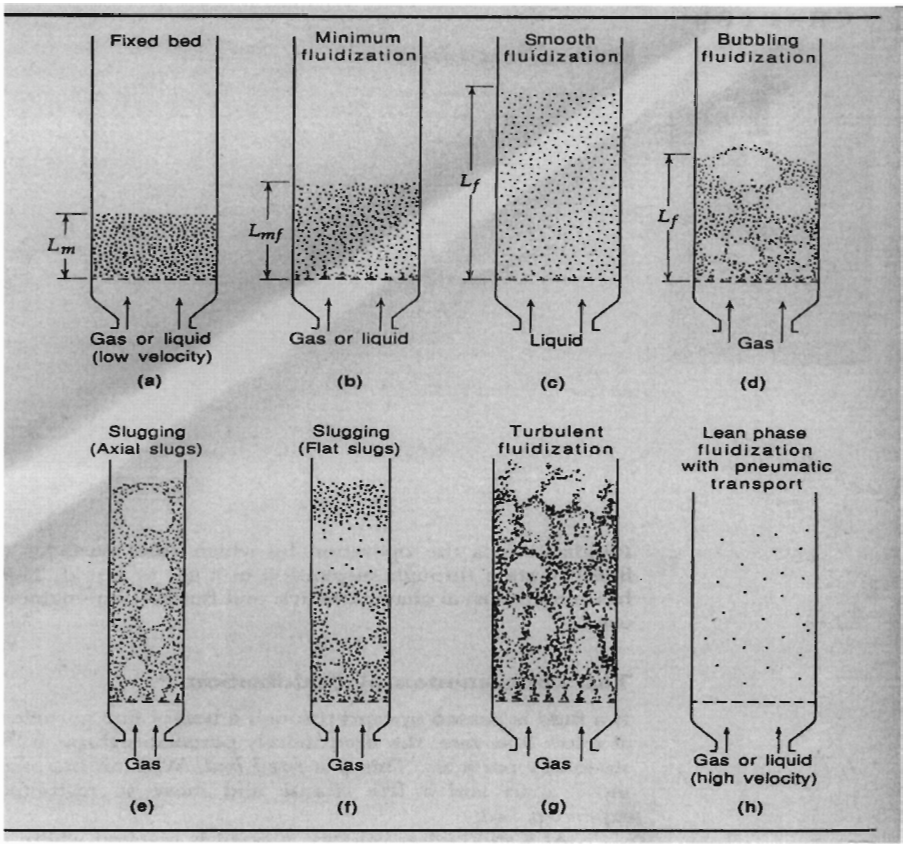

Figure: 2-12. Various methods of contacting (Kunii and Levenspiel, 1991)

The ease with which particles fluidize, and the range of operating conditions varies greatly among gas-solid systems. The behaviour of a fluidised bed is influenced by many factors including particle size. Geldart did an empirical classification of fluidised particles and divided powders into four groups depending on their size and density. From smallest to largest particle, they are as follows: (Kunii and Levenspiel, 1991)

Group C particles are cohesive or very fine powders. In these particles, the inter-particle forces are greater than those resulting from the action of the gas. These are difficult to fluidise. An example is flour and starch.

Group A particles are aeratable particles with a small mean particle size and low particle density (< 1.4 g/cm^3). These particles fluidise easily at low gas velocities and form small bubbles at higher gas velocities.

Group B particles are sand like particles of mean particle diameter from 40 μm and 500 μm and density of between 1.4 and 4 g/cm^3. They exhibit vigorous bubbling actions and the bubbles enlarge as they rise.

Group D particles are large and or dense particles. Deep beds are very difficult to fluidise and they have an erratic bubbling behaviour. Behaviours such as channelling can be observed on these particles.
Geldart's classification of particles can be graphically represented as follows:

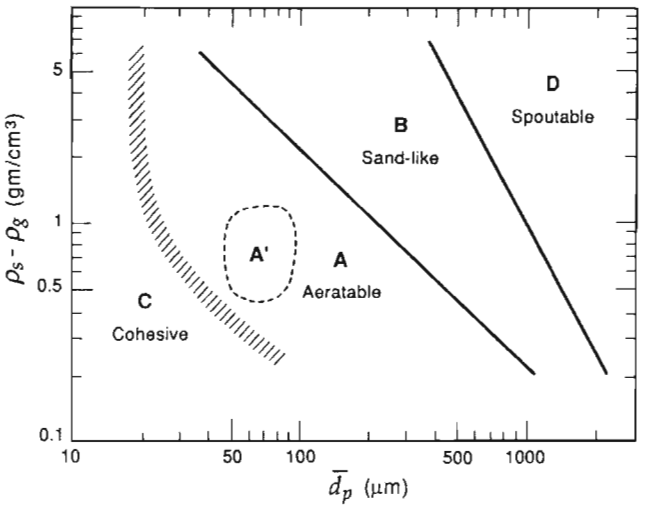

Figure 2-13: The Geldart classification of particles for air at ambient conditions. (Kunii and Levenspiel, 1991)

Fluidization principles have found a lot of industrial applications due to their efficient mass and heat transfer among other advantages. Kunii and Levenspiel, (1991) list the following as the advantages of using fluidized beds:

1) The rapid mixing of solids leads to close to isothermal conditions through out the bed, hence the process is easy to control.
2) The system is resistant to rapid temperature changes and responds slowly to rapid changes in the operating conditions. This gives a margin of safety especially in avoiding uncontrollable temperature rises for highly exothermic reactions
3) Heat and mass transfer rates between gas and particles are very high compared with other modes of contacting. This in turn lowers reaction induction times and increases the reaction rates(Bodas *et al.,* 1996)
4) Since most fluidized beds have small particle sizes, the resistance to diffusion through the particle is smaller and this is of benefit to diffusion controlled reactions

Fluidization has found many industrial applications. In metallurgical operations, the roasting of sulphide ores is done in fluidized beds. Polymerization of gaseous ethylene

Kunii and Levenspiel mention the extensive use of the fluidized bed driers due to low construction cost, easy operability and high thermal efficiency. Iron and steel companies are known to use large driers to dry coal before feeding it into the coke ovens. In the pharmaceutical industry, the dryers are small but efficient. Examples of driers are shown in Figure 2-14 below:

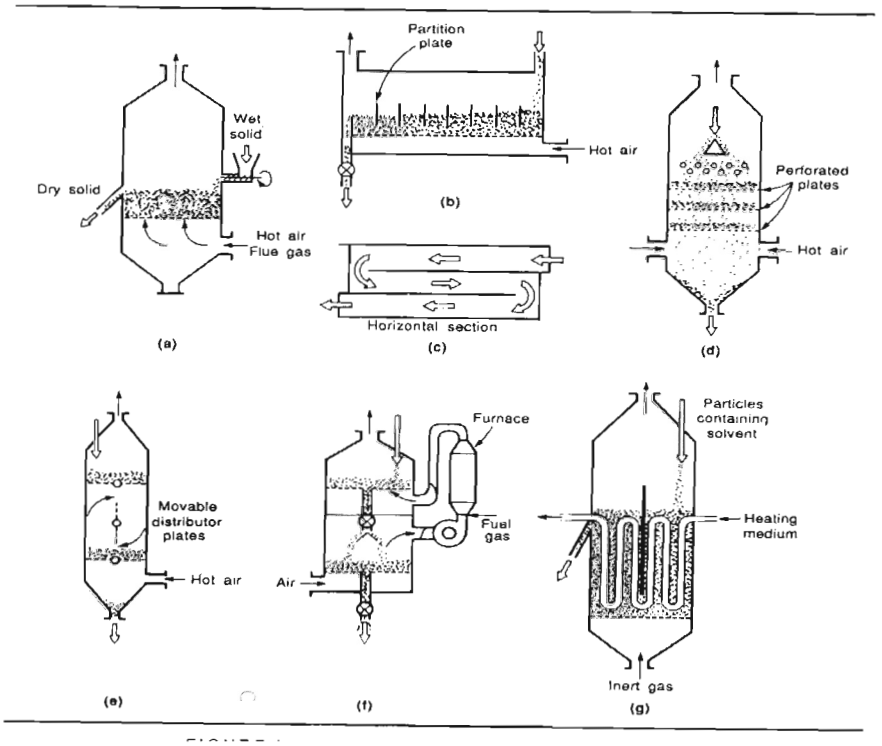

Figure 2-14: Various designs of driers (Kunii and Levenspiel, 1991)

2.8.1. Designing a fluidized Bed

The design of the fluidized bed is described and illustrated in detail in Chapter 3. The following sections describe the important aspects of fluidized bed design and the related design calculations.

2.8.2. The Distributor

A distributor mainly supports the bed materials, distributes the fluidizing gas uniformly. Distributor malfunctions have been known to affect fluidization quality (Sathiyamoorthy and Horio, 2003). Sathiyamoorthy and Horio, (2003) mentioned, maldistribution of fluidizing fluid, defluidization of the bed material on the grid plate, and attrition of the bed material at the gas issuing sites as some of the unwanted properties for an inefficient distributor.

For a specified bed height, there is a critical value of pressure drop of the gas distributor to produce a high quality fluidized bed (Luo *et al.,* 2004). The larger the pressure drop of a gas distributor and the ratio of aperture, the better the fluidizing performance. The overall distributor performance has to be optimized with respect to factors such as the economics of operation (Luo *et al.,* 2004).
Further investigations into the relationship between pressure drop of distributor and fluidization quality, Luo *et al,* (2004) mentions of a critical value of the gas distributor pressure drop in order to have a uniform and stable fluidized bed. This value C_p as a pressure drop number relative to ΔP_D and ΔP_B according to the following equation:

$$C_p = \frac{\Delta P^2{}_D + \Delta P^2{}_B}{(\Delta P_D + \Delta P_B)\Delta P_D} \tag{7}$$

Let

$$n = \frac{\Delta P_B}{\Delta P_D} \tag{8}$$

hence

$$C_p = \frac{1 + n^2}{1 + n} \tag{9}$$

Where P_D is pressure of gas distributor and P_B is the bed pressure drop. According to

2.8.3 Calculations for Minimum Fluidization Velocity for different Particle Sizes

In the designing of fluidized beds, an accurate prediction of the minimum fluidization velocity is of great importance since the minimum fluidization is a hydrodynamic parameter that strongly influences the overall behavior of fluidized beds (Reina *et al*, 2000).

At the onset of fluidization, the drag force by the upward moving gas equals the weight of particles (Kunii and Levenspiel., 1991). According to Kunii and Levenspiel (1991), the voidage is slightly larger at the onset of fluidization and the void fraction (ε_{mf}) can be estimated for random packing. The minimum fluidization velocity U_{mf} can be calculated using the following equations according to Kunii and Levenspiel:

$$\frac{\Delta P}{L} = \frac{150(1-\varepsilon)^3 \mu U_{mf}}{\varepsilon_{mf}^{\ 3}(\phi_s d_p)^2} + \frac{1.75(1-\varepsilon_{mf})\rho_g U_{mf}^{\ 2}}{\varepsilon_{mf}^{\ 3}\phi_s d_p} \qquad (10)$$

Where

U_{mf}	Minimum fluidization velocity (m/s)
ρ_g	Gas density
ρ_s	Density of solids
μ	Viscosity of gas (kg/m.s)
ϕ	Sphericity of a particle (dimensionless)
ε_{mf}	Void fraction at minimum fluidization conditions
d_p	Particle diameter
g	Acceleration due to gravity
L	Bed height

Different workers represent the above equation differently. Most of the terms in the equation can be determined experimentally and some are provided in references. Sathiyamoorthy and Horio, (2003) highlighted that the uniformity of fluidization is related to a critical velocity and the distributor pressure drop which in turn is related to the bed pressure drop. The critical velocity $\mathbf{U_C}$ is defined as the fluidizing-medium velocity when the resistance caused by the stagnant zone is overcome resulting in complete fluidization. As quoted by Sathiyamoorthy and Horio, (2003), Chyang and Huang introduce *The Real Minimum Fluidization Velocity* as the one which would give the same distributor pressure drop as of that obtained in an empty column.

2.8.4. Calculations for Pressure Drops at various positions on the Fluidized Bed

In industry, pressure drop measurements indicate the approximate bulk density or the fluidized bed height (Van Ommen *et al.,* 2004). Frequent pressure monitoring can be used to monitor the hydrodynamic behavior of the bed and can be used as a tool to forecast hydrodynamic changes such as agglomeration (Van Ommen *et al.,* 2004).
Plots of pressure drop (Δp) versus gas velocity u_o are used to determine the minimum fluidization velocity.
Δp can be calculated using the following equation according to Kunii and Levenspiel (1991)

$$\frac{\Delta p_b}{L_{mf}} = (1-\varepsilon_{mf})(\rho_s - \rho_g)\left(\frac{g}{g_c}\right) \qquad (11)$$

Where g_c is a conversion factor
g_c = 1kg.m/N.s^2

Pressure drops in fluidized beds can be measured and from different positions in the bed. However it is of importance to have a clear understanding of the origins of pressure signals and all the pressure variations or fluctuations that occur in practical situations. Such information assists in the overall understanding of the bed behavior, and identifying the positions of pressure probes relative to the sources of pressure waves (Van Ommen *et al.*, 2004).
The average pressure drop, usually measured over part of a fluidized bed gives an estimate of the average bulk density or fluidized bed height. (Van Ommen *et al.*, 2004, Z. Luo *et al.*, 2004). The weight of the solids minus their buoyancy per unit cross-sectional area of the bed, estimates the pressure drop Δp of the fluidizing gas. (Werther, 1999)

$$\Delta p \approx (\rho_s - \rho_f) C_v g \Delta h \qquad (12)$$

ρ_s Density of solids kg m^{-3}

ρ_f Density of fluid kg m^{-3}

C_v Is the average solids volume concentration in the volume element $A_t \Delta h$ (Werther, 1999)

In a pilot scale bubbling bed of Geldart B particles, Van Ommen, (2004) found that the pressure fluctuations are as a result of high amplitude compression waves, bubble passage and low amplitude compression waves. In small-diameter columns, moving bed mass results in significant pressure changes. According to Ommen and Colleagues (2004), the bubbles formed below a pressure measurement position, result

As mentioned by Werther (1999), bubbling fluidized beds' average solids volume concentration C_v can be assumed independent of bed height, and this leads to a linear relationship between pressure values and height (Figure 2-15.) such that a series of pressure measurements along the height **h** above the gas distributor, can be used to extrapolate the bed height **H.**

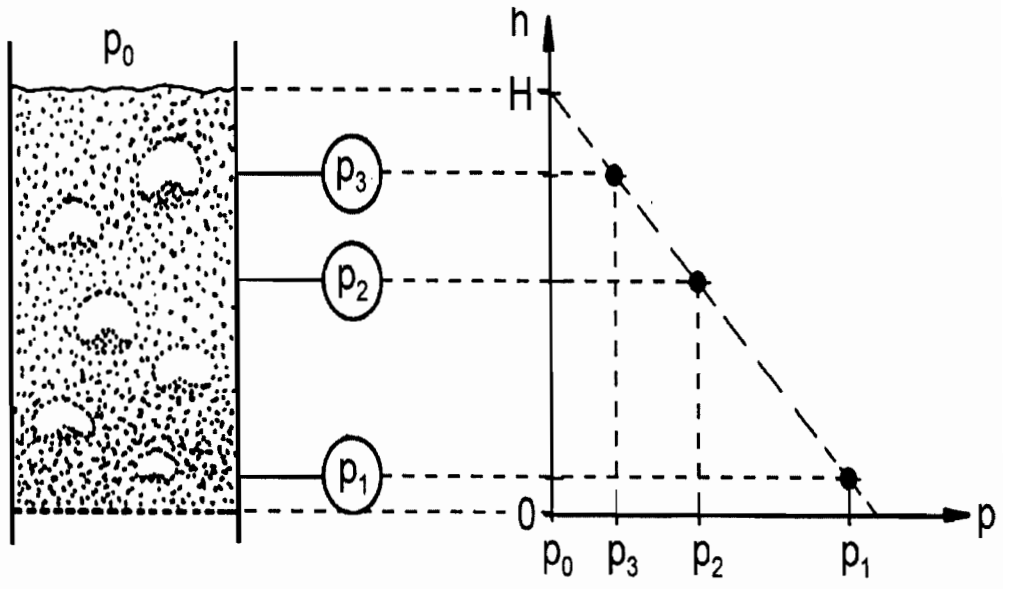

Figure 2-15: Determination of the expanded bed height in a bubbling fluidized bed (Werther, 1999)

The pressure drop across a distributor ΔP_d is expressed as a ratio to the bed pressure drop ΔP_b hence $\Delta P_d/\Delta P_b$ gives the pressured drop across a distributor and the ratio is usually within the range 0.1 – 0.4 for uniform fluidization (Sathiyamoorthy and Horio., 2003). The aspect ratio of a fluidized bed is defined as the ratio of the bed height, H to the diameter of the bed, D.

2.9. Conclusion

As literature suggests, high lime COPR will contain calcium chromite phases and other phases of Mg, Fe, Cr, Al, oxides. Various studies have shown that, in the presence of moisture, and ambient oxygen, the calcium chromite phases will oxidize to calcium chromate. Chromium rich phases such as hydrocalumite and hydrogarnet have been observed to influence the release of Cr(VI) as the slag ages (Farmer *et al.,* 2005). Due to the high concentrations of calcium oxide in these phases, the leach solution pH ranges between 10-12, mobilizing the Cr(VI). However with a CaO:SiO2 ratio below 2, the chromium rich phases (refer to Table 2-3) are stable phases of magnesium and silicates (Kilau and Shah, 1984) resistant to oxidation. In landfill situations and other natural environments, the Cr(VI)-rich phases would slowly release Cr(VI) into the environment, whilst the oxidation of calcium chromite phases to calcium chromate would compound to serious environmental consequences. However the oxidation reaction takes a very long time and only a small fraction of the chromium oxidizes (Pillay *et al.,* 2003). In production situations, the long-term environmental performance of a waste needs to be ascertained shortly after production to ensure safe disposal practices.

Studies done on reagent grade $Cr_2O_3 - CaO$ chemical mixtures identified the key parameters affecting the oxidation reaction, and a probable reaction mechanism. The mechanism proposed the diffusion of oxygen to the $Cr_2O_3 - CaO$ phase boundaries, resulting in the probable movement of Cr^{3+} across the phase boundary. The diffusion of oxygen to the phase boundaries is limited to the pores and fissures along grain boundaries (Pillay *et al,* 2003) hence a smaller diffusion path and a high oxygen concentration gradient will probably influence the reaction induction time.

Literature has shown that the alternative use of fluidized bed techniques in some processes has resulted in higher yields, better heat and mass transfers, and better product quality. In this study fluidized bed techniques were chosen as means to enhance the oxygen diffusion to the reacting phase boundaries consequently affecting the reaction rate.

CHAPTER 3

EXPERIMENTAL APPROACH AND METHODS

Previous workers (Pillay, 2001 and Petersen, 1998) have indicated that the ageing of Cr(III) in CaO-containing COPR under normal ambient conditions is a very slow process. Various scholars have established that moisture, oxygen and calcium oxide, besides other physical characteristics of the chromium containing solid waste, play a major role in the ageing of Cr(III) to Cr(VI).

It has been speculated that the oxidation of slag is limited by the diffusion of oxygen to the grain boundaries. It can therefore be hypothesised that using fluidised bed techniques one can effectively increase the oxygen mass transfer to the reacting particles, thereby increasing the rate of oxidation. This chapter presents the experimental approach and the methodology used to test this hypothesis. The chapter also describes the materials and the equipment used in this study.

3.1. Experimental Approach

A fluidised bed suitable for fine-grained fractions of typical chromium-bearing slags was designed and constructed. It was commissioned using a slag from platinum ore processing.

Slag obtained from a chrome smelter was dried, sieved and characterised to determine its elemental composition. Three particle sizes were selected for fluidisation.

Representative samples of the three different particle sizes were fluidised for up to 72 hours with regular sampling and leaching for Cr(VI) abundance. Similar samples were left to age on laboratory benches as control experiments. Bench samples were sampled regularly to establish a Cr(VI) abundance profile with time.

3.2. Equipment

The basic design of the fluidized bed was adopted from Mawatari *et al.,* (2003). The fluidized bed was constructed using a 'Plexiglas' acrylic tube of an inside diameter of 65 mm. A glass-sintered disk was attached at the bottom of the fluidized bed as a gas distributor. In order to minimise the entrainment of slag particles out of the bed, as well as increasing gas-particle contact time, a disengagement zone (refer to figure 3.1) was incorporated in the design. According to Bernoulli's equation, the increase in cross-sectional area results in a drop in gas velocity causing the particles to fall back

fluidizing-gas line to measure the superficial gas velocity. Bone-dry compressed air was used as the fluidising medium. The design of the humidifier was such that, dry air would bubble through a column of water absorbing water in the process (refer to Figure 3.1). A hygrometer attached to the main airline was used to indicate the changes in the moisture of the fluidising air. Post the bed, exhaust gas scrubbers (Master Pneumatic Detroit, FC10 Filter) were fitted to trap any chromium containing dust.

Below is a schematic representation of the Experimental Rig

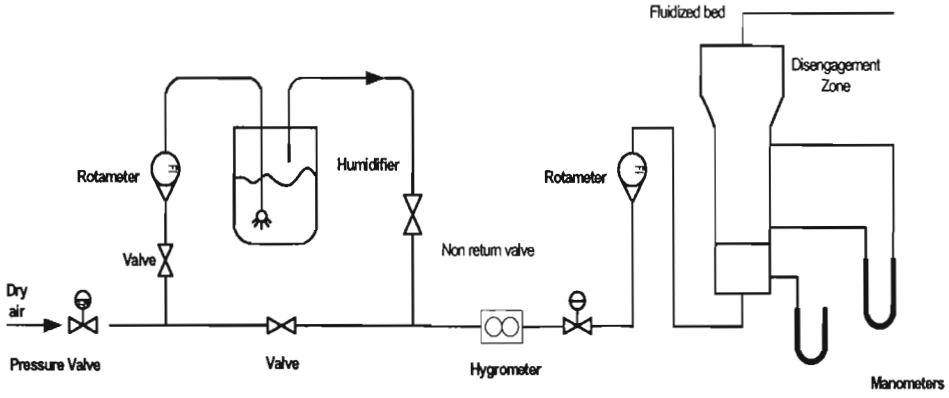

Figure 3.1 Schematic outline of the fluidization rig

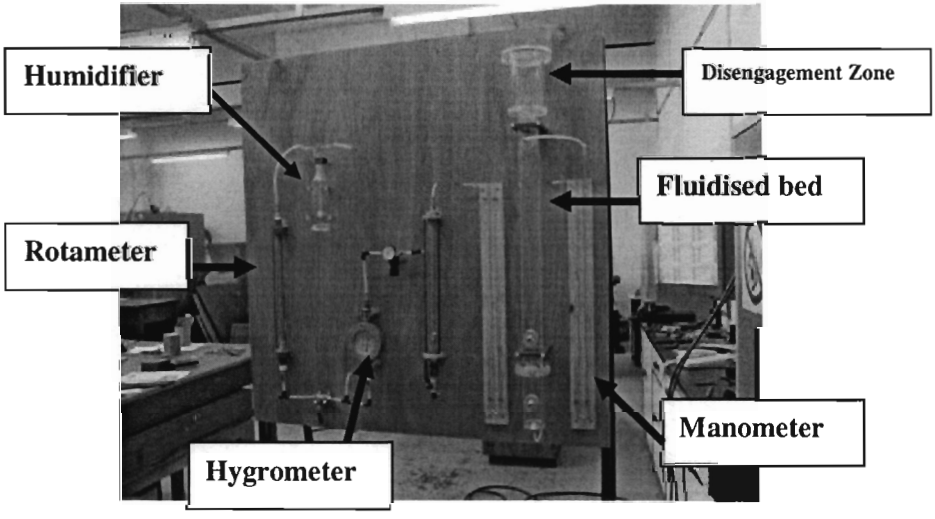

Figure 3.2: Picture of the fluidization rig used in the experiment

Before commissioning the rig, a hazard analysis was conducted. The air line and the bed were tested for leaks, hairline fractures and general operational safety by operating the rig at maximum pressure (6bars) for 24 hours (without any sample) whilst regularly sprinkling soapy water on joints.

A safety 'overspill pipe' into a glass container was added to the manometers as a precaution in the event of mercury being pushed out of the manometers. This can happen if the scrubbers are chocked or blocked. Slow release valves were fitted on the main airline in order to gently and gradually fluidise the bed.

A standard operating procedure was written and approved by the laboratory safety officer and the supervisor. The commission of the rig is described in Chapter 4.

3.3. Materials

The tests were conducted on Low Carbon Ferrochrome (LCFeCr) slag as well as UG-2 ore slag from the smelting of PGM-bearing concentrates. These materials are described below:

3.3.1. Low Carbon Ferrochrome Slag (LCFeCr)

The LCFeCr slag was obtained from a local integrated stainless steel smelter. Two 20 kg buckets of the slag were sampled fresh, on-site from a granulator. The slag was not milled before sampling although the largest particle size was > 1000μm and the finest particle size was < 38μm.

On arrival at the laboratory, 20 kg of the slag was air dried and classified into different particle sizes using a sieve shaker (refer to Table 3-1). The density was determined using an AccuPyc 1330 Pycnometer and the actual particle size distribution of selected sieved particle size ranges was determined using Malvern Mastersizer. The coarse fraction (> 1000μm) was further milled to ensure reasonable quantities of the different sample sizes.

Table 3-1: The particle size distribution of the LCFeCr slag

Particle Size [μm]	Mass[g]	% Fraction
>1000 μm	12271	64.4
300-1000 μm	6183	32.4
106-300 μm	443	2.3
90-106 μm	30	0.2
63-90 μm	81	0.4
38-63 μm	39	0.2
<38 μm	20	0.1
Total mass	19069	

Table 3-2: The elemental composition of each particle size class (before milling)

	CHEMICAL COMPOSITION				
PARTICLE SIZE CLASS[μm]	**% Cr**	**%Fe**	**%Al**	**%Mg**	**%Ca**
38-63μm	1.45	0.17	12.19	10.05	29.07
63-90μm	1.34	0.14	10.42	9.02	27.88
90-106μm	1.28	0.15	10.89	8.79	26.92
106-300μm	1.50	0.05	5.58	9.04	28.40
300-1000μm	1.40	0.05	3.92	8.17	26.10
>1000μm	0.97	0.06	4.30	8.39	28.20

XRPD patterns from the slag are provided in appendix.

3.3.2. PGM Slag

The PGM slag was obtained from a local PGM smelter. The slag was from the smelting of a chromite seam for valuable PGMs. The slag was milled by the supplier to under 1000μm. On arrival to the laboratory, it was further milled into the predetermined particle sizes. The density and actual particle size distributions were determined by Pycnometer and Malvern Mastersizer respectively. The slag was used to commission the fluidised bed, determine important fluidisation parameters and overall bed performance.

3.4. Methods

3.4.1. Sampling Procedure

(i) Bulk of the Sample

The LCFeCr slag sample originated from tapped slag from the Submerged Arc Furnace, quenched in water, producing a highly porous granular material. The sampling was done from an intermediate storage bin such that the two 20 kg samples were representative of one production batch.

A power–driven front-end loader (load capacity exceeding 200 litres) was used to randomly collect five samples from the storage bin. The five samples were mixed, coned and quartered obtaining two representative 20 kg samples.

In the laboratory, the sample was air dried and then sieved out to >1000 μm, 300

(ii) Fluidisation Sample

The selected particle size fractions for fluidisation (38-63 μm; 63-90 μm; 90-106 μm), obtained by further milling of the coarse fractions of the slag, were each mixed thoroughly and a 200 g sample was then charged into the fluidised bed. A 10 g sample was also sampled and leached for initial Cr(VI) analysis. After predetermined fluidisation duration, the fluidised bed reactor was dismantled carefully without loss of sample. The sample was discharged onto a flat surface, mixed and 10 g was sampled for Cr(VI) analysis. The remaining sample was reweighed and recharged into the fluidised bed reactor for continued fluidisation. This procedure was repeated whenever sampling was necessary.

3.4.2. Elemental Analysis of Ferrochrome Slag

For elemental analysis, about 0.10g each of the three particle sizes was digested with a mixture of hydrofluoric acid/hydrochloric acid/nitric/perchloric acid. Each digest solution was analysed for Ca, Fe, Mg, Al and Cr using Atomic Absorption Spectroscopy (AAS). Parallel to the AAS method, the XRF method was used to confirm the AAS figures. The chromium values obtained by AAS method were regarded as the total chromium content of the selected particle size.

3.4.3. Density Measurements

The density measurements were done using a Helium Pycnometer model AccuPyc 1330. The machine was set to conduct 10 purges, 10 runs at an equilibration rate of 0.0050 psig/min. (Note that the default machine setting for the equilibration rate was 0.01 psig/min and a lower value increases the accuracy of the machine). These parameters were set constant through out this study.

3.4.4. Particle Size Analysis

Particle size analysis was done using a Malvern Mastersizer. A 300RF lens, for size particle range 0.05- 880μm was selected. Water was used as the sample dispersant.

3.4.5. Determination of Minimum Fluidisation Velocity

To determine the minimum fluidisation velocity (U_{mf}) of the selected particle size

through the bed, were measured using a mercury manometer. The pressure drop values were plotted against the gas velocity to then determine the minimum fluidisation velocity. The experiments were conducted at atmospheric pressure and temperature. Only pressure drops as gas velocities increased were studied. The experimental values were compared with the values predicted by a modified Ergun equation.

3.4.6. Calculation of Minimum Fluidisation Velocity

Parallel to the experiments, U_{mf} predictions were done using suitable correlations whose parameters used for calculating U_{mf}. were available. In these calculations, Reynolds number (at minimum fluidisation) and Galileo number were used to modify the Ergun equation as illustrated below.

$$\frac{\Delta P}{L} = \frac{150(1-\varepsilon)^3 \mu U}{\varepsilon^3 (\phi d_p)^2} + \frac{1.75(1-\varepsilon)\rho_g U^2}{\varepsilon^3 \phi d_p} \quad (1)$$

$$\mathrm{Re_{mf}} = \sqrt{33.7^2 + 0.0408Ga} - 33.7 \quad (2)$$

$$\mathrm{Re_{mf}} = \frac{d_p U_{mf} \rho_g}{\mu} \quad (3)$$

$$\mathrm{Ga} = \frac{d_p^3 g \rho_g (\rho_p - \rho_g)}{\mu^2} \quad (4)$$

Combining equations 2, 3 and 4

$$\frac{d_p U_{mf} \rho_g}{\mu} = \sqrt{33.7^2 + \frac{0.0408 d_p^3 g \rho_g (\rho_p - \rho_g)}{\mu^2}} - 33.7$$

Where;

$\mathrm{Re_{mf}}$	Particle Reynolds number at U_{mf}
Ga	Galileo number
d_p	Diameter of the particles
g	Gravitational acceleration
ρ_g	Density of fluidizing gas
ρ_p	Density of the particles (slag)
μ	Viscosity of air
U_{mf}	Minimum fluidisation velocity
ε	Void fraction

ϕ Shape factor

3.4.7. Bench Ageing of Slag Samples

From the different particle sizes, representative samples were weighed into open weighing boats and left to age under ambient atmosphere on laboratory benches. Before bench ageing, a sample was taken to give the initial Cr(VI) content of the sample. Sampling and subsequent leaching for Cr(VI) was done after 4 and 8 weeks.

3.5. Effect of Fluidisation Time on Oxidation of Residual Cr(III)

In order to establish the effects of fluidisation time, weighed samples were charged into the fluidised bed reactor and fluidised for up to 72 hours. Sampling and leaching for Cr(VI) abundance was done after 3, 6, 24, 27, 48, and 72 hours. A selected coarse sample was fluidised for up to 2 weeks.

Analysis for Cr(VI) was done immediately after 24 hrs of leaching and the samples were kept in a refrigerator as a reference samples. The leach residues were chemically digested for total chrome analysis.

3.6. Analysis of Samples for Cr(VI)

Different methods are used to analyse for Cr(VI) although Cr(VI) is commonly detected as a colourful Cr(VI)-DPC (1,5 diphenylcarbazide) complex using UV-Visible Spectroscopy at 540 nm. The choice of the analytical method to use for Cr(VI) analysis depends on the Cr(VI) concentrations expected in samples. For very low Cr(VI) concentrations, most methods include a highly sensitive pre-concentration or separation step such as ion chromatography coupled with a UV-Visible Spectrometer.

Due to high levels (> 0.05 ppm) of Cr(VI) in the slag samples considered in this study, UV-Visible Spectroscopy was selected for Cr(VI) analyses. For a detailed description of the analytical protocol refer to Pillay's June 2001 thesis.

CHAPTER FOUR

RESULTS

This chapter will give results of all the experiments done during the course of this investigation. Results from the ageing of slag in the fluidised bed will be presented and compared to those of the bench ageing tests. Particle size analysis results of fluidised samples will be presented to establish the possible loss and formation of fines during fluidisation. Residual chrome data for specific residues after leaching for Cr(VI) is presented parallel to Cr(VI) abundance data in graphical form. An error analysis is included. This chapter will also present results from exploratory work on the effects of microwaves on slag in section 4.5. The chapter is concluded by a discussion of the results presented.

4.1. Commissioning of Fluidised Bed Reactor

The fluidised bed, built as discussed in Chapter 3, was commissioned using the UG-2 ore slag. Size fractions in the 38-63μm and 63-90μm range were used to assess the performance of the fluidised bed reactor. The specific gravity of this slag was determined to be 2.9 g/cm^3. The selected particle sizes ranges for fluidisation include Geldart's Group A and B particles. They should thus be easily fluidizable within the 0- 6 bars pressure range available in the laboratory.

4.1.1. Determination of Minimum Fluidisation Velocities

Figure 4.1 shows the plots of pressure drop against gas velocity for the 38-63μm and 63-90μm particle sizes.

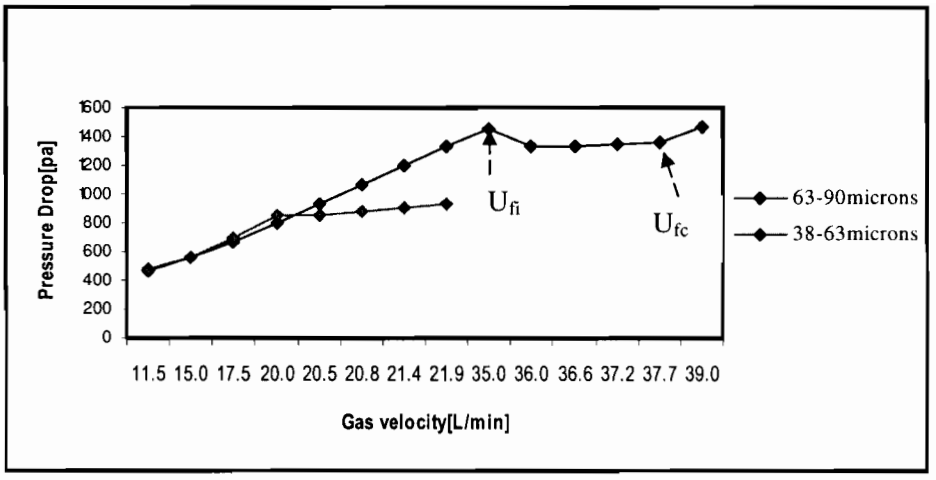

Figure 4-1: Determination of the minimum fluidization velocity for 38- 63μm and 63-90μm particle size fractions of a UG2 smelter slag

The two distinct kinks observed for the 63-90μm sample (compared to 38-63μm sample) can be attributed to the particle size distribution within the 63-90μm particle size range, as shown in Table 4.2. As the average diameter of particles increase, the presence of what Gauthier *et al.*, (1999) refer to as 'extreme-sized' particles affect fluidisation hydrodynamics resulting in the observed two break points.
The two velocities can be identified as one representing the incipient fluidization of most fluidizable particles (U_{fi}), and complete fluidization of the all the particles in the sample (U_{fc}).
For the 38-63μm sample the absence of the kinks can therefore be attributed to the absence of significant gas-particle and inter-particle interaction as the particle diameter decreases (Gauthier *et al.*, 1999). The calculated value for the minimum fluidization velocity of the 38-63μm samples was in close agreement with the experimental value. The 21 % difference in the 63-90μm values can be attributed to increasing pressure fluctuations as the particle size increases and the error resulting from the correlation used to calculate minimum fluidization velocity (Gauthier *et al.*, 1999).

Table 4-1: Experimental and calculated minimum fluidisation velocities for 38-63μm and 63-90μm

Particle Size [μm]	**Calculated U_{mf} [cm/s]***	**Experimental U_{mf} [cm/s]**
38-63 μm	2.5	2.5
63-90 μm	5.7	4.5

Table 4-2a: Quantities (volume %) of different particle size 'cuts' within the 38-63μm as reported by Malvern Mastersizer (mean d_p = 51μm)[Raw data in Appendix B3]

Particle size range [μm]	0.1 - 1	1 – 10	10 - 36	36 - 66	66 - 104
Volume percent	6.9	9.3	37.0	35.84	10.97

Table 4-2b: Quantities (volume %) of different particle size 'cuts' within the 63-90μm sample as reported by Malvern Mastersizer (mean d_p = 77μm)

Particle size range [μm]	0.2 - 1	1 - 10	10 - 66	66 - 89	89 - 164
Volume percent	4.0	5.4	41.6	24.9	24.2

4.2. Ageing of Slag in the Fluidised Bed

Once it had been shown that fine fractions of slag could be successfully fluidized, and the operational parameters had been established, ageing tests were run in the apparatus with a slag believed to be prone to oxidative ageing.

4.2.1. Effect of Fluidisation Time on Cr(VI) Abundance

Fluidisation of the ferrochrome slag was done with bone-dry compressed air for a maximum of 72 hours as described in Chapter 3. Figures 4.2 and 4.3 show the hexavalent chromium concentrations determined in samples retrieved from these experiments.

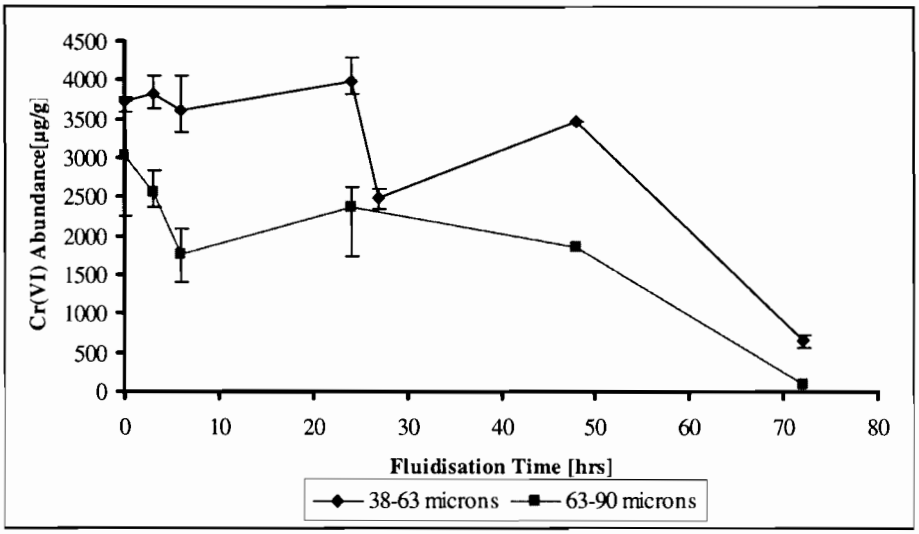

Contrary to expectations, the Cr(VI) abundance in the samples dropped, rather than increased, from an initial concentration of 2717 µg/g and 2329 µg/g, to a minimum of 473 µg/g and 89 µg/g for the 36-63µm and 63-90µm samples, respectively.

It was suspected that two effects might have caused Cr(VI) concentrations to decrease: (i) a loss of fine particles [known to be enriched in Cr(VI)] over time, and (ii) insufficient time for oxidation to occur to a significant extent. In order to check on these hypotheses, another run was performed with a coarser slag sample, and over a longer fluidization time.

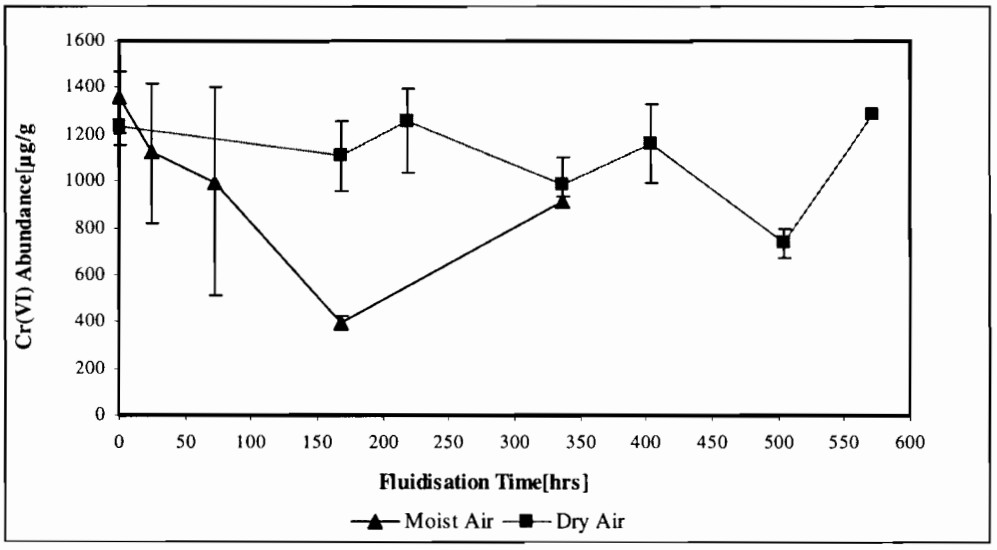

Figure 4-3: Cr(VI) abundance in most and dry air fluidised ferrochrome slag for the 90-106 µm particle size

A sample in the 90-106 µm range was therefore fluidised for 3 weeks with regular sampling for Cr(VI) analysis. A similar run was done using moist air as the fluidising medium for two weeks. It is important to note the Cr(VI) abundance profile for the 90-106 µm sample (dry air) (Figure 4.3) does not show a similar trend as observed with the 38-63 µm, and 63-90 µm samples as fluidisation time increased. The Cr(VI) abundance profile for the same particle size fluidized with moisture (flow rate of approximately $10\times10^{-6} m^3 H_2O / m^3 Air$) for up to 2 weeks did not indicate a gradual increase in Cr(VI) to suggest oxidation of Cr(III) although there was evidence (in the form of weight increases) of possible hydration of CaO during fluidisation. (See Appendix A14)

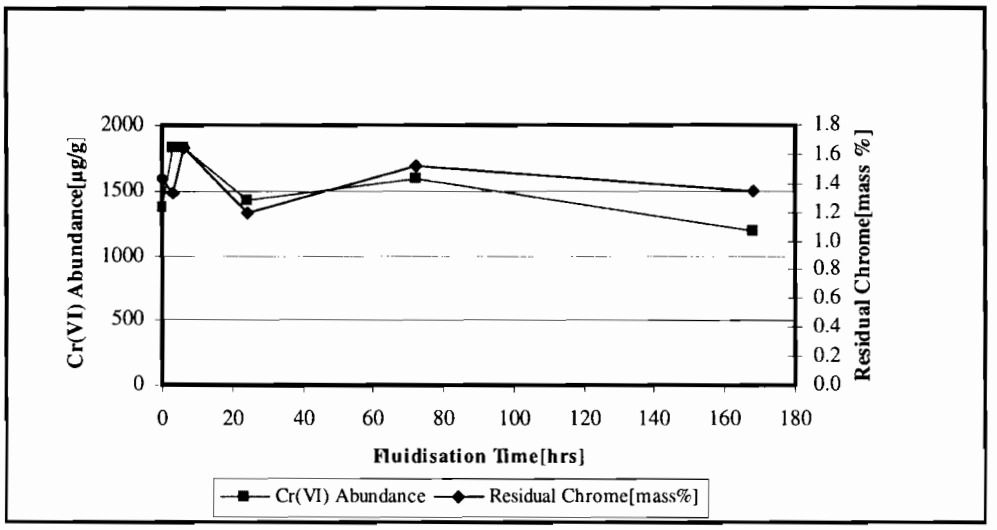

Figure 4-4: Cr(VI) abundance and residual chrome in a fluidised 90-106µm ferrochrome sample

Figure 4.4 shows results of a further experiment with a sample in the for 90-106 µm range, in which total residual chrome was determined alongside Cr(VI) concentrations. This was a repeat experiment in which the 90-106 µm samples were screened of fines and fluidised for up to2 weeks.

In order to determine whether fluidisation resulted in the oxidation of residual Cr(III) in the 38-63 µm samples, the residual chrome of the residues after leaching for Cr(VI) was plotted against time. Figure 4.5 shows a comparison of residual chrome and Cr(VI) abundance in the 38-63 µm samples after fluidisation.

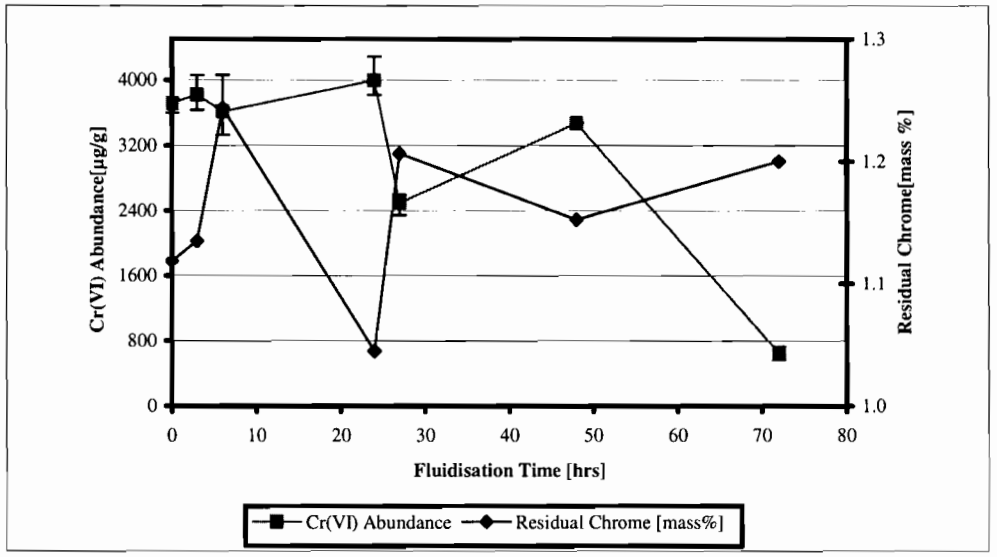

4.2.2. Effect of Fluidisation Time on Particle Sizes

This work was done to investigate the hypothesis that a loss of ultrafines from the bed resulted in the observed decrease of Cr(VI) concentrations as shown in Figure 4.2. The data from particle size analysis would also indicate whether fines were generated during fluidisation.

Figures 4.6a and 4.6b show that there was a decrease in the amount of ultrafines (< 2 μm) in the 6 hr and the 72 hrs sample in comparison to the 3 hr sample

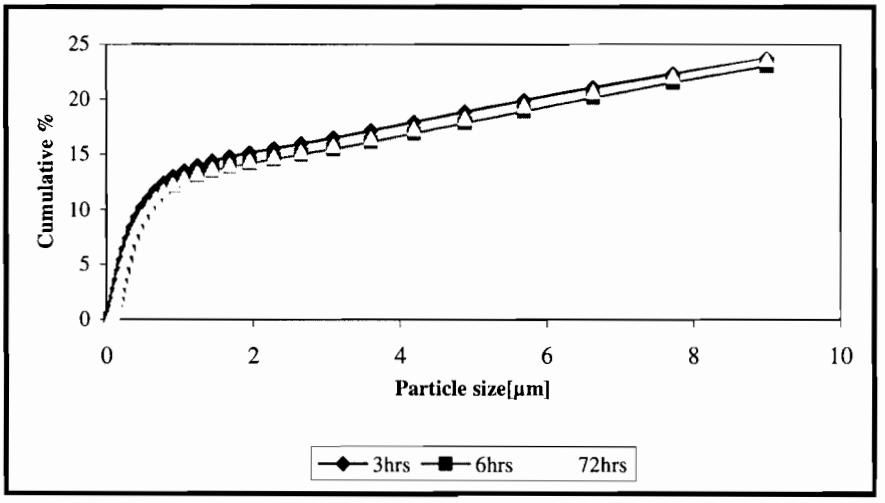

Figure 4-6a: Abundance of fines (< 10 μm) in the 3 hr, 6 hr, and 72 hr fluidised samples of the 38-63 μm particle size

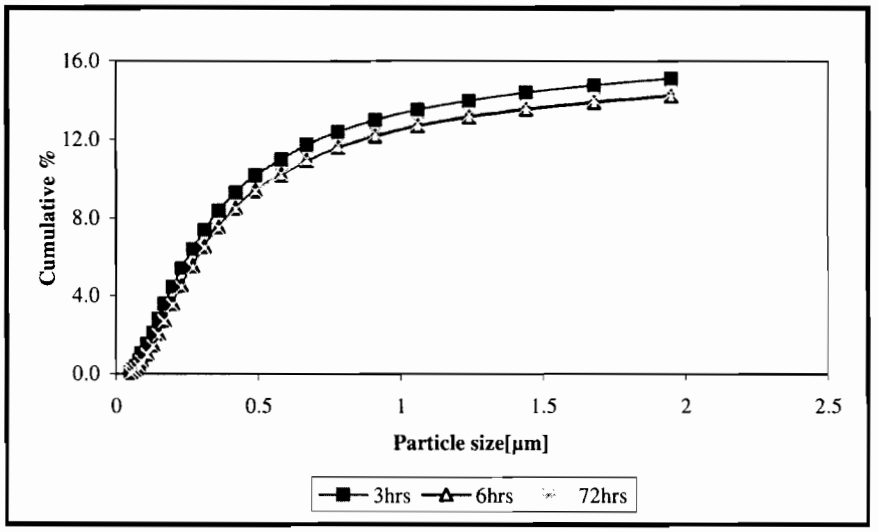

Figures 4.7 and 4.8 present particle size analysis data of the two fluidisation tests on the 90-106 μm size fraction, both after screening of ultrafines.

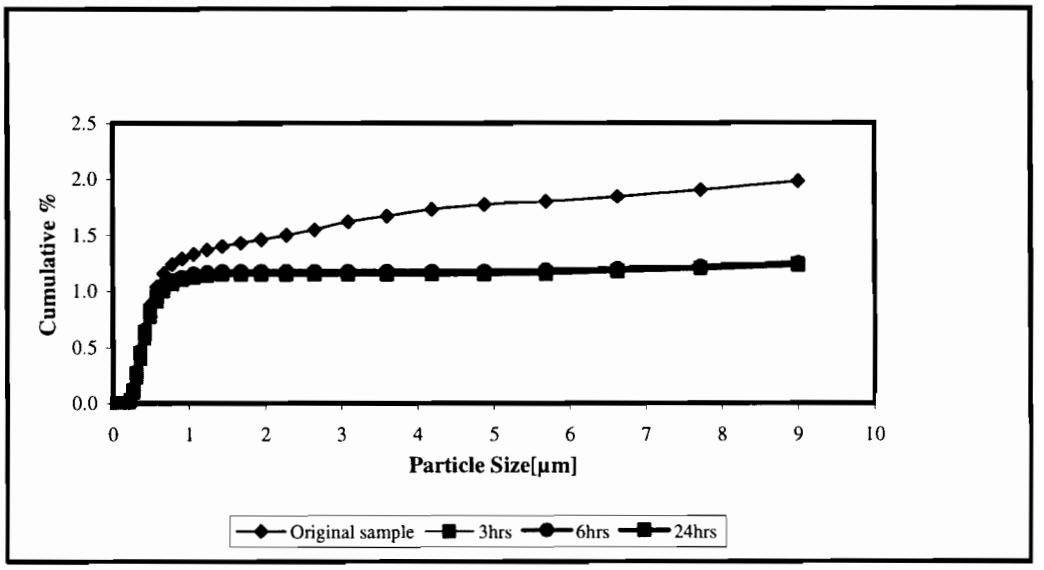

Figure 4-7: Abundance of ultrafines (<10μm) of the 0 hr, 3 hr, 6 hr, and 24 hr fluidised samples of the 90-106 μm particle size

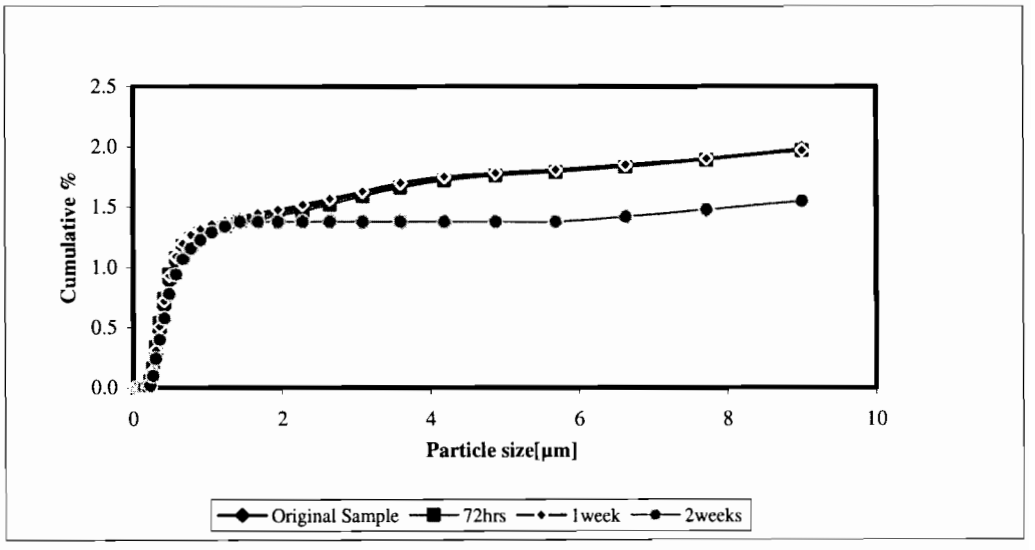

Figure 4-8: Particle size distribution (< 10 μm) of the 0 hr, 72 hr, 1 week and 2 week fluidised sample of the 90-106 μm particle size

It is of interest to note that, in the 90-106 µm sample, the amount of the particles under 10 µm (ultrafines) decreases in the first 24 hrs of fluidisation (Figure 4.7) and then increase in the 72 hrs to 1week fluidisation followed by a decrease after 2 weeks. Repeat experiments were not conducted to verify the reliability of the particle size data hence the overlap of the original and 1 week sample is viewed with.

4.3. Error Analysis

Whilst the obtained Cr(VI) abundance data does not present any evidence of the oxidation of residual chrome to Cr(VI), it is of concern that large variations were observed between repeat samples. Such variation is proposed to be as a result of the Cr(VI) analytical method and the sampling methods employed.

Tables 4.3 to 4.4 show the errors obtained in the repeat readings on samples. A repeat is when excess leachate of the same sample in question is analysed for Cr(VI) with a scheduled sample. The excess samples are stored in glass containers in the fridge immediately after analysis. This was done to check the consistency of the analytical method used in this study. Hence the samples near the end of a fluidisation run (48hrs, 72 hrs, Table 4.2; 24hrs, Table 4.3; 336 hrs, 408 hrs, Table 4.4) could only be repeated twice or otherwise once.

Table 4-3: Cr(VI) abundance variations between repeat samples of 38-63 µm size fraction.

Sample ID	38-63 µm	Cr(VI) Abundance [µg/g]						
Fluidisation Time	Original Sample	Repeat 1	Repeat 2	Repeat 3	Ave	Min	Max	Error (%)
0 hrs	3749	3769	3596	3753	3717	3596	3769	5
3 hrs	3918	4061	3661	3632	3818	3632	4061	11
6 hrs	3737	4061	3330	3342	3617	3330	4061	20
24 hrs	4287	3816	3880	n.d	3994	3816	4287	12
27 hrs	2590	2344	2550	n.d	2495	2344	2590	10
48 hrs	3476	3470	n.d	n.d	3473	3470	3476	0.2
72 hrs	565	728	n.d	n.d	646	565	728	25

Table 4-4: Cr(VI) abundance variations between repeat samples of 63-90µm size fraction

Sample ID	63-90 µm	Cr(VI) Abundance [µg/g]						
Fluidisation Time	Original Sample	Repeat 1	Repeat 2	Repeat 3	Ave	Min	Max	Error (%)
0 hrs	2248	3725	3117	n.d	3030	2248	3725	49
3 hrs	2369	2834	2462	n.d	2555	2369	2834	20
6 hrs	1742	1416	2084	n.d	1747	1416	2084	38
24 hrs	2490	2243	n.d	n.d	2367	1732	2117	16

Table 4-5: Cr(VI) abundance variations between repeat samples of 90-106μm size fraction

Sample ID	90-106 μm	Cr(VI) Abundance [μg/g]						
Fluidisation Time	Original Sample	Repeat 1	Repeat 2	Repeat 3	Ave	Min	Max	Error (%)
0hrs	1330	1156	1160	1287	1233	1156	1330	14
168 hrs	958	1155	1080	1254	1111	958	1254	27
216 hrs	1399	1211	1035	1380	1256	1035	1399	29
336 hrs	932	934	1103	n.d	990	932	1103	17
408 hrs	1114	1041	1330	n.d	1162	1041	1330	25

It can be observed that the Cr(VI) analytical method had large errors between repeat samples. However the changes in Cr(VI) abundance with fluidisation time can be clearly observed.

4.4. Ageing of Slag in Bench Tests

The results from the bench ageing tests of the different particle sizes of the ferrochrome slag are shown in Figures 4.9 to 4-11. An increase in Cr(VI) abundance is observed as the sample ages in contact with air.

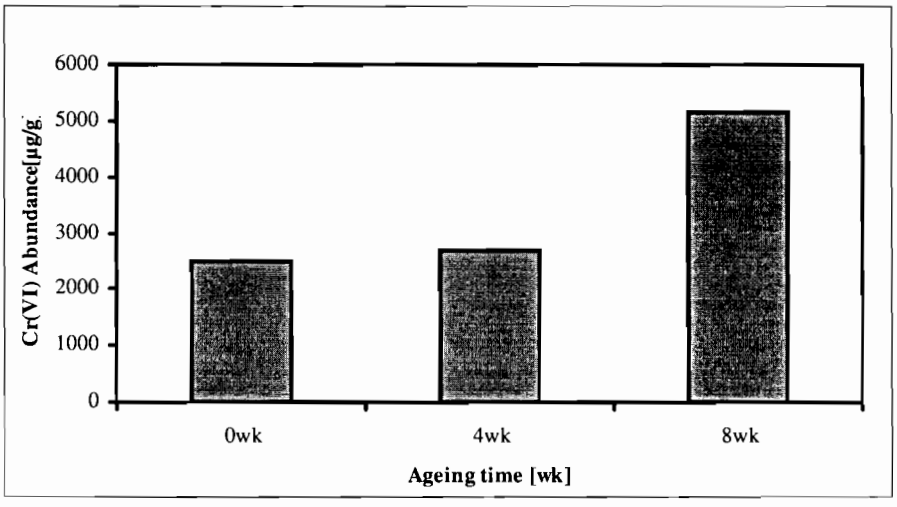

Figure 4-9: Cr(VI) abundance for a 38-63μm ferrochrome sample after 8 weeks ageing in an ambient atmosphere on laboratory benches

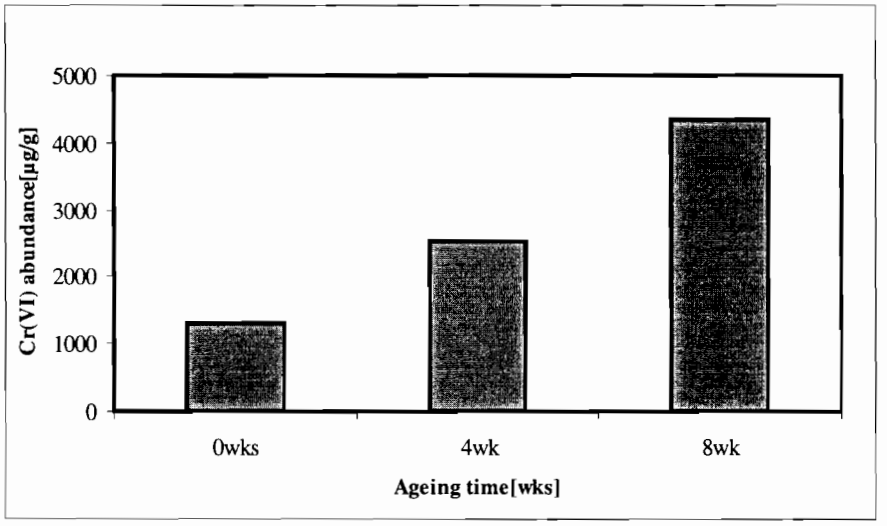

Figure 4-10: Cr(VI) abundance for a`63-90 µm ferrochrome sample after 8 weeks ageing in an ambient atmosphere on laboratory benches

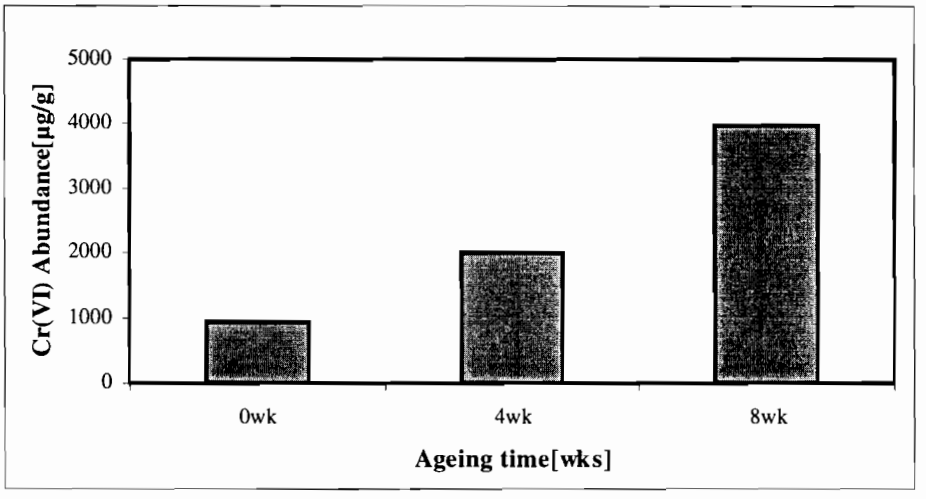

Figure 4-11: Cr(VI) abundance for a 90-106µm ferrochrome sample after 8 weeks ageing in an ambient atmosphere on laboratory benches

4.5. Effect of Microwaves on Slag*

This work was done to establish whether microwave irradiation of slag samples might have any oxidative ageing accelerating effects. The effects of microwaves were noted as overall temperature changes in the sample and changes in Cr(VI) concentration

compared to the control samples. The mineralogy of the slag used in this test was not determined except for Cr(VI) analysis of duplicate samples of the two particle sizes tested. The duplicate samples that were not irradiated were used as controls. Table 4.6 presents the results obtained from this exploratory work conducted on AOD slag of different particle sizes.

Table 4-6: Effect of microwave irradiation on Cr(VI) release and overall sample temperature

Sample ID	Particle size[μm]	Irradiation Time[sec]	Mass of sample[g]	T_1[°C]	T_2[°C]	ΔT[°C]	Abs [Å]	Cr(VI) [ppm]
2A	>425	300	60	18	30	12	0.533	1.03
2B	>425	900	60	18	30	12	0.592	1.14
3A	>4000	300	60	18	29	11	0.643	1.24
1a*	>425	n.d	n.d	n.d	n.d	n.d	0.601	1.16
1b*	>4000	n.d	n.d	n.d	n.d	n.d	0.615	1.18

*1a and 1b are control samples of 2A, 3A and 2B respectively.

It can be observed that exposing the slag to microwave irradiation for as long as 900 seconds increased the temperature of the slag by a magnitude of 12 °C with no evidence to suggest microwave influence on the amount of Cr(VI) leached from the slag. Changing the slag's particle size does not seem to have an effect on the slag's microwave coupling properties.

A growing body of data seems to suggest the possibility of microwave-enhanced solid-state diffusion in heterogeneous reactions in ceramics, glass and polymer materials. Freeman *et al.* (1995) observed an enhancement of an ionic driving force rather than intrinsic-vacancy mobility during microwave irradiation. A proposed reaction mechanism (Pillay *et al.*, 2003) for the oxidation of Cr(III) in slag suggests Cr^{3+} ion diffusion across the grain boundary: hence any microwaves-slag interactions that enhance solid-state transport are likely to affect the reaction kinetics. In majority cases, the microwave effect can be explained with thermal effects whilst other proposed effects remain speculative. The preliminary tests on slag did not produce significant temperature changes, suggesting little or no coupling between microwaves and slag.

4.6. Discussion

From Figure 4.2 it is observed that, fluidizing the 38-63μm and 90-63μm samples for up to 72 hours, resulted in a decrease of the Cr(VI) abundance with fluidising time. This is indicative of either a gradual loss (with fluidization time) of leachable Cr(VI) or oxidisable chromium.

The Cr(VI) abundance profile produced after fluidizing a coarse sample for 3 weeks (Figure 4.3) does not show any obvious relationship between fluidization time and the sample's Cr(VI) abundance, although there is a clear indication of very little or no generation of Cr(VI) as a result of the oxidation of the Cr_2O_3 phases.

Figures 4.6a and 4.6b (abundance of ultrafines in the 38-63 μm samples < 10 μm) indicate a decrease in ultrafines in the 6hr and 72hr samples compared to the 3 hr sample. As a result of the few samples taken during this run, the data does not provide a clear pattern of generation and or loss of ultrafines from the bed (although there is a notable decrease in ultrafines). Cr(VI) containing phases such as hydrogarnet are known to occur in COPR as small crystals of a magnitude in the order of 2 μm in diameter (Hillier *et al.,* 2003). Hence, a loss of fines from the bed could be synonymous with the loss of the Cr(VI) containing fraction.

In the repeat test conducted on the 90-106 μm size fractions, it is interesting to note that the quantity of ultrafines in the 3 hr, 6 hr and 24 hr samples decreased from between 1.5-2 % to between 1-1.5 % (Figure 4.7). The observed early decrease in fines (< 10 μm) concurs with evidence presented by Gravina and colleagues in 2004, however the decrease (Figure 4-6b) does not coincide with the observed decrease in leachable Cr(VI) in finer samples (see figure 4-2). According to Gravina *et al.* (2004), this could be due to attrition removing surface irregularities from fresh angular materials followed by particle-rounding-off resulting in a decrease in attrition. However, in the coarse samples analysed, the Cr(VI) enriched fines are not in large quantities such that a loss of ultrafines of such a magnitude would not significantly affect the amount leachable Cr(VI), hence the observed variations in ultrafines could be regarded as an instrument error.

About 10-15 %, and 6-8 % of solids in the 38-63 μm and 63-90 μm size ranges respectively are below 10 μm, compared to only about 2% in the 90-106 μm range hence a loss of fines from the 38-63μm and 63-90μm size ranges would significantly affect the quantities leachable Cr(VI).

Evidence by Pillay (2001), suggests that oxidation of Cr_2O_3 requires intimate contact with CaO. As was observed by Hellier and colleagues (2003), a significant part of fines is CaO; hence a loss of fines from the 38-63 μm and 63-90 μm size ranges would mean that the size fraction most prone to oxidation would be lost from the bed.

Microwave irradiation on slag produced no obvious increases of Cr(VI) in slag (Table 4.6) and showed no signs of significant coupling with slag. Evidence from literature mentions microwaves to improve leaching and dissolution of minerals. In this context it would be desirable for the microwaves to increase the average pore sizes within the slag particles subsequently reducing the internal diffusion limitations. However more work needs to be done and probably coupling microwave irradiation with fluidisation should be investigated.

From the data obtained in this study, it can be concluded that:

(i) The fluidisation of fine particle ranges resulted in a possible generation of ultrafines and their subsequent loss from the bed, thus making this test unreliable. Compounding to this problem was a wide particle size range in the finer size ranges tested: only 36 %(vol %) of the particles was within the defined size range.

(ii) The problem of elutriation of ultrafines can be managed by fluidising a coarser slag and using a narrowly 'cut' particle size range. However no oxidation was observed in up to 3 weeks of fluidisation with bone dry air and moist air whilst during bench ageing Cr(VI) abundance doubled in 4 weeks.

4.7. Concluding Notes

Although the data produced from this study did not show any evidence of rapid oxidation of residual Cr(III) in the tested slag, it has become clear that in further studies the fluidization of coarse particles should be considered in the light of the loss of fines from the bed. The method of introducing moisture to the fluidization medium, should be improved as Pillay *et al.* (2003) observed significant Cr(III) conversions in the presence of moisture.

CHAPTER FIVE

CONCLUSION

This dissertation set out to develop an accelerated laboratory test for determining whether residual trivalent chromium in slags generated in the metallurgical industry is prone to slow long-term oxidation.

The production of ferrochrome and stainless steel is a major source of chrome-containing slag as a waste product. Residual chrome in basic slags had been observed in previous research to slowly oxidise in the presence of oxygen in ambient atmosphere, producing the mobile and toxic Cr(VI) form. In landfill scenarios, the oxidation of residual Cr(III) can result in the subsequent leaching of Cr(VI) into underground waterways and surrounding areas posing an environmental hazard.

Pillay *et al.* (2003) observed 0.1-1% conversions of residual Cr(III) in ferrochrome slag to Cr(VI) in ambient atmosphere within a period of 6-9 months. The slow kinetics of the oxidation reaction in ambient atmosphere makes it difficult to ascertain, the long term stability (towards atmospheric oxidation) of fresh slag coming off the production line.

It is therefore important that a method that can accelerate the oxidation of residual Cr(III), (from observed periods of months to hours) in ambient atmosphere be developed to ascertain the stability of COPR towards atmospheric oxidation before disposal on landfills. Fluidised bed techniques were selected as a suitable way of enhancing gas-solid mass transfer, and it was also decided to carry out a preliminary study on the use of microwave radiation.

The following discussion revisits the objectives of this study as presented in the earlier chapters. The chapter also discusses the hypothesis and whether it has been validated in the study. Outcomes of the work, shortcomings and the broader implications of the study will be reviewed, and recommendations presented for future work on this topic.

5.1. Summary of Findings

This study was undertaken with the aim of achieving the following objectives:

1. Designing and constructing a laboratory scale fluidized bed reactor capable of fluidizing a selected particle size class and reproducing particular fluidization parameters to within expected error margins.

2. Determining whether this apparatus achieves the desired result of developing a rapid laboratory method that gives an indication of the environmental stability of slag towards oxidation before disposal. As fluidization enhances mass transfer, and as the atmospheric oxidation of residual chromium (III) is believed to be a diffusion controlled reaction, a fluidized bed was believed to be a suitable apparatus for enhancing the rate of oxidation.

3. Specifically accelerating the oxidation of residual Cr(III) in slag to Cr(VI) from the waiting time of weeks to months associated with bench ageing, to a matter of hours to days using fluidization techniques with dry and moist air at ambient temperatures.

The apparatus was successfully built from the design and was commissioned using an inert platinum slag. The apparatus posed no occupational safety hazards during its operation and the individual units (e.g. humidifier, dust filters, manometers) performed satisfactorily. Experimental values of the minimum fluidization velocity for the selected particle sizes were in close agreement with the values obtained using the Ergun equation. One weakness of the study was that the Cr(VI) detection method was disappointingly inaccurate in terms of repeatability (as already discussed in section 4.3). Despite this, the results obtained were robust enough to allow for some conclusions to be drawn with respect to chromium oxidation

It has been observed that ageing of slag in the fluidized bed with bone-dry air did not present obvious evidence of rapid oxidation of residual Cr(III) as expected. Fluidization of fine particle sizes (38-63μm, 63-90μm) resulted in the loss of ultrafines by elutriation, hence it can be concluded that, although the finer particle sizes are easy to fluidize and mostly likely to oxidize (as observed by Pillay *et al.*, 2003), the loss of ultrafines introduced uncertainties in the test method. Fluidizing coarser particle size samples in bone-dry air rectified the problem of sample loss but the generated Cr(VI) profile indicated that there was no detectable oxidation of Cr(III) in slag. Ageing the coarse slag in the fluidized bed reactor, with moist air (for up to two weeks) resulted in a mass increase in the bulk of the slag sample due to possible hydration of CaO to $Ca(OH)_2$ during fluidization. Despite the large error margins observed in the Cr(VI) values, the Cr(VI) abundance profiles did not provide evidence suggesting accelerated oxidation of residual Cr(III) during the two week fluidization

Irradiating selected slag samples of different particle sizes with microwaves did not result in a noticeable increase in the quantity of leached Cr(VI) to suggest any Cr(III) oxidation. The slight temperature increase in the irradiated slag suggested very little or no coupling of slag and microwaves. However the effects of microwaves need to be thoroughly investigated.

As observed in the bench ages, the Cr(III) in the slag in question does however oxidize in ambient atmosphere, as significant oxidation was observed after 8 weeks in bench tests. However contrary to the hypothesis, ageing slag in a fluidized bed reactor seems to only improve the external diffusion resistance of the bulk of the slag particles to mass transfer, which is normally limited in a landfill situation. However the internal diffusion limitations to the reactive phases within a particle cannot be addressed in this test thereby failing to accelerate the oxidation reaction.

Whilst the method failed to accelerate the oxidation of Cr(III) in the slag, the results of the bench ageing tests emphasize the need for further investigations into accelerated laboratory methods. Section 5.2 provides recommendations for further work.

5.2. Recommendations

Based on the conclusions of the investigation, the following recommendations are made for further research:

1) Further work on the oxidative ageing of chromium-containing slags needs to start from considerations of overcoming the internal rather than external diffusion resistances.
2) It is also recommended that an oxygen enriched medium be used as a oxidizing medium. This will increase the overall oxygen partial pressure and hence provide a steeper oxygen concentration gradient.
3) Although the exploratory work with microwaves did not establish any effect of microwaves, suggestions by Freeman *et al.* (1998) of possible microwave-excited ionic currents resulting in 'solid state ionic mass transfers' across grain boundaries should be further investigated as a way to possibly accelerate the solid-state diffusion of the Cr^{3+} ions across grain boundaries as proposed by Pillay *et al.*, (2003) in the reaction mechanism of the oxidation of residual Cr(III) in slag.
4) The effects of subjecting slag, in its fluidized state to microwave irradiation should be investigated. Since the fluidization will eliminate the gas-solid diffusion resistances, the only probable rate limiting step would then be the proposed ionic diffusion of Cr^{3+} ion across the grain boundaries and the formed product layer. It is therefore apparent that a new rig design that includes a microwave source, probably designed in the form of a jacket around

5) The cause of the large errors observed on the Cr(VI) analytical method and possible Cr(VI) leachate pretreatment (to eliminate possible interferences) should be investigated.

The following recommendation is made concerning industrial practices:
Whilst there is not yet an accelerated laboratory ageing test, it is recommended that the ferrochrome and stainless steel industry should avoid possible formation of $CaO \cdot Cr_2O_3$ phases (which are known to be susceptible to oxidative atmospheric ageing leading to Cr(VI) formation) by careful control of CaO/SiO_2 ratios during smelting.

REFERENCES

Allison, J.D., Brown, D.S., Novo-Gradac, S.L., (1991) "A geochemical assessment model for environmental systems version 3.0, Georgia, Athens

Al-Harahsheh, M. and Kingman, S.W. (2004), "Microwave-assisted leaching- a review", *Hydrometallurgy,* vol 73, pp 189-203

Apte, A.D., Verma, S., Tare, V. and Bose, P. (2005), "Oxidation of Cr(III) in tannery sludge to Cr(VI): Field observations and theoretical assessment", *Journal of Hazardous Materials* B121, pp. 215 - 222

Bab, M.A. and Mendoza-Zelis, L. (2004), "A model for kinetics of mechanically assisted gas-solid reactions", *Scripta Materialia*, no. 50, pp. 99-104

Bade, S., Hoffmann, U., Schonert, K. (1996), "Mechano-chemical Reaction of Metallurgical Grade Silicon with gaseous hydrogen chloride in a vibration mill", *Int. J. Miner. Process*, vol. 44-45, pp. 167-179

Bartie, N., Eksteen, J., Jahanshahi, S. and Sun, S. (2003), "The effect of Temperature, Oxygen Potential and Slag Chemistry on the Stability of Chromium Spinels in Melter Slags in the Base Metals Industry", *XXII International Mineral Processing Congress*, pp. 1364-1369

Bartlett, R.J., James, B.R. (1988), 'Mobility and Bioavailability of Chromium in Soils', *Chromium in the Human and Natural Environment*, pp. 267-299

Bartlett, R.J and Kimble, J.M. (1976), "Behavior of Chromium in Soils: I. Trivalent Forms", *J. Environ. Qual*, 5, pp.379-382

Bartlett, R.J and Kimble, J.M. (1976), "Behavior of Chromium in Soils: II. Trivalent Forms", *J. Environ. Qual*, 5, pp.383-386

Berlan, J. (1995), "Microwaves in chemistry: Another way of heating reaction mixtures", *Radiat. Phys. Chem*, vol. 45, no. 4, pp. 581-589

Bhattacharya, A.K., Bandopadhyay, P. and Das, P. (2003), "Oxidation reaction in graphite-role of particle characteristics", *Ceramics International*, vol. 29, pp. 967-969

Bodas, M.G., Dash, D.R. and Sivaramakrishnan, C.S. (1996), "Oxidation of Iron Powder In a Fluidized Bed Reactor", *Material and Design*, vol. 17, no. 3, pp. 167-172

kinetics in ceramics", *Mat Res Innovat,* vol 1 pp 77-84

Calder, L.M., (1998), "Chromium Contamination in Ground Water, In. Nriagu J. (Ed.) *Chromium in the Human and Natural Environment",* pp.215-229, New York, John Wiley and Sons

Deltombe, E., De Zoubov, N. and Pourbaix, M. (1966), "Atlas of Electrochemical Equilibria", (pp. 256-271). Oxford Pergamon Press

Drew, D., Izuchukwu, S.I. and Tucker, P. (1992); 'Chromium Toxicity', From *http://www.atsdr.cdc.gov/HEC/CSEM/chromium/index.html*

Erdem, M. and Tumen, F. (2004), "Chromium removal from aqueous solution by ferrite process", *Journal Of Hazardous Materials*, no. B109, pp. 71-77

Farmer J G., Paterson E., Bewley, R.J.F., Geelhoed, J. S., Hillier, S., Meeussen, J. C. L., Lumsdon, D. G., Thomas, R. P. and Graham, M. C. (2006), "The implications of integrated assessment and modeling studies for the future remediation of chromite ore processing residue disposal sites", *Science of the Total Environment*, no. 360, pp. 90-97

Fini, A. and Breccia, A. (1999), "Chemistry by Microwaves", *Pure Appl. Chem*, vol. 71, no. 4, pp. 573-579

Freeman, S.A., Booske, J.H. and Cooper, R.F. (1998), "Modeling and numerical simulations of microwave-induced ionic transport", *Journal of Applied Physics*, vol. 83, no. 11, pp. 5761-5771

Gaunthier, D., Zerguerras, S. and Flamant G. (1999), "Influence of the particle size distribution of powders on the velocities of minimum and complete fluidization", *Chemical Engineering Journal,* vol 74 pp181-196

Geelhoed, J.S., Meeussen, J.C.L., Hillier, S., Lumsdon, D.G., Thomas, R. P., Farmer, J.G. and Paterson, E. (2002), "Identification and geochemical modeling of processes controlling leaching of Cr(VI) and other major elements from chromite ore processing residue", *Geochimica et Cosmochimica Acta*, vol. 66, no. 22, pp. 3927-3942

Gravina, T., Lirer, L., Marzocchella, A., Petrosino, P. and Salatino, P. (2004) "Fluidization and attrition of pyroclastic granular solids", *Journal of Volcanology and Geothermal Research,* Vol 138, 27-42

Hillier, S., Roe, M. J., Geelhoed, J. S., Fraser, A. R., Farmer, J. G., and Paterson, E. (2003), "Role of quantitative mineralogical analysis in the investigation of site contaminated by chromite ore processing residue", *Science of the Total Environment*, vol. 308, no. 308, pp. 195-210

Thermodynamics of $FeO.Cr_2O_3$-$MgO.Cr_2O_3$-$MgO.Al_2O_3$ Spinel Structure Solid Solution Saturated with $(Cr,Al)_2O_3$", *ISIJ International,* Vol. 35, no 7, pp 851-858

Holappa, L. and Xiao Y. (2004), "Slags in ferroalloys production- review of present knowledge", *The South African Institute of Mining and Metallurgy Conference: VII International Conference of Molten Slag Fluxes and Salts (25-28 January 2004)*

James, B.R. and Bartlett, R.J. (1983b) "Behavior of Chromium in Soils: VII: Interactions Between Oxidation-Reduction and Organic Complexation", *J. Environ.Qual.,*12, pp.173-176

Jones, J.A.T. (2005), "Electric Arc Furnace Steel Making", *ww.steel.org/learning/howmade/eaf.htm.*

Jones, R.T. (1999) "Platinum Smelting in South Africa", *South African Journal of Science,* 95

Kunii, D and Levenspiel, O. (1991) "Fluidisation" *Chem. Eng. Scie.* Pp 69-180

Karthikeyan, T., Rajgopal, S. and Lima, R.M. (2005), "Chromium (VI) adsorption from aqueous solution by Hevea Brasilinesis saw dust activated carbon", *Journal Of Hazardous Materials* B124 pp 192-199

Kilau, H.W., and Shah, I.D. (1984), "Chromium-Bearing Waste Slag: Evaluation Of Leachability when Exposed to Simulated Acid Precipitation", *Hazardous and Industrial Waste Management and Testing: Third Symposium,* Philadelphia, ASTM STP, 851. Jackson, L.P., Rohlik A.R (Eds), pp. 61-81

Lee, Y. and Nassaralla C.L. (1998), "Formation of Hexavalent Chromium by reaction between Slag and Magnesite-Chrome Refractory," *Metallurgical and Materials Transactions B*, vol. 29B, pp. 405-410

Lind, B. B., Fallman, A.-M. and Larson, L. B. (2001), "Environmental impact of ferrochrome slag in road construction", *Waste Management*, vol 21 pp 255-264

Luo, Z., Zhao, Y., Chen, Q., Tao, X. and Fan, M. (2004), "Effect of gas distributor on performance of dense phase high density fluidized bed for separation," *Int. J. Miner. Process*, vol. 74, pp. 337-341

Makino, T., Kamewada, K., Hatta, T., Takahashi, Y. and Sakurai, Y. (1998), "Determination of Optimal Chromium Oxidation Conditions and Evaluation of Soil Oxidative Activity in Soils", *Journal of Geochemical Exploration*, vol. 64, pp. 435-441

Marmo, L., Rovero, G. and Baldi G. (1999), "Modeling of Catalytic Gas-Solid Fluidized Bed Reactors", *Catalysis Today*, vol 52, pp 235-247

Motz, H. and Geiseler, J. (2001) "Products of steel slags an opportunity to save natural resources" *Waste Management* vol 21, pp 285-293

Nell, J. (2004), "Melting of Platinum Group Metal Concentrates in South Africa", *The South African Institute Of Mining and Metallurgy,* SA ISSN 0038-223X/3.0+0.00.

Palmer, C. D. and Puls, R. W. (1994), "Natural attenuation of hexavalent chromium in groundwater and soils" *EPA Ground Water Issue*, EPA/540/5-94/505

Petersen, J., Petrie, J.G. (2000), "Modelling and assessment of the long-term leachate generation potential in deposits of ferro-chromium slags" *The Journal of The South African Institute of Mining and Metallurgy*. SA ISSN 0038-223X/3.00+0.00

Petersen, J. (1998), "Assessment and Modeling of Chromium Release in Minerals Processing Waste Deposits," PhD Thesis, University Of Cape Town

Pillay, K. (2001), "A Kinetic and Mechanistic Study on The Oxidation of Chromium Oxide in Pure Chemicals and In Ferro metallurgical Slags," Masters Thesis, University of Cape Town

Pillay, K., Von Blottnitz, H. and Petersen, J. (2003), 'Ageing of Chromium(III)-bearing Slag and its Relation to The Atmospheric Oxidation Of Solid chromium(III)-Oxide in the Presence of Calcium Oxide', *Chemosphere*, vol. 52, pp. 1771-1779

Pretorius E B., and Nunnington, R. C. (2000), "Stainless Steel Slag Fundamentals- From furnace to Tundish", *Sixth International Conference on Molten Slags, Fluxes and Salts-Topics/Contents, Paper126,* http: www.print.kth.se/slags/SLAGS/CONTENTS.htm (14 February 2001)

Pretorius E.B., Snellgrove, R. and Maun, A. (1992), "Oxidation State of Chromium in CaO-Al2O3-CrOx-SiO2 Melts under Strongly Reducing Conditions at 1500oC", *Journal of American Ceramic Society*, vol. 6, no. 75, pp. 1378-1381

Proctor, D.M., Fehling, K.A., Shay, E.C., Witterborn, J.L., Green, J.J., Avent, C., Bigham, R.D., Connolly, M., Lee, B., Shepker, T.O., and Zak, M.A. (2000), "Physical and Chemical Characteristics of Blast Furnace, Basic Oxygen Furnace, and Electric Arc Furnace Steel Industry Slags", *Environ. Sci. Technol.* 34, pp1576-1582

Raner, K.D., Strauss, R.C., Vyskoc, F. and Mokbel, L. (1993), "A Comparison of Reaction Kinetics Observed under Microwave Irradiation and Conventional Heating", *Journal of Organic Chemistry*, vol. 58, pp. 950-953

Rai, D., Sass, B.M. and Moore, D.A (1987), "Chromium(III) hydrolysis constants and solubility of Chromium(III) hydroxide", *Inorg.Chem.* Vol 26, pp 345

Rao, K.J., Ramakrishnan, P.A. and Gadagkar, R. (1999), "Microwave Preparation of Oxide Bronzes", *Journal of Solid State Chemistry*, vol. 148, pp. 100-107

Reina, J., Velo, E. and Puigjaner, L. (2000), "Predicting the minimum fluidization velocity of polydisperse mixtures of scrap-wood particles", *Powder Technology*, 111 pp 245-251

Richard, F.C and Bourg, A.C.M. (1991), "Aqueous Geochemistry of Chromium: A Review", Water Reserves, 25 pp. 807-816

Ruud van Ommen, J., John van der Schaaf., Schouten, J.C., Van Wachen, b.G.M., Coppens, M.-O. and van den Bleek, C. M. "Optimal placement of probes for dynamic pressure measurements in large-scale fluidized beds", *Powder Technology,* vol 139 pp 264-276

Rybakov, K.I., Semenov, V.E., Freeman, S.A., Booske, J.H and Cooper, R.F. (1997), "Dynamics of microwave-induced currents in ionic crystals", *The American Physical Society"* Vol 55, no 6 pp 3559-3567

Sathiyamoorthy, D. and Horio, M. (2003), "On the influence of aspect ratio and distributor in gas fluidized beds", *Chemical Engineering Journal*, vol. 93, pp. 151-161

Schroeder, D.C. and Lee, G.F. (1975), "Potential transformations of chromium in natural waters", *Water, Air and Soil Pollution,* vol 4, pp 355-365

Shen, H., Forssberg, E. and Nordstrom, U. (2004), "Physicochemical and mineralogical properties of stainless steel slags oriented to metal recovery", *Resources, Conservation and Recycling,* vol40, pp 245-271

Takahashi, T., and Yabuta K. (2002) "New Applications for Iron and Steelmaking Slag", *NKK Technical Review,* No.87, pp 38-44

Van Ommen, R.J., De Korte R-J. and Van den Bleek C. M. (2004), "Rapid detection of defluidization using the standard deviation of pressure fluctuations", *Chemical Engineering and Processing*, vol. 43, pp. 1329-1335.

Wang, H., Dlugogorski, B.Z. and Kennedy, E.M. (2003), "Coal oxidation at Low Temperatures: Oxygen consumption, Oxidation Products, Reaction Mechanism and Kinetic Modeling", *Progress in Energy and Combustion science*, vol. 29, pp. 487-513

Werther. J. (1999) "Measurement techniques in fluidized beds", *Powder Technology,* vol 102 pp 15-36

Xiao, Y. and Holappa, L. (1993), "Determination of Activities in Slags Containing Chromium Oxides", *ISIJ International*, vol. 33, no. 1, pp. 66-74

Yoon B.-H., Heo K.H. and Sohn H-S. (2002), "Improvement of steel cleanliness by controlling slag composition", *Iron and Steelmaking*, vol. 29, no. 3, pp. 215 – 218

Ziemkiewiez, P. (1998), "Steel Slag: Applications for AMD control", *Proceedings of the 1998 Conference on Hazardous Waste Research*, pp 44- 62

OVERVIEW OF APPENDICES

Appendix A: Cr(VI) calculations, minimum fluidization data, AA and XRF data

Appendix A1: Cr(VI) calculations from absorbance readings
Appendix A2: Data used to determine the minimum fluidisation velocity for the 63-90 μm samples
Appendix A3: Data used to determine the minimum fluidisation velocity for the 38-63 μm samples
Appendix A4: Calculations to determine the minimum fluidization velocity
Appendix A5: Estimating the volumetric flow rate of moist air through the bed
Appendix A6: Cr(VI) abundance calculations
Appendix A7: Cr(VI) abundance data for 38-63 μm samples after fluidisation
Appendix A8: Cr(VI) abundance data for 63-90 μm samples after fluidisation
Appendix A9: Cr(VI) abundance data for 90-63 μm samples after fluidisation
Appendix A10: Cr(VI) abundance data for 90-160 μm samples after fluidisation with moisture
Appendix A11: XRF results for UG-2 slag
Appendix A12: XRF results for LCFeCr slag (milled)
Appendix A13: AA results for LCFeCr slag for milled and original sample
Appendix A14: Weight changes during fluidization with moist air for the 90-106 μm particle size

Appendix B: Particle Size Distribution Analysis Data

Appendix B1: Particle size distribution for 90-106 μm samples fluidised for up to 24 hrs
Appendix B2: Particle size distribution for 90-106 μm samples fluidised for up to 2 weeks
Appendix B3: Particle size distribution for 38-63 μm samples fluidised for up to 72 hrs
Appendix B4: Particle size distribution for38-63 μm, 63-90 μm and 90-106 μm original samples.

Appendix C: Density Measurements Data

Appendix C1 Density measurements for 38-63 μm, 63-90 μm and 90-106 μm LCFeCr milled samples
Appendix C2 Density measurements for 38-63 μm, 63-90 μm UG2 milled samples

Appendix D: XRPD Patterns for LCFeCr Sample

Appendix D1 XRPD patterns for LeCFeCr original sample

A1. Cr(VI) CALCULATIONS FROM ABSORBANCE READINGS

TABLE: 1 Absorbance readings for standards

Cr(VI) [ppm]	Absorbance
0.05	0.008
0.1	0.026
0.2	0.064
0.4	0.132
1	0.337
2	0.624

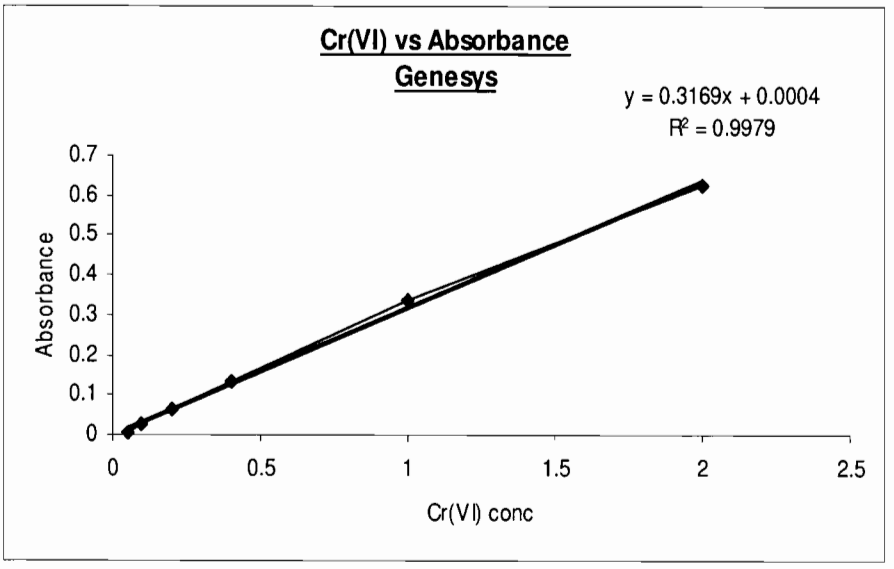

FIGURE: 1 Standards Calibration graph

From the calibration equation $Y = 0.3169x + 0.0004$ the y-intercept is 0.004 and the slope is 0.3169

TABLE 2: LEACHED SAMPLES

Sample ID	Absorbance	Cr(VI)[ppm]
0hrs	0.648	2.04
3hrs	0.685	2.16
6hrs	0.600	1.89

$X = \left(\frac{y - 0.0004}{0.3169} \right)$ where X is the Cr(VI) concentration and Y is absorbance. For example, the 0hr sample:

$$\text{Cr(VI)} = \left(\frac{0.648 - 0.0004}{0.3169} \right)$$

$$= 2.04\text{ppm}$$

The values of Y-intercept vary with the calibration standards.

A2. DATA USED TO DETERMINE THE MINIMUM FLUIDISATION VELOCITY FOR THE 63-90μm SAMPLE

Rotameter Reading	h_1	h_2	Δh [mmHg]	Δp [pa]	Air flow [L/min]
1	15.3	18.7	3.4	467	12
2	14.9	19.1	4.2	560	15
3	14.5	19.5	5.0	667	18
4	14.0	20.0	6.0	800	20
5	13.5	20.5	7.0	933	24
6	13.0	21.0	8.0	1067	26
7	12.5	21.5	9.0	1200	30
8	12.0	22.0	10.0	1333	33
9	11.5	22.5	11.0	1460	35
9.2	12.0	22.0	10.0	1333	36
9.4	12.0	22.0	10.0	1333	37
9.6	11.9	22.0	10.1	1347	37
9.8	11.9	22.1	10.2	1360	38
10	11.5	22.5	11.0	1467	39

Bed cross-sectional area $=133cm^2$

A3. DATA USED TO DETERMINE THE MINIMUM FLUIDISATION VELOCITY FOR THE 38-63μm SAMPLE

Rotameter Reading	h_1	h_2	Δh [mmHg]	Δp [pa]	Air flow [L/min]
1	15.2	18.8	3.6	480	12
2	14.9	19.1	4.2	560	15
3	14.4	19.6	5.2	693	18
4	13.8	20.2	6.4	853	20
4.1	13.8	20.2	6.4	853	20.5
4.2	13.7	20.3	6.6	880	20.8
4.4	13.6	20.4	6.8	907	21.4
4.6	13.5	20.5	7.0	933	21.9
4.8	13.4	20.7	7.3	973	22.5

Bed cross-sectional area $=133cm^2$

A4. CALCULATIONS TO DETERMINE THE MINIMUM FLUIDISATION VELOCITY

The calculations were done using Ergun equation in combination with Reynold's equation and Galileo number.

$$\frac{\Delta P}{L} = \frac{150(1-\varepsilon)\mu U}{\varepsilon^3(\phi d_p)^2} + \frac{1.75(1-\varepsilon)\rho_g U^2}{\varepsilon^3 \phi d_p} \quad 1$$

$$\mathrm{Re_{mf}} = \sqrt{33.7^2 + 0.0408Ga} - 33.7 \quad 2$$

$$\mathrm{Re_{mf}} = \frac{d_p U_{mf} \rho_g}{\mu} \quad 3$$

$$\mathrm{Ga} = \frac{d^3{}_p g \rho_g (\rho_p - \rho_g)}{\mu^3} \quad 4$$

Equating equations 2 and 3

$$\frac{d_p U_{mf} \rho_g}{\mu} = \sqrt{33.7^2 + 0.0408Ga} - 33.7 \text{ and substituting for Ga}$$

$$\frac{d_p U_{mf} \rho_g}{\mu} = \sqrt{33.7^2 + 0.0408 d^3{}_p g \rho_g \left(\frac{d_p{}^3 g \rho_g (\rho_p - \rho_g)}{\mu^3} \right)} - 33.7$$

Minimum fluidization velocity for 38-63µm size fraction

d_p = Diameter of slag [cm] = $\left(\frac{0.0063 + 0.0038}{2} \right) = 0.0051\text{cm}$

ρ_s = density of slag [g/cm^3] = 2.9211g/cm^3

ρ_g = density of air [g/cm^3] = 0.0012g/cm^3

μ_{air} = viscosity of air [g/cm.s] = 0.00018g/cm.s

$g_{freefall}$ = acceleration due to gravity [cm/s^2] = 980cm/s^2

$$U_{mf} = \frac{0.0018}{0.0051 \times 0.0012} \left[\left(33.7^2 + 0.0408 \frac{(0.0051)^3 (0.0012)(2.8988)(980)}{(0.00018)^2} \right)^{\frac{1}{2}} - 33.7 \right]$$

U_{mf} = 294.12×0.0084

Experimental value read off the graph of Pressure Vs Air velocity

Tube reading = 4cm
Graphical reading = 20L/min
= $333cm^3/s$
Area of fluidized bed = πr^2
= $\pi(6.5)^2 = 132.7cm^2$
Superficial gas velocity = $\frac{333cm^3}{s} \times \frac{1}{132.7cm^2} = \underline{\underline{2.5cm/s}}$

Minimum fluidisation velocity for 63-90μm size fraction

$d_p \approx$ Diameter of slag [cm] $= \left(\frac{0.009 + 0.0063}{2}\right) = 0.0077cm$

ρ_s = density of slag [g/cm^3] = 2.9211g/cm^3

ρ_g = density of air [g/cm^3] = 0.0012g/cm^3

μ_{air} = viscosity of air [g/cm.s] = 0.00018g/cm.s

$g_{freefall}$ = acceleration due to gravity [cm/s^2] = 980cm/s^2

$$U_{mf} = \frac{0.0018}{0.007 \times 0.0012}\left[\left(33.7^2 + 0.0408\frac{(0.0077)^3(0.0012)(2.9188)(980)}{(0.00018)^2}\right)^{\frac{1}{2}} - 33.7\right]$$

$U_{mf} = 194.805 \times 0.02927$

$U_{mf} = \underline{\underline{5.70cm/s}}$

Experimental value read off the graph of Pressure drop Vs Air velocity

Tube reading = 9cm
Graphical reading = 36L/min
= $600cm^3/sec$
Area of fluidized bed = πr^2
= $\pi(6.5)^2 = 132.7cm^2$
Superficial gas velocity= $\frac{600cm^3}{s} \times \frac{1}{132.7cm^2} = \underline{\underline{4.51cm/s}}$

A5. ESTIMATING THE VOLUMETRIC FLOW RATE OF MOIST AIR THROUGH THE BED

Humidifier ID		6.5cm
Height of water eluted daily		15cm
Volume of water eluted daily		$\Pi \times \left(\frac{6.5}{2}\right)^2 \times 15$
	=	$498cm^3$ of water per day
Air Flow rate	=	$52m^3$/day
Water Eluted	=	$\frac{0.000498}{52}$
	=	$10 \times 10^{-6} m^3 H_2O / m^3 Air / day$

A6. Cr (VI) ABUNDANCE CALCULATIONS

These calculations show how the Cr(VI) abundance figure were arrived at after leaching a certain mass of sample and getting the absorbance readings.

For example;
When a 10.15g sample from a 38-63µm size of total chrome content of 1.06% was leached with 200ml of 1M NaOH the average absorbance was 0.693Å which extrapolated to 2.02ppm

Cr(VI) leached = 2.02ppm = 2020µg/L

⇒ 1000ml	= 2020 µg
200ml	= 404 µg
% Cr prior to leaching	=1.06%
Mass of sample	=10.15g
Mass of Cr in the sample	$=(1.06\% \times 10.15g) = 0.1076g$
Conversion	$=\left(\frac{`404\mu g}{0.1076g}\right)$ = 3754µg/g

A7. Cr (VI) ABUNDANCE DATA FOR 38-63µm SAMPLES AFTER FLUIDISATION

Mass [g]	Date Leached	Date Analyzed	Fluidization Time[hrs]	Abs 1	Abs 2	Cr(VI) 1 [ppm]	Cr(VI) 2 [ppm]	Cr(VI) Abundance [µg/g]
10.15	5 Oct	6 Oct	0	0.648	0.630	2.04	1.99	3749
	5 Oct	7 Oct	0	0.664	0.636	2.07	1.98	3769
	5 Oct	10 Oct	0	0.614	0.615	1.95	1.91	3596
	5 Oct	10 Oct	0	0.633	0.651	2.01	2.02	3753
10.22	5-Oct	6 Oct	3	0.685	0.660	2.16	2.08	3918
	5 Oct	7 Oct	3	0.716	0.709	2.24	2.21	4061
	5 Oct	10 Oct	3	0.625	0.635	1.99	1.98	3661
	5 Oct	10 Oct	3	0.622	0.629	1.98	1.96	3632
10.12	5-Oct	6 Oct	6	0.600	0.670	1.89	2.12	3737
	5 Oct	7 Oct	6	0.700	0.696	2.19	2.17	4061
	5 Oct	10 Oct	6	0.562	0.573	1.79	1.78	3661
	5 Oct	10 Oct	6	0.566	0.574	1.80	1.79	3632
10.22	6 Oct	7 Oct	24	0.744	0.744	2.32	2.32	4287
	6 Oct	10 Oct	24	0.653	0.660	2.08	2.06	3816
	6 Oct	10 Oct	24	0.683	0.653	2.17	2.03	3880
10.12	6-Oct	7 Oct	27	0.451	0.441	1.37	1.41	2590
	6 Oct	10 Oct	27	0.397	0.402	1.25	1.26	2344
	6 Oct	10 Oct	27	0.439	0.431	1.34	1.40	2550
10.56	7 Oct	10 Oct	48	0.610	0.626	1.94	1.95	3476
	7 Oct	10 Oct		0.615	0.620	1.96	1.93	3470
10.28	8 Oct	10-Oct	72	0.101	0.095	0.32	0.29	565
	8 Oct	10-Oct		0.127	0.126	0.40	0.39	728

A8. Cr (VI) ABUNDANCE DATA FOR 63-90µm SAMPLES AFTER FLUIDISATION

Mass	Date Leached	Date Analyzed	Fluidization Time	Abs	Cr(VI) [ppm]	Cr(VI) Abundance [µg/g]
10.03	26 Sep	27 Sep	0	0.378	1.16	2248
	26 Sep	28-Sep	0	0.567	1.92	3725
	26 Sep	30-Sep	0	0.539	1.61	3117
10.19	26 Sep	27 Sep	3	0.405	1.24	2369
	26 Sep	28-Sep	3	0.439	1.49	2834
	26 Sep	30-Sep	3	0.433	1.29	2462
10.15	26 Sep	27 Sep	6	0.297	0.91	1742
	26 Sep	28-Sep	6	0.220	0.74	1416
	26 Sep	30-Sep	6	0.366	1.09	2084
10.08	27 Sep	28-Sep	24	0.382	1.29	2490
	27 Sep	30-Sep	24	0.391	1.16	2243
10.10	29 Sep	30-Sep	48	0.421	1.26	1862
10.06	30 Sep	30- Sep	72	0.022	0.06	89

A9. Cr(VI) ABUNDANCE DATA FOR 90-106μm SAMPLES AFTER FLUIDISATION

Mass	Date Leached	Date Analysed	Fluidization Time[hrs]	Abs 1	Abs 2	Cr(VI) 1 [ppm]	Cr(VI) 2 [ppm]	Cr(VI) Abundance [μg/g]
10.01	28 Oct	4 Nov	84	0.238	0.240	0.756	0.762	1330
	28 Oct	11 Nov	84	0.222	0.212	0.674	0.644	1156
	28 Oct	15 Nov	84	0.222	0.219	0.666	0.657	1160
	17 Nov	18 Nov	84	0.228	0.238	0.744	0.725	1287
10.15	31 Oct	04 Nov	168	0.171	0.176	0.546	0.562	958
	31 Oct	11 Nov	168	0.222	0.218	0.674	0.662	1155
	31 Oct	15 Nov	168	0.207	0.192	0.622	0.628	1080
	31 Oct	18 Nov	168	0.230	0.226	0.731	0.719	1254
10.03	2 Nov	4 Nov	216	0.252	0.252	0.800	0.800	1399
	2 Nov	11 Nov	216	0.222	0.234	0.674	0.710	1211
	2 Nov	15 Nov	216	0.202	0.192	0.607	0.577	1035
	2 Nov	15 Nov	216	0.247	0.250	0.784	0.793	1380
10.06	7 Nov	11 Nov	336	0.170	0.184	0.519	0.561	932
	7 Nov	15 Nov	336	0.182	0.178	0.377	0.398	934
	7 Nov	15 Nov	336	0.198	0.202	0.632	0.645	1103
10.02	10 Nov	11 Nov	408	0.215	0.208	0.653	0.632	1114
	10 Nov	15 Nov	408	0.201	0.199	0.604	0.598	1041
	10 Nov	15 Nov	408	0.243	0.240	0.772	0.762	1330
10.04	14 Nov	15 Nov	504	0.125	0.132	0.377	0.398	671
	14 Nov	15 Nov	504	0.142	0.144	0.459	0.465	799
	17 Nov	18 Nov	576	0.232	0.238	0.738	0.756	1289

A10. Cr(VI) ABUNDANCE DATA FOR 90-106 µm SAMPLES AFTER FLUIDIZATION WITH MOIST AIR

Mass	Date Leached	Date Analysed	Fluidization Time[hrs]	Abs [HCl]	Abs [H_2SO_4]	Cr(VI) [HCl] [ppm]	Cr(VI) [H_2SO_4] [ppm]	Cr(VI) Abundance [H_2SO_4] [µg/g]	Cr(VI) Abundance [HCl] [µg/g]
10.19	24 Aug	6 Sept	0	0.301	0.210	0.901	0.634	0.634	1717
	24 Aug	29 Aug	0	0.210	0.257	0.630	0.769	0.769	1200
	24 Aug	25 Aug	0	0.300	0.242	0.905	0.737	0.737	1723
10.16	24-Aug	6-Sep	24	0.212	0.246	0.640	0.740	1224	1414
	28-Aug	29-Aug	24	0.175	0.199	0.526	0.597	1005	1141
	24-Aug	25-Aug	24	0.194	0.135	0.598	0.427	1142	816
10.02	24-Aug	6-Sep	72hrs	0.172	0.084	0.523	0.265	1013	513
	24-Aug	29-Aug	72hrs	0.121	0.181	0.366	0.544	709	1054
	24-Aug	25-Aug	72hrs	0.300	0.242	0.905	0.737	1723	1404
10.43	28-Aug	6-Sep	1 week	0.080	0.071	0.253	0.227	472	423
	28-Aug	29-Aug	1 week	0.077	0.063	0.236	0.194	439	362
	5-Sep	6-Sep	2week	0.210	0.155	0.634	0.473	1228	916

A11. XRF RESULTS FOR UG-2 SLAG

Cr_2O_3	Fe_2O_3	Fe_3O_4	MgO	CaO	Al_2O_3	SiO_2
1.0%	18.3%	17.7%	13.2%	4.4%	1.7%	31.9%

A12. XRF RESULTS FOR LCFeCr SLAG (MILLED SAMPLE)

Cr_2O_3	Fe_2O_3	Fe_3O_4	MgO	CaO	Al_2O_3
2.11%	0.18%	0.17%	4.83%	30.9%	8.80%

A13. AA RESULTS FOR LCFeCr SLAG (MILLED SAMPLES)

		Cr tot	Fe	Al	Mg	Ca
Sample ID	Sample Mass	Mass%	Mass%	Mass%	Mass%	Mass%
90-106µm	0.103	1.14	0.369	13.9	10.2	32.1
63-90µm	0.105	1.03	0.355	13.0	10.2	29.6
38-63µm	0.103	1.06	0.327	12.8	10.4	31.1

AA RESULTS FOR LCFeCr SLAG (ORIGINAL SAMPLES)

		Cr tot	Fe	Al	Mg	Ca
Sample ID	Sample Mass	Mass%	Mass%	Mass%	Mass%	Mass%
106 - 90µm	0.126	1.28	0.15	10.9	8.79	26.9
90 - 63µm	0.132	1.34	0.14	10.4	9.02	27.9
63 - 38µm	0.116	1.45	0.17	12.2	10.0	29.1

A14. WEIGHT CHANGES DURING FLUIDIZATION WITH MOIST AIR FOR THE 90-106 µm PARTICLE SIZE

Date	Fluid Time	Bulk Mass	Mass after fluidization	Mass Sampled for leaching	Mass of water absorbed
21-Aug	0hr	200.27	200.27		
22-Aug	24hr	200.27	204.73	10.16	4.46
24-Aug	72hr	194.39	196.02	10.02	1.63
28-Aug	1 week	187.77	186.62	10.43	
5-Sep	2 week	176.17	175.85	10.03	

APPENDIX B1: PARTICLE SIZE DISTRIBUTION FOR 90 – 106 μm SAMPLES FLUIDISED FOR 24HOURS

APPENDIX D1: XRPD PATTERNS FOR LCFeCr SLAG ORIGINAL SAMPLE

Result: Analysis Table

ID: Teboes 0 hrs | Run No: 2 | Measured: 1/31/06 9:35AM
File: HELEN | Rec. No: 461 | Analysed: 1/31/06 9:35AM
Path: C:\SIZERS\DATA\ | Source: Analysed

Range: 300RF mm Beam: 2.40 mm Sampler: MS17 Obs: 6.9 %
Presentation: 3OHD Analysis: Polydisperse Residual: 0.575 %
Modifications: None

Conc. = 0.0428 %Vol Density = 3.100 g/cm^3 S.S.A.= 0.0752 m^2/g
Distribution: Volume D[4, 3] = 126.38 um D[3, 2] = 25.73 um
D(v, 0.1) = 83.67 um D(v, 0.5) = 124.35 um D(v, 0.9) = 178.37 um
Span = 7.616E-01 Uniformity = 2.433E-01

Size (um)	Volume In %	Size (um)	Volume In %	Size (um)	Volume In %	Size (um)	Volume In %
0.05	0.00	0.58	0.16	6.63	0.04	76.32	5.81
0.06	0.00	0.67	0.12	7.72	0.06	88.91	12.46
0.07	0.00	0.78	0.08	9.00	0.08	103.58	20.32
0.08	0.00	0.91	0.05	10.48	0.09	120.67	22.79
0.09	0.00	1.06	0.04	12.21	0.09	140.58	16.01
0.11	0.00	1.24	0.04	14.22	0.09	163.77	9.55
0.13	0.00	1.44	0.03	16.57	0.08	190.80	5.26
0.15	0.00	1.68	0.03	19.31	0.06	222.26	0.97
0.17	0.00	1.95	0.03	22.49	0.03	258.95	0.00
0.20	0.00	2.28	0.04	26.20	0.02	301.68	0.00
0.23	0.03	2.65	0.05	30.53	0.03	351.46	0.00
0.27	0.09	3.09	0.07	35.56	0.08	409.45	0.00
0.31	0.16	3.60	0.07	41.43	0.21	477.01	0.00
0.36	0.19	4.19	0.06	48.27	0.47	555.71	0.00
0.42	0.20	4.88	0.04	56.23	1.07	647.41	0.00
0.49	0.21	5.69	0.03	65.51	2.49	754.23	0.00
0.58		6.63		76.32		878.67	0.00

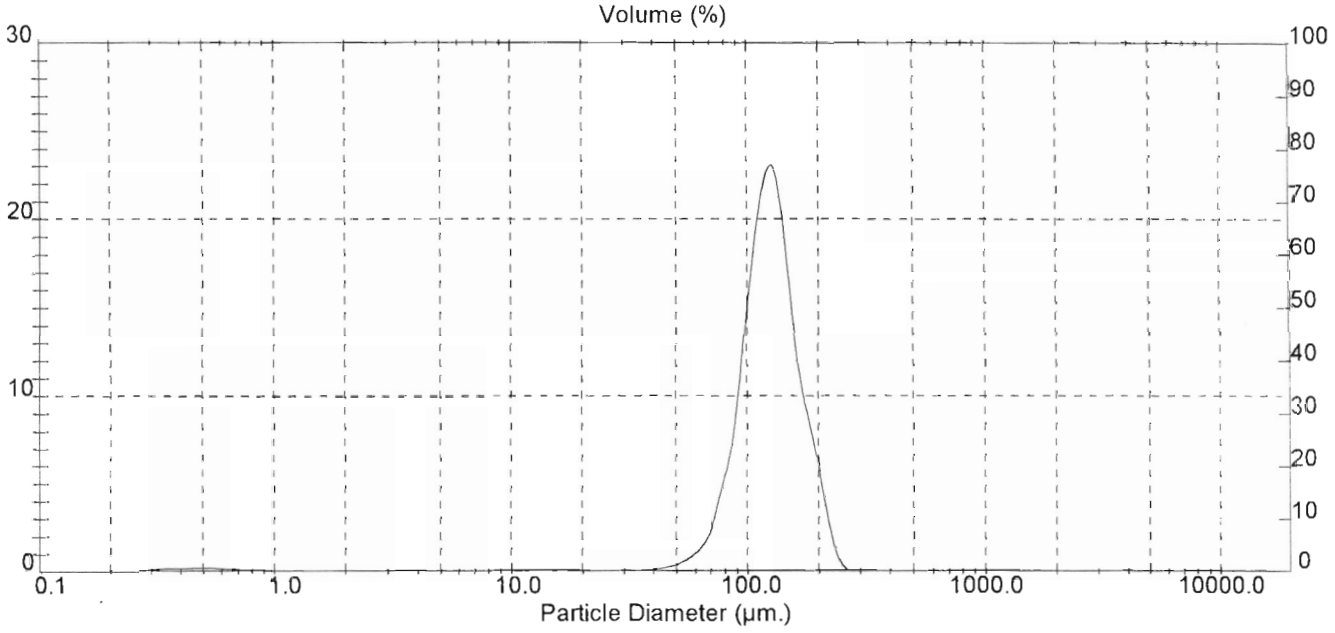

90 – 106µm

Result: Analysis Table

ID: Teboes 3 hrs	Run No: 3	Measured: 1/31/06 9:44AM
File: HELEN	Rec. No: 462	Analysed: 1/31/06 9:45AM
Path: C:\SIZERS\DATA\		Source: Analysed

Range: 300RF mm	Beam: 2.40 mm	Sampler: MS17 Obs': 6.0 %
Presentation: 3OHD	Analysis: Polydisperse	Residual: 0.488 %
Modifications: None		

Conc. = 0.0447 %Vol	Density = 3.100 g/cm^3	S.S.A.= 0.0635 m^2/g
Distribution: Volume	D[4, 3] = 128.94 um	D[3, 2] = 30.49 um
D(v, 0.1) = 86.72 um	D(v, 0.5) = 124.91 um	D(v, 0.9) = 180.42 um
Span = 7.502E-01	Uniformity = 2.398E-01	

Size (um)	Volume In %	Size (um)	Volume In %	Size (um)	Volume In %	Size (um)	Volume In %
0.05	0.00	0.58	0.14	6.63	0.02	76.32	5.64
0.06	0.00	0.67	0.09	7.72	0.03	88.91	12.49
0.07	0.00	0.78	0.06	9.00	0.04	103.58	20.86
0.08	0.00	0.91	0.04	10.48	0.05	120.67	23.20
0.09	0.00	1.06	0.02	12.21	0.05	140.58	15.85
0.11	0.00	1.24	0.02	14.22	0.05	163.77	9.16
0.13	0.00	1.44	0.01	16.57	0.04	190.80	4.93
0.15	0.00	1.68	0.00	19.31	0.03	222.28	2.40
0.17	0.00	1.95	0.00	22.49	0.02	258.95	0.00
0.20	0.00	2.28	0.00	26.20	0.01	301.68	0.00
0.23	0.02	2.65	0.00	30.53	0.02	351.46	0.00
0.27	0.07	3.09	0.00	35.56	0.06	409.45	0.00
0.31	0.14	3.60	0.00	41.43	0.17	477.01	0.00
0.36	0.17	4.19	0.00	48.27	0.41	555.71	0.00
0.42	0.18	4.88	0.00	56.23	0.97	647.41	0.00
0.49	0.19	5.69	0.00	65.51	2.33	754.23	0.00
0.58		6.63		76.32		878.67	0.00

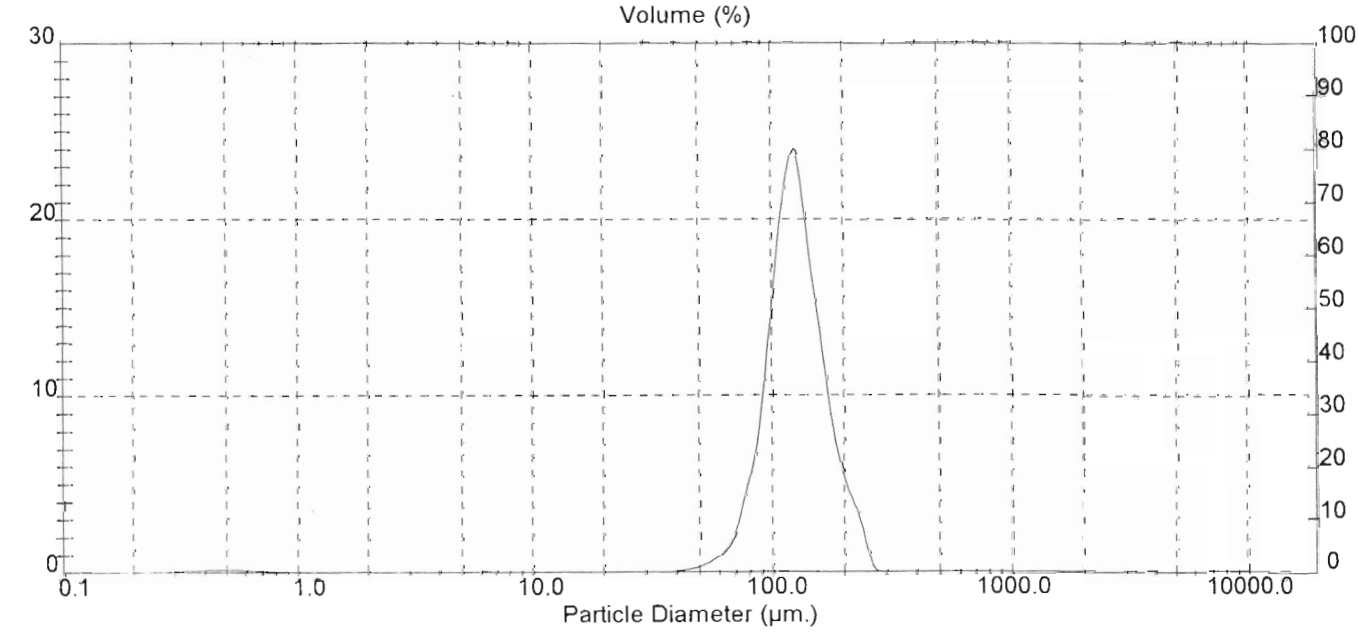

Result: Analysis Table

ID: Teboes 6h | Run No: 6 | Measured: 10/25/05 3:01PM
File: HELEN | Rec. No: 423 | Analysed: 10/25/05 3:03PM
Path: C:\SIZERS\DATA\ | Source: Analysed

Range: 300RF mm | Beam: 2.40 mm | Sampler: MS17 | Obs': 13.8 %
Presentation: 3OHD | Analysis: Polydisperse | Residual: 1.242 %
Modifications: None

Conc. = 0.0127 %Vol | Density = 3.500 g/cm^3 | S.S.A.= 0.8802 m^2/g
Distribution: Volume | D[4, 3] = 37.98 um | D[3, 2] = 1.95 um
D(v, 0.1) = 0.64 um | D(v, 0.5) = 35.39 um | D(v, 0.9) = 78.55 um
Span = 2.202E+00 | Uniformity = 6.766E-01

Size (um)	Volume In %	Size (um)	Volume In %	Size (um)	Volume In %	Size (um)	Volume In %
0.05	0.03	0.58	0.81	6.63	1.22	76.32	5.17
0.06	0.07	0.67	0.73	7.72	1.35	88.91	3.57
0.07	0.12	0.78	0.66	9.00	1.48	103.58	1.98
0.08	0.18	0.91	0.59	10.48	1.64	120.67	0.39
0.09	0.25	1.06	0.52	12.21	1.86	140.58	0.00
0.11	0.35	1.24	0.45	14.22	2.19	163.77	0.00
0.13	0.46	1.44	0.39	16.57	2.67	190.80	0.00
0.15	0.58	1.68	0.35	19.31	3.34	222.28	0.00
0.17	0.71	1.95	0.33	22.49	4.18	258.95	0.00
0.20	0.84	2.28	0.35	26.20	5.16	301.68	0.00
0.23	0.94	2.65	0.41	30.53	6.20	351.46	0.00
0.27	1.01	3.09	0.51	35.56	7.25	409.45	0.00
0.31	1.02	3.60	0.64	41.43	8.28	477.01	0.00
0.36	0.99	4.19	0.78	48.27	8.47	555.71	0.00
0.42	0.95	4.88	0.94	56.23	7.94	647.41	0.00
0.49	0.89	5.69	1.08	65.51	6.76	754.23	0.00
0.58		6.63		76.32		878.67	

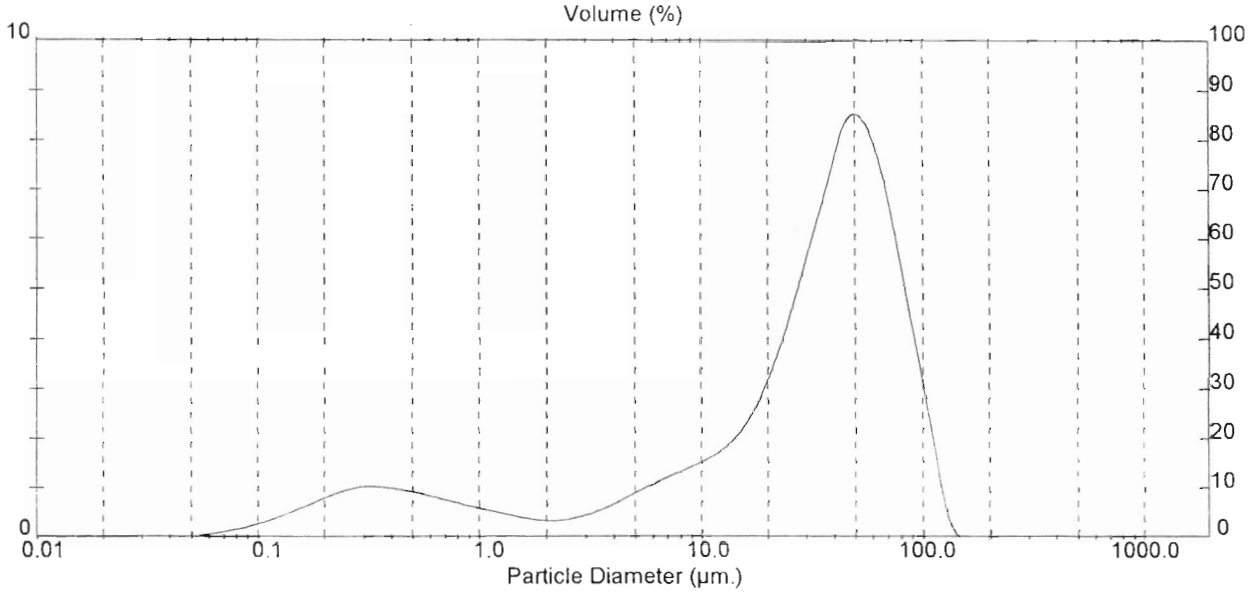

Result: Analysis Table

ID: Teboes 24 hrs | Run No: 5 | Measured: 1/31/06 10:01AM
File: HELEN | Rec. No: 464 | Analysed: 1/31/06 10:01AM
Path: C:\SIZERS\DATA\ | Source: Analysed

Range: 300RF mm | Beam: 2.40 mm | Sampler: MS17 | Obs': 7.5 %
Presentation: 3OHD | Analysis: Polydisperse | Residual: 0.588 %
Modifications: None

Conc. = 0.0561 %Vol | Density = 3.100 g/cm^3 | S.S.A. = 0.0653 m^2/g
Distribution: Volume | D[4, 3] = 127.37 um | D[3, 2] = 29.66 um
D(v, 0.1) = 85.92 um | D(v, 0.5) = 124.29 um | D(v, 0.9) = 177.27 um
Span = 7.350E-01 | Uniformity = 2.337E-01

Size (um)	Volume In %	Size (um)	Volume In %	Size (um)	Volume In %	Size (um)	Volume In %
0.05	0.00	0.58	0.13	6.63	0.02	76.32	5.87
0.06	0.00	0.67	0.08	7.72	0.02	88.91	12.80
0.07	0.00	0.78	0.05	9.00	0.03	103.58	20.96
0.08	0.00	0.91	0.03	10.48	0.04	120.67	23.04
0.09	0.00	1.06	0.02	12.21	0.04	140.58	16.03
0.11	0.00	1.24	0.01	14.22	0.04	163.77	9.50
0.13	0.00	1.44	0.01	16.57	0.04	190.80	5.21
0.15	0.00	1.68	0.00	19.31	0.03	222.28	0.91
0.17	0.00	1.95	0.00	22.49	0.02	258.95	0.00
0.20	0.00	2.28	0.00	26.20	0.01	301.68	0.00
0.23	0.03	2.65	0.00	30.53	0.02	351.46	0.00
0.27	0.09	3.09	0.00	35.56	0.07	409.45	0.00
0.31	0.15	3.60	0.00	41.43	0.18	477.01	0.00
0.36	0.18	4.19	0.00	48.27	0.44	555.71	0.00
0.42	0.19	4.88	0.00	56.23	1.04	647.41	0.00
0.49	0.18	5.69	0.01	65.51	2.48	754.23	0.00
0.58		6.63		76.32		878.67	

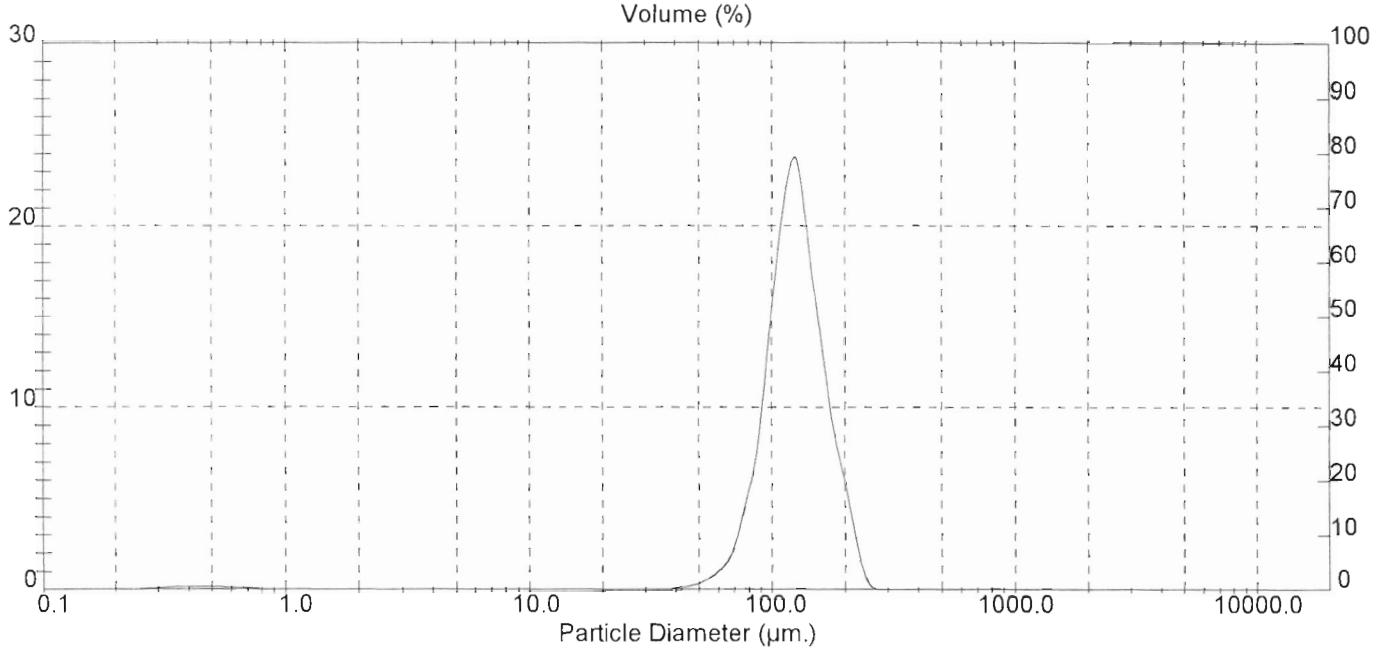

APPENDIX B2: PARTICLE SIZE DISTRIBUTION FOR 90 – 106 μm SAMPLES FLUIDISED FOR 2WEEKS

Result: Analysis Table

ID: Tebogo - 72hrs	Run No: 2	Measured: 2/6/06 11:23AM
File: TEBOG0	Rec. No: 22	Analysed: 2/6/06 11:23AM
Path: C:\SIZERS\DATA\		Source: Analysed

Range: 300RF mm	Beam: 2.40 mm	Sampler: MS17 Obs' 8.7 %
Presentation: 3OHD	Analysis: Polydisperse	Residual: 0.654 %
Modifications: None		

Conc. = 0.0552 %Vol	Density = 3.100 g/cm^3	S.S.A = 0.0768 m^2/g
Distribution: Volume	D[4, 3] = 127.07 um	D[3, 2] = 25.22 um
D(v, 0.1) = 83.80 um	D(v, 0.5) = 124.63 um	D(v, 0.9) = 179.97 um
Span = 7.716E-01	Uniformity = 2.458E-01	

Size (um)	Volume In %	Size (um)	Volume In %	Size (um)	Volume In %	Size (um)	Volume In %
0.05	0.00	0.58	0.14	6.63	0.04	76.32	5.87
0.06	0.00	0.67	0.10	7.72	0.06	88.91	12.47
0.07	0.00	0.78	0.06	9.00	0.08	103.58	20.09
0.08	0.00	0.91	0.04	10.48	0.09	120.67	22.36
0.09	0.00	1.06	0.03	12.21	0.08	140.58	16.01
0.11	0.00	1.24	0.03	14.22	0.07	163.77	9.78
0.13	0.00	1.44	0.02	16.57	0.06	190.80	5.49
0.15	0.00	1.68	0.02	19.31	0.04	222.28	1.20
0.17	0.00	1.95	0.03	22.49	0.03	258.95	0.00
0.20	0.01	2.28	0.04	26.20	0.02	301.68	0.00
0.23	0.04	2.65	0.05	30.53	0.03	351.46	0.00
0.27	0.11	3.09	0.07	35.56	0.08	409.45	0.00
0.31	0.18	3.60	0.07	41.43	0.20	477.01	0.00
0.36	0.20	4.19	0.06	48.27	0.47	555.71	0.00
0.42	0.20	4.88	0.04	56.23	1.09	647.41	0.00
0.49	0.20	5.69	0.03	65.51	2.53	754.23	0.00
0.58		6.63		76.32		878.67	

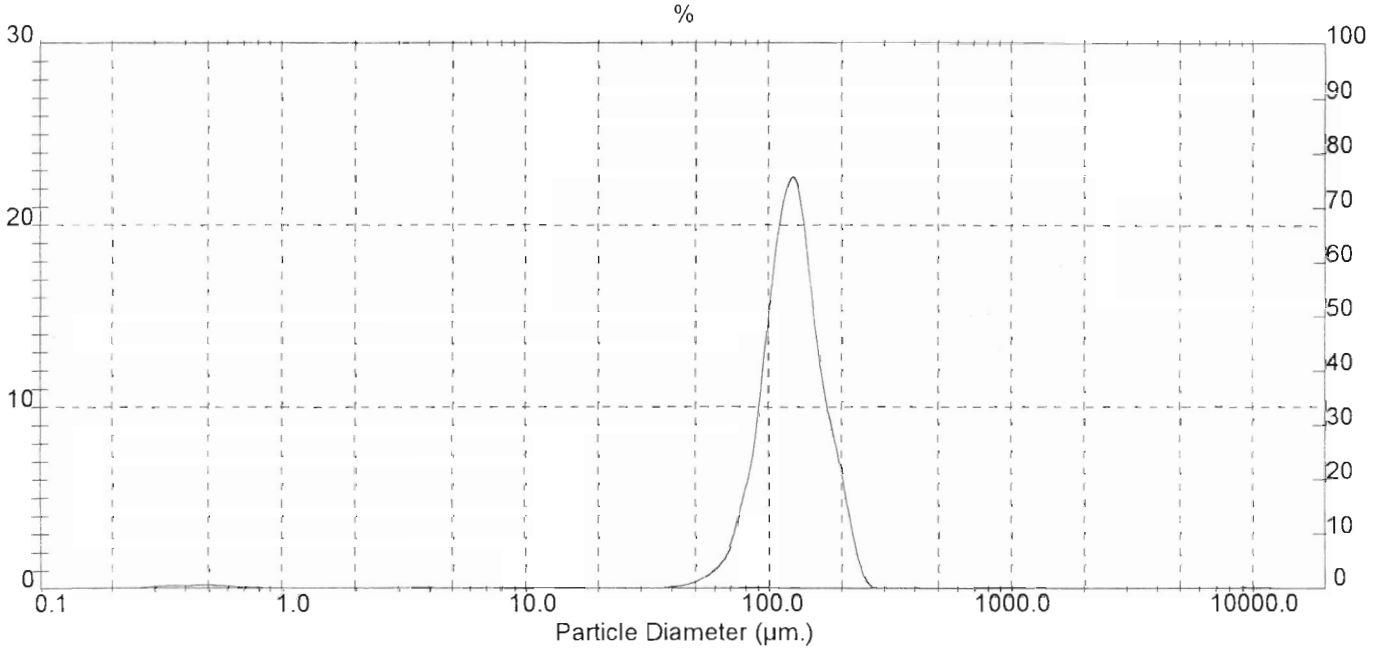

Result: Analysis Table

ID: Tebogo - C7 1 week | Run No: 3 | Measured: 2/6/06 11:30AM
File: TEBOG0 | Rec. No. 23 | Analysed: 2/6/06 11:30AM
Path: C:\SIZERS\DATA\ | Source: Analysed

Range: 300RF mm Beam: 2.40 mm Sampler: MS17 Obs: 8.5 %
Presentation: 3OHD Analysis: Polydisperse Residual: 0.643 %
Modifications: None

Conc. = 0.0529 %Vol Density = 3.100 g/cm^3 S.S.A. = 0.0776 m^2/g
Distribution: Volume D[4, 3] = 126.11 um D[3, 2] = 24.96 um
D(v, 0.1) = 83.35 um D(v, 0.5) = 123.86 um D(v, 0.9) = 178.17 um
Span = 7.655E-01 Uniformity = 2.442E-01

Size (um)	Volume In %	Size (um)	Volume In %	Size (um)	Volume In %	Size (um)	Volume In %
0.05	0.00	0.58	0.16	6.63	0.04	76.32	6.04
0.06	0.00	0.67	0.11	7.72	0.05	88.91	12.75
0.07	0.00	0.78	0.07	9.00	0.07	103.58	20.41
0.08	0.00	0.91	0.05	10.48	0.07	120.67	22.52
0.09	0.00	1.06	0.04	12.21	0.07	140.58	15.77
0.11	0.00	1.24	0.03	14.22	0.06	163.77	9.47
0.13	0.00	1.44	0.03	16.57	0.05	190.80	5.22
0.15	0.00	1.68	0.03	19.31	0.04	222.28	0.97
0.17	0.00	1.95	0.03	22.49	0.02	258.95	0.00
0.20	0.01	2.28	0.04	26.20	0.02	301.68	0.00
0.23	0.03	2.65	0.05	30.53	0.03	351.46	0.00
0.27	0.10	3.09	0.06	35.56	0.08	409.45	0.00
0.31	0.17	3.60	0.07	41.43	0.21	477.01	0.00
0.36	0.20	4.19	0.05	48.27	0.50	555.71	0.00
0.42	0.21	4.88	0.03	56.23	1.14	647.41	0.00
0.49	0.21	5.69	0.03	65.51	2.62	754.23	0.00
0.58		6.63		76.32		878.67	

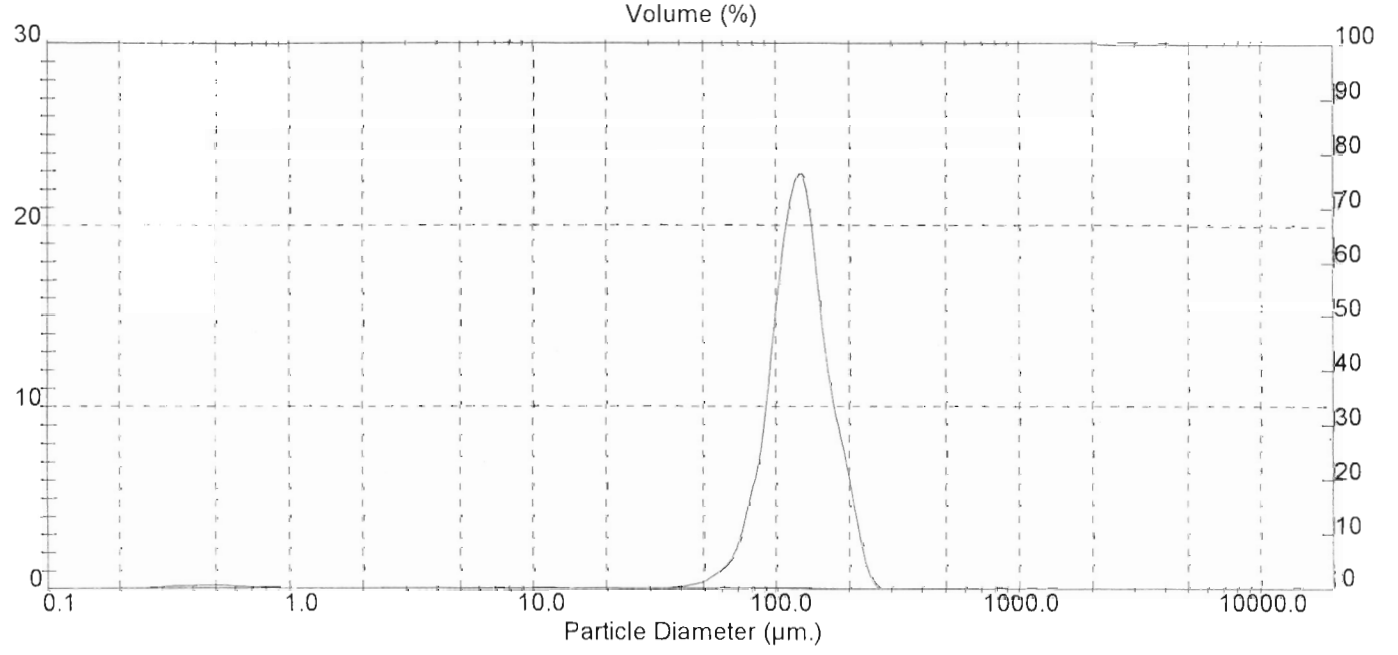

Result: Analysis Table

ID: Teboho 2week fluid | Run No: 1 | Measured: 2/14/06 9:56AM
File: TEBOG0 | Rec. No: 24 | Analysed: 2/14/06 9:56AM
Path: C:\SIZERS\DATA\ | Source: Analysed

Range: 300RF mm Beam: 2.40 mm Sampler: MS17 | Obs: 6.9 %
Presentation: 3OHD | Analysis: Polydisperse | Residual: 0.613 %
Modifications: None

Conc. = 0.0455 %Vol | Density = 3.100 g/cm^3 | S.S.A. = 0.0698 m^2/g
Distribution: Volume | D[4, 3] = 127.61 um | D[3, 2] = 27.75 um
D(v, 0.1) = 83.08 um | D(v, 0.5) = 124.28 um | D(v, 0.9) = 181.54 um
Span = 7.923E-01 | Uniformity = 2.519E-01

Size (um)	Volume In %	Size (um)	Volume In %	Size (um)	Volume In %	Size (um)	Volume In %
0.05	0.00	0.58	0.16	6.63	0.04	76.32	6.07
0.06	0.00	0.67	0.13	7.72	0.06	88.91	12.52
0.07	0.00	0.78	0.09	9.00	0.07	103.58	20.03
0.08	0.00	0.91	0.07	10.48	0.08	120.67	22.24
0.09	0.00	1.06	0.06	12.21	0.08	140.58	15.53
0.11	0.00	1.24	0.05	14.22	0.08	163.77	9.20
0.13	0.00	1.44	0.04	16.57	0.07	190.80	5.00
0.15	0.00	1.68	0.00	19.31	0.06	222.28	2.44
0.17	0.00	1.95	0.00	22.49	0.04	258.95	0.00
0.20	0.00	2.26	0.00	26.20	0.03	301.68	0.00
0.23	0.02	2.65	0.00	30.53	0.04	351.46	0.00
0.27	0.08	3.09	0.00	35.56	0.11	409.45	0.00
0.31	0.14	3.60	0.00	41.43	0.26	477.01	0.00
0.36	0.16	4.19	0.00	48.27	0.58	555.71	0.00
0.42	0.18	4.88	0.00	56.23	1.25	647.41	0.00
0.49	0.20	5.69	0.00	65.51	2.74	754.23	0.00
0.58		6.63		76.32		878.67	

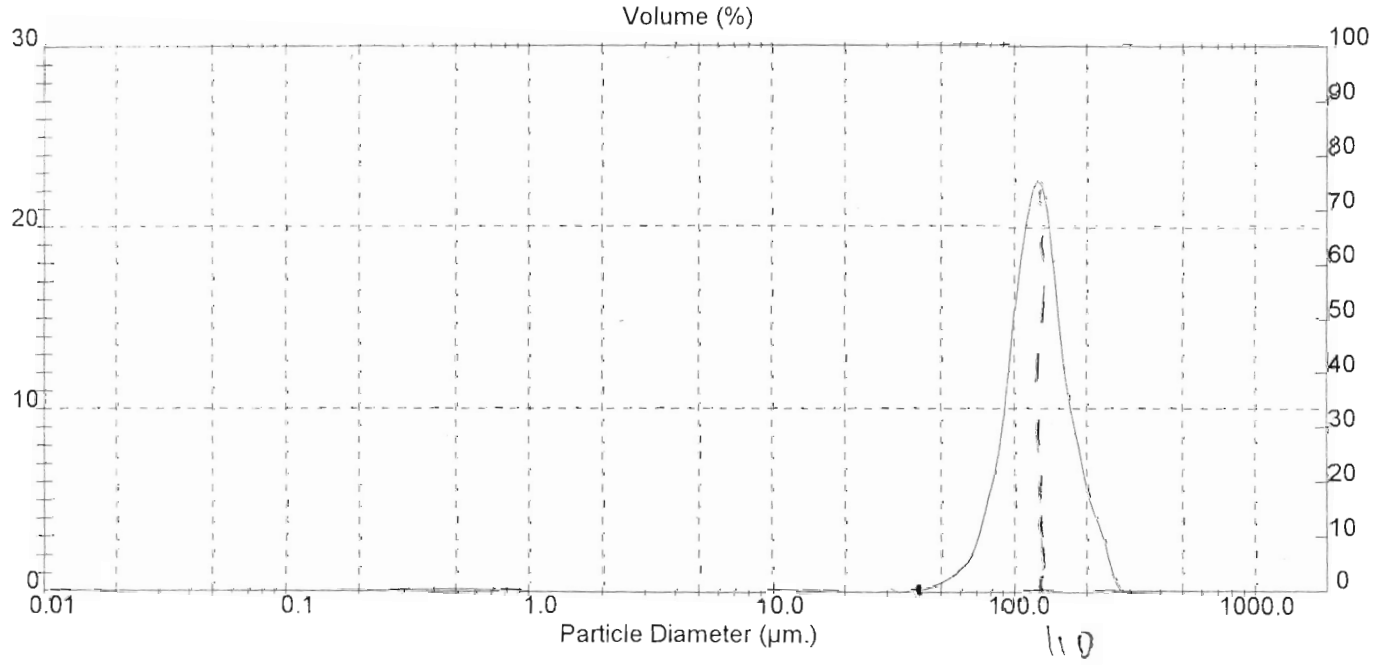

APPENDIX B3: PARTICLE SIZE DISTRIBUTION FOR 38 - 63 μm SAMPLES FLUIDISED FOR UP TO 72HRS

Result: Analysis Table

ID: Teboes 3h	Run No: 4	Measured: 10/25/05 2:56PM
File: HELEN	Rec No: 422	Analysed: 10/25/05 2:56PM
Path: C:\SIZERS\DATA\		Source: Analysed

Range: 300RF mm	Beam: 2.40 mm	Sampler: MS17 Obs: 10.5 %
Presentation: 3OHD	Analysis: Polydisperse	Residual: 1.592 %
Modifications: None		

Conc. = 0.0092 %Vol	Density = 3.500 g/cm^3	S.S.A.= 1.0191 m^2/g
Distribution: Volume	D[4, 3] = 37.47 um	D[3, 2] = 1.68 um
D(v, 0.1) = 0.56 um	D(v, 0.5) = 35.02 um	D(v, 0.9) = 77.85 um
Span = 2.207E+00	Uniformity = 6.798E-01	

Size (um)	Volume In %	Size (um)	Volume In %	Size (um)	Volume In %	Size (um)	Volume In %
0.05	0.06	0.58	0.81	6.63	1.15	76.32	5.20
0.06	0.13	0.67	0.74	7.72	1.25	88.91	3.53
0.07	0.20	0.78	0.67	9.00	1.36	103.58	1.86
0.08	0.28	0.91	0.60	10.48	1.51	120.67	0.19
0.09	0.38	1.06	0.53	12.21	1.74	140.58	0.00
0.11	0.48	1.24	0.47	14.22	2.10	163.77	0.00
0.13	0.58	1.44	0.41	16.57	2.63	190.80	0.00
0.15	0.69	1.68	0.37	19.31	3.34	222.26	0.00
0.17	0.79	1.95	0.36	22.49	4.23	258.95	0.00
0.20	0.86	2.28	0.38	26.20	5.22	301.68	0.00
0.23	0.95	2.65	0.44	30.53	6.25	351.46	0.00
0.27	0.99	3.09	0.54	35.56	7.27	409.45	0.00
0.31	0.99	3.60	0.66	41.43	8.25	477.01	0.00
0.36	0.97	4.19	0.79	48.27	8.40	555.71	0.00
0.42	0.93	4.88	0.93	56.23	7.88	647.41	0.00
0.49	0.87	5.69	1.04	65.51	6.75	754.23	0.00
0.58		6.63		76.32		878.67	

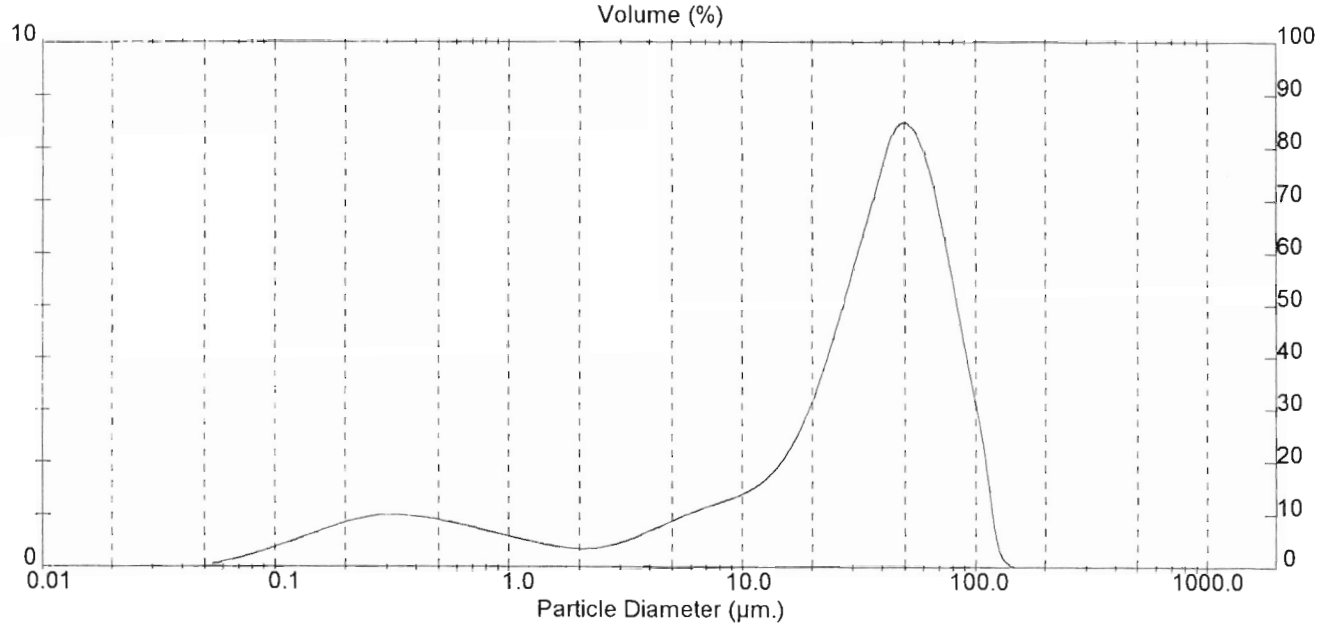

Result: Analysis Table

ID: Teboes 6h | Run No: 6 | Measured: 10/25/05 3:01PM
File: HELEN | Rec. No: 423 | Analysed: 10/25/05 3:03PM
Path: C:\SIZERS\DATA\ | Source: Analysed

Range: 300RF mm | Beam: 2.40 mm | Sampler: MS17 | Obs: 13.8 %
Presentation: 3OHD | Analysis: Polydisperse | Residual: 1.242 %
Modifications: None

Conc. = 0.0127 %Vol | Density = 3.500 g/cm^3 | S.S.A. = 0.8802 m^2/g
Distribution: Volume | D[4, 3] = 37.98 um | D[3, 2] = 1.95 um
D(v, 0.1) = 0.64 um | D(v, 0.5) = 35.39 um | D(v, 0.9) = 78.55 um
Span = 2.202E+00 | Uniformity = 6.766E-01

Size (um)	Volume In %	Size (um)	Volume In %	Size (um)	Volume In %	Size (um)	Volume In %
0.05	0.03	0.58	0.81	6.63	1.22	76.32	5.17
0.06	0.07	0.67	0.73	7.72	1.35	88.91	3.57
0.07	0.12	0.78	0.66	9.00	1.48	103.58	1.98
0.08	0.18	0.91	0.59	10.48	1.64	120.67	0.39
0.09	0.25	1.06	0.52	12.21	1.86	140.58	0.00
0.11	0.35	1.24	0.45	14.22	2.19	163.77	0.00
0.13	0.46	1.44	0.39	16.57	2.67	190.80	0.00
0.15	0.58	1.68	0.35	19.31	3.34	222.28	0.00
0.17	0.71	1.95	0.33	22.49	4.18	258.95	0.00
0.20	0.84	2.28	0.35	26.20	5.16	301.68	0.00
0.23	0.94	2.65	0.41	30.53	6.20	351.46	0.00
0.27	1.01	3.09	0.51	35.56	7.25	409.45	0.00
0.31	1.02	3.60	0.64	41.43	8.28	477.01	0.00
0.36	0.99	4.19	0.78	48.27	8.47	555.71	0.00
0.42	0.95	4.88	0.94	56.23	7.94	647.41	0.00
0.49	0.89	5.69	1.08	65.51	6.76	754.23	0.00
0.58		6.63		76.32		878.67	0.00

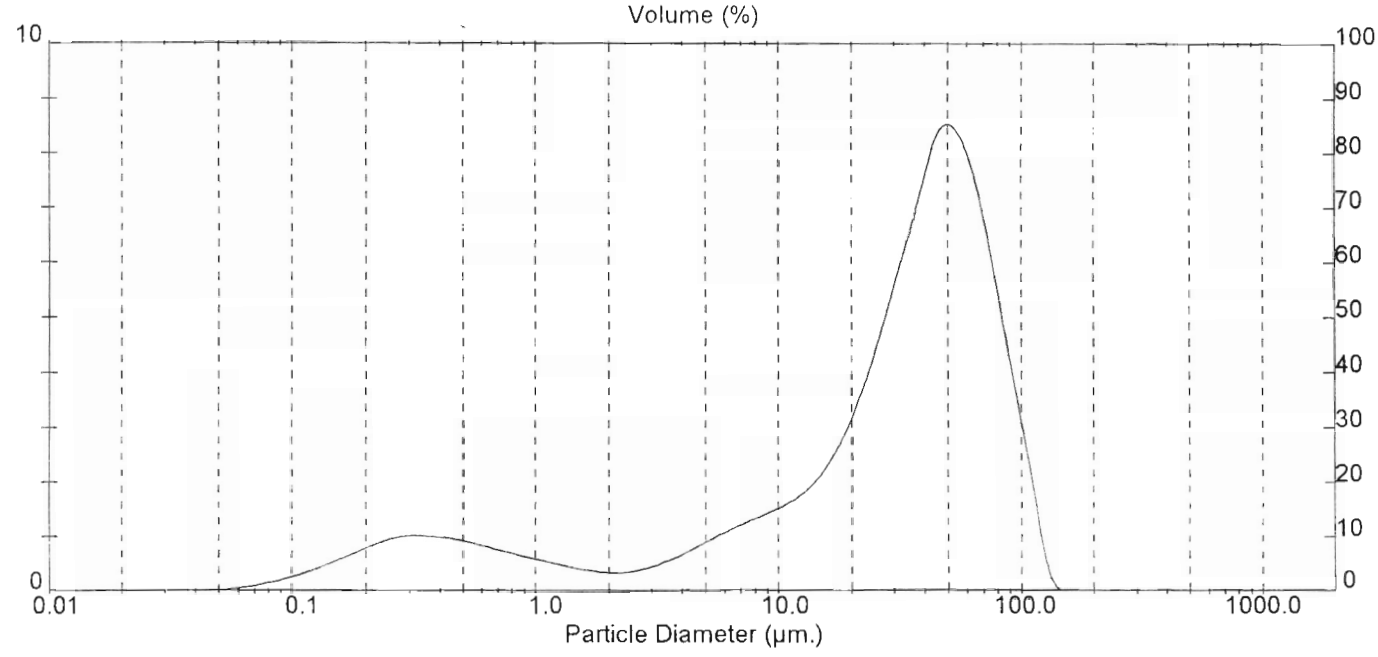

Result: Analysis Table

ID: Teboes 24h | Run No: 7 | Measured: 10/25/05 3:20PM
File: HELEN | Rec. No: 424 | Analysed: 10/25/05 3:20PM
Path: C:\SIZERS\DATA\ | Source: Analysed

Range: 300RF mm | Beam: 2.40 mm | Sampler: MS17 | Obs: 13.2 %
Presentation: 3OHD | Analysis: Polydisperse | Residual: 1.192 %
Modifications: None

Conc. = 0.0122 %Vol | Density = 3.500 g/cm^3 | S.S.A. = 0.8716 m^2/g
Distribution: Volume | D[4, 3] = 37.46 um | D[3, 2] = 1.97 um
D(v, 0.1) = 0.66 um | D(v, 0.5) = 35.34 um | D(v, 0.9) = 76.83 um
Span = 2.155E+00 | Uniformity = 6.587E-01

Size (um)	Volume In %	Size (um)	Volume In %	Size (um)	Volume In %	Size (um)	Volume In %
0.05	0.03	0.58	0.81	6.63	1.19	76.32	5.13
0.06	0.07	0.67	0.73	7.72	1.30	88.91	3.42
0.07	0.12	0.78	0.66	9.00	1.42	103.58	1.70
0.08	0.18	0.91	0.59	10.48	1.57	120.67	0.00
0.09	0.25	1.06	0.53	12.21	1.79	140.58	0.00
0.11	0.35	1.24	0.46	14.22	2.14	163.77	0.00
0.13	0.45	1.44	0.40	16.57	2.66	190.80	0.00
0.15	0.57	1.68	0.36	19.31	3.38	222.26	0.00
0.17	0.70	1.95	0.34	22.49	4.27	258.95	0.00
0.20	0.82	2.28	0.36	26.20	5.30	301.68	0.00
0.23	0.93	2.65	0.42	30.53	6.39	351.46	0.00
0.27	0.99	3.09	0.52	35.56	7.47	409.45	0.00
0.31	1.01	3.60	0.64	41.43	8.53	477.01	0.00
0.36	0.98	4.19	0.79	48.27	8.65	555.71	0.00
0.42	0.94	4.88	0.93	56.23	8.04	647.41	0.00
0.49	0.88	5.69	1.06	65.51	6.78	754.23	0.00
0.58		6.63		76.32		878.67	

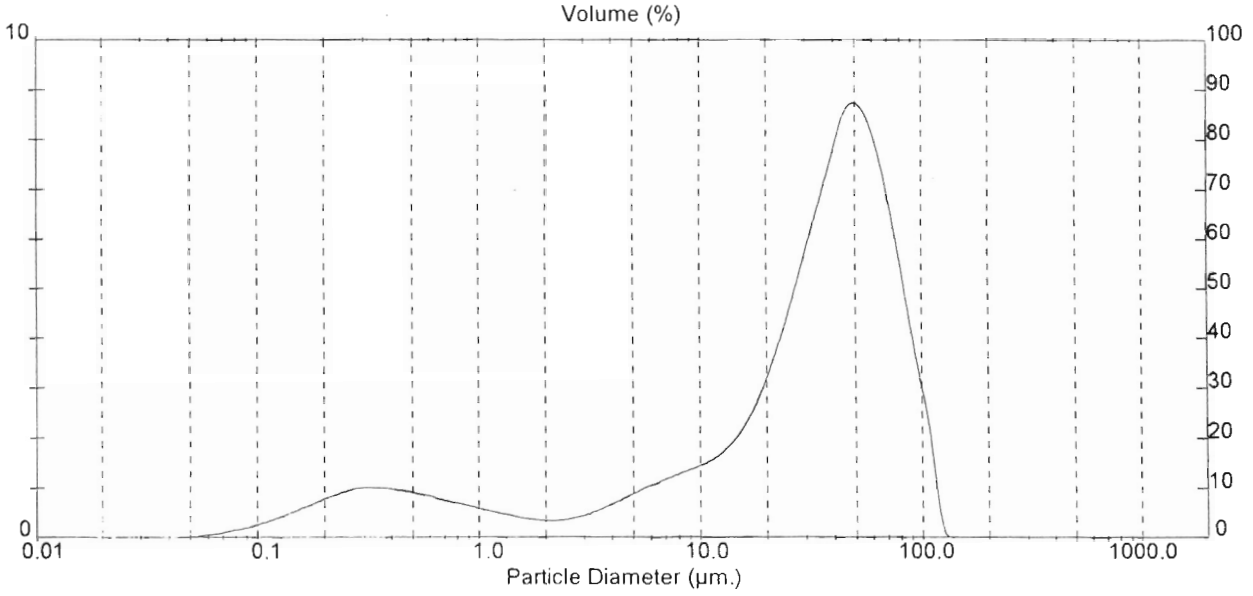

Result Analysis Table

ID: Teboes 27h | Run No: 8 | Measured: 10/25/05 3:29PM
File: HELEN | Rec. No: 425 | Analysed: 10/25/05 3:33PM
Path: C:\SIZERS\DATA\ | Source: Analysed

Range: 300RF mm | Beam: 2.40 mm | Sampler: MS17 | Obs: 11.0 %
Presentation: 3OHD | Analysis: Polydisperse | Residual: 1.179 %
Modifications: None

Conc. = 0.0111 %Vol | Density = 3.500 g/cm^3 | S.S.A. = 0.5097 m^2/g
Distribution: Volume | D[4, 3] = 39.71 um | D[3, 2] = 3.36 um
D(v, 0.1) = 1.18 um | D(v, 0.5) = 36.29 um | D(v, 0.9) = 79.63 um
Span = 2.162E+00 | Uniformity = 6.660E-01

Size (um)	Volume In %	Size (um)	Volume In %	Size (um)	Volume In %	Size (um)	Volume In %
0.05	0.00	0.58	0.94	6.63	1.18	76.32	4.81
0.06	0.00	0.67	0.86	7.72	1.31	88.91	3.12
0.07	0.00	0.78	0.75	9.00	1.47	103.58	1.83
0.08	0.00	0.91	0.65	10.48	1.67	120.67	1.04
0.09	0.01	1.06	0.55	12.21	1.95	140.58	0.72
0.11	0.01	1.24	0.47	14.22	2.33	163.77	0.00
0.13	0.03	1.44	0.40	16.57	2.87	190.80	0.00
0.15	0.07	1.68	0.35	19.31	3.58	222.28	0.00
0.17	0.13	1.95	0.33	22.49	4.44	258.95	0.00
0.20	0.24	2.28	0.35	26.20	5.43	301.68	0.00
0.23	0.42	2.65	0.41	30.53	6.47	351.46	0.00
0.27	0.64	3.09	0.52	35.56	7.44	409.45	0.00
0.31	0.85	3.60	0.64	41.43	8.31	477.01	0.00
0.36	0.97	4.19	0.78	48.27	8.91	555.71	0.00
0.42	1.00	4.88	0.92	56.23	8.13	647.41	0.00
0.49	1.02	5.69	1.05	65.51	6.62	754.23	0.00
0.58	1.01	6.63	1.18	76.32		878.67	

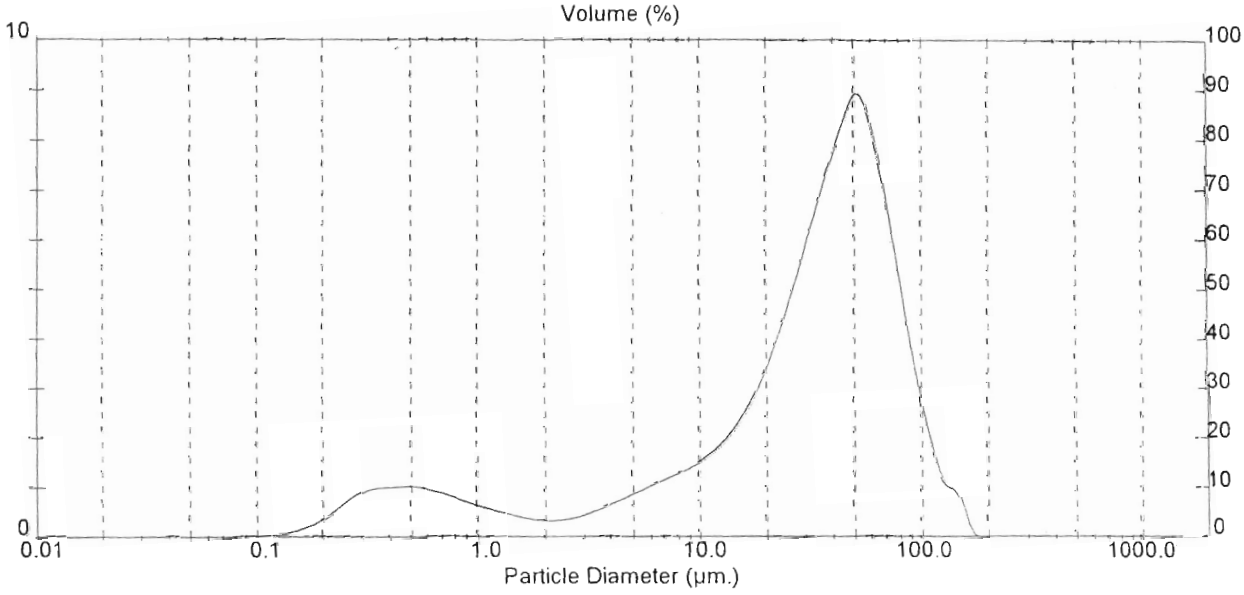

Result: Analysis Table

ID: Teboes 48h | Run No: 9 | Measured: 10/25/05 3:41PM
File: HELEN | Rec. No. 426 | Analysed: 10/25/05 3:44PM
Path: C:\SIZERS\DATA\ | Source: Analysed

Range: 300RF mm | Beam: 2.40 mm | Sampler: MS17 | Obs': 12.1 %
Presentation: 3OHD | Analysis: Polydisperse | Residual: 1.292 %
Modifications: None

Conc. = 0.0113 %Vol | Density = 3.500 g/cm^3 | S.S.A. = 0.7556 m^2/g
Distribution: Volume | D[4, 3] = 37.11 um | D[3, 2] = 2.27 um
D(v, 0.1) = 0.76 um | D(v, 0.5) = 34.64 um | D(v, 0.9) = 76.26 um
Span = 2.179E+00 | Uniformity = 6.650E-01

Size (um)	Volume In %	Size (um)	Volume In %	Size (um)	Volume In %	Size (um)	Volume In %
0.05	0.02	0.58	0.86	6.63	1.23	76.32	5.01
0.06	0.04	0.67	0.78	7.72	1.37	88.91	3.32
0.07	0.06	0.78	0.69	9.00	1.52	103.58	1.64
0.08	0.10	0.91	0.60	10.48	1.71	120.67	0.00
0.09	0.16	1.06	0.52	12.21	1.97	140.58	0.00
0.11	0.23	1.24	0.45	14.22	2.35	163.77	0.00
0.13	0.33	1.44	0.38	16.57	2.88	190.80	0.00
0.15	0.45	1.68	0.35	19.31	3.58	222.28	0.00
0.17	0.59	1.95	0.34	22.49	4.43	258.95	0.00
0.20	0.74	2.28	0.37	26.20	5.40	301.68	0.00
0.23	0.88	2.65	0.43	30.53	6.42	351.46	0.00
0.27	0.98	3.09	0.53	35.56	7.42	409.45	0.00
0.31	1.01	3.60	0.66	41.43	8.40	477.01	0.00
0.36	1.00	4.19	0.81	48.27	8.50	555.71	0.00
0.42	0.98	4.88	0.95	56.23	7.89	647.41	0.00
0.49	0.93	5.69	1.09	65.51	6.64	754.23	0.00
0.58		6.63		76.32		878.67	

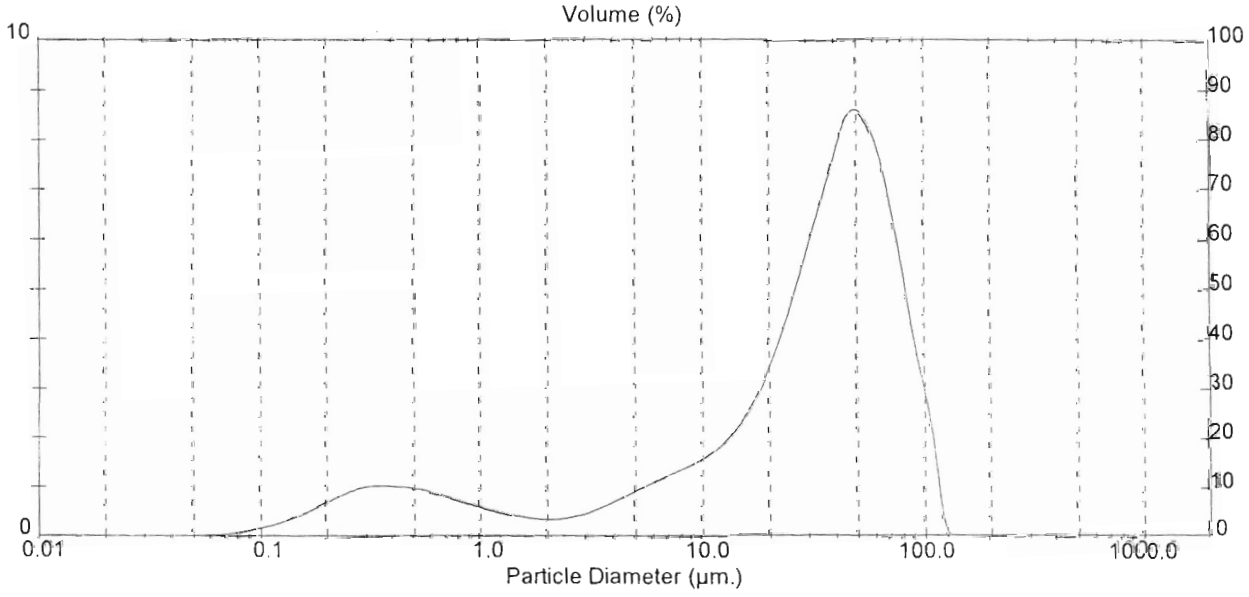

Result: Analysis Table

ID: Teboes 72h — Run No: 10 — Measured: 10/25/05 3:49PM
File: HELEN — Rec No: 427 — Analysed: 10/25/05 3:49PM
Path: C:\SIZERS\DATA\ — Source: Analysed

Range: 300RF mm Beam: 2.40 mmSampler: MS17 — Obs: 11.4 %
Presentation: 3OHD — Analysis: Polydisperse — Residual: 1.586 %
Modifications: None

Conc. = 0.0102 %Vol — Density = 3.500 g/cm^3 — S.S.A. = 0.8755 m^2/g
Distribution: Volume — D[4, 3] = 36.56 um — D[3, 2] = 1.96 um
D(v, 0.1) = 0.64 um — D(v, 0.5) = 33.71 um — D(v, 0.9) = 76.26 um
Span = 2.243E+00 — Uniformity = 6.890E-01

Size (um)	Volume In %	Size (um)	Volume In %	Size (um)	Volume In %	Size (um)	Volume In %
0.05	0.03	0.58	0.85	6.63	1.26	76.32	4.79
0.06	0.07	0.67	0.77	7.72	1.39	88.91	3.26
0.07	0.11	0.78	0.69	9.00	1.53	103.58	1.73
0.08	0.17	0.91	0.61	10.48	1.71	120.67	0.19
0.09	0.23	1.06	0.53	12.21	1.97	140.58	0.00
0.11	0.34	1.24	0.46	14.22	2.35	163.77	0.00
0.13	0.45	1.44	0.40	16.57	2.88	190.80	0.00
0.15	0.57	1.68	0.36	19.31	3.59	222.28	0.00
0.17	0.70	1.96	0.35	22.49	4.45	258.95	0.00
0.20	0.82	2.28	0.38	26.20	5.41	301.68	0.00
0.23	0.93	2.65	0.45	30.53	6.39	351.46	0.00
0.27	1.00	3.09	0.56	35.56	7.34	409.45	0.00
0.31	1.03	3.60	0.69	41.43	8.23	477.01	0.00
0.36	1.01	4.19	0.84	48.27	8.23	555.71	0.00
0.42	0.97	4.88	0.99	56.23	7.56	647.41	0.00
0.49	0.90	5.69	1.13	65.51	6.33	754.23	0.00
0.58		6.63		76.32		878.67	0.00

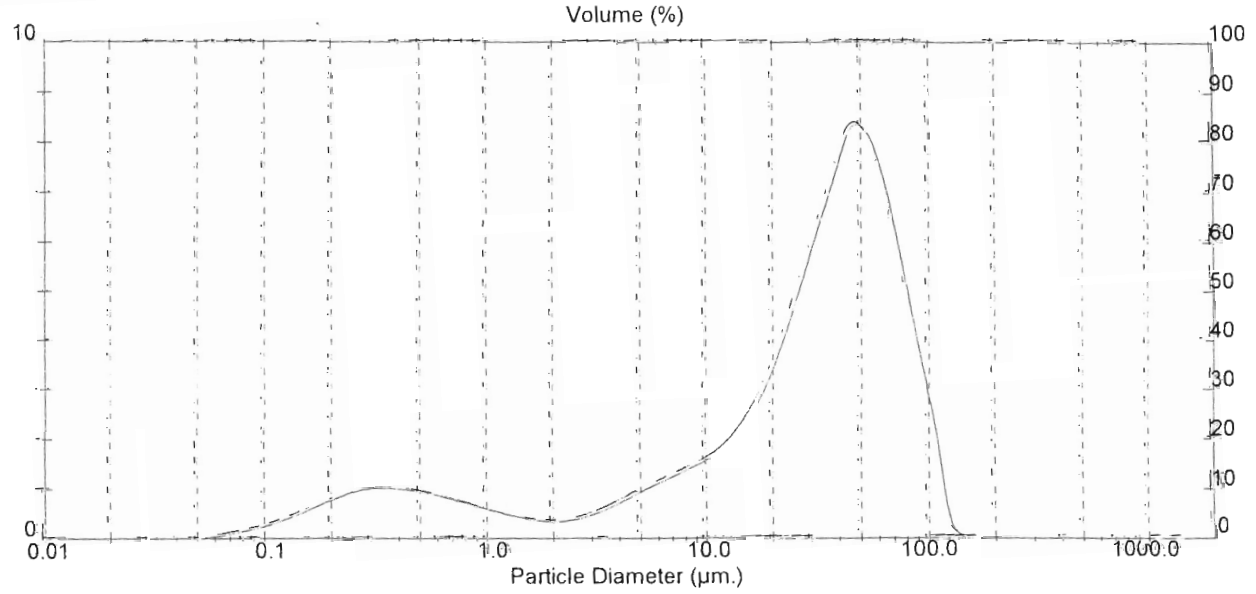

APPENDIX B4: PARTICLE SIZE DISTRIBUTION FOR 38 - 63 µm, 63 – 90 µm, 90 - 106µm ORIGINAL SAMPLES

Result: Analysis Table

ID: Tebogo-63+38 Run No: 1 Measured: 7/11/05 11:57AM
File: HELEN Rec. No: 327 Analysed: 7/11/05 11:57AM
Path: C:\SIZERS\DATA\ Source: Analysed

Range: 300RF mm Beam: 2.40 mmSampler: MS17 Obs: 15.0 %
Presentation: 3OHD Analysis: Polydisperse Residual: 0.467 %
Modifications: None

Conc. = 0.0205 %Vol Density = 3.100 g/cm^3 S.S.A.= 0.3865 m^2/g
Distribution: Volume D[4, 3] = 41.11 um D[3, 2] = 5.01 um
D(v, 0.1) = 4.96 um D(v, 0.5) = 39.19 um D(v, 0.9) = 78.10 um
Span = 1.866E+00 Uniformity = 5.551E-01

Size (um)	Volume In %	Size (um)	Volume In %	Size (um)	Volume In %	Size (um)	Volume In %
0.05	0.00	0.58	0.67	6.63	0.94	76.32	5.59
0.06	0.00	0.67	0.62	7.72	1.09	88.91	3.66
0.07	0.00	0.78	0.54	9.00	1.27	103.58	1.72
0.08	0.00	0.91	0.47	10.48	1.52	120.67	0.00
0.09	0.00	1.06	0.42	12.21	1.85	140.58	0.00
0.11	0.01	1.24	0.36	14.22	2.32	163.77	0.00
0.13	0.01	1.44	0.31	16.57	2.96	190.80	0.00
0.15	0.04	1.68	0.26	19.31	3.77	222.28	0.00
0.17	0.09	1.95	0.23	22.49	4.75	258.95	0.00
0.20	0.20	2.28	0.24	26.20	5.88	301.68	0.00
0.23	0.38	2.65	0.27	30.53	7.09	351.46	0.00
0.27	0.57	3.09	0.35	35.56	8.33	409.45	0.00
0.31	0.69	3.60	0.45	41.43	9.56	477.01	0.00
0.36	0.71	4.19	0.57	48.27	9.73	555.71	0.00
0.42	0.73	4.88	0.68	56.23	9.03	647.41	0.00
0.49	0.73	5.69	0.80	65.51	7.52	754.23	0.00
0.58		6.63		76.32		878.67	

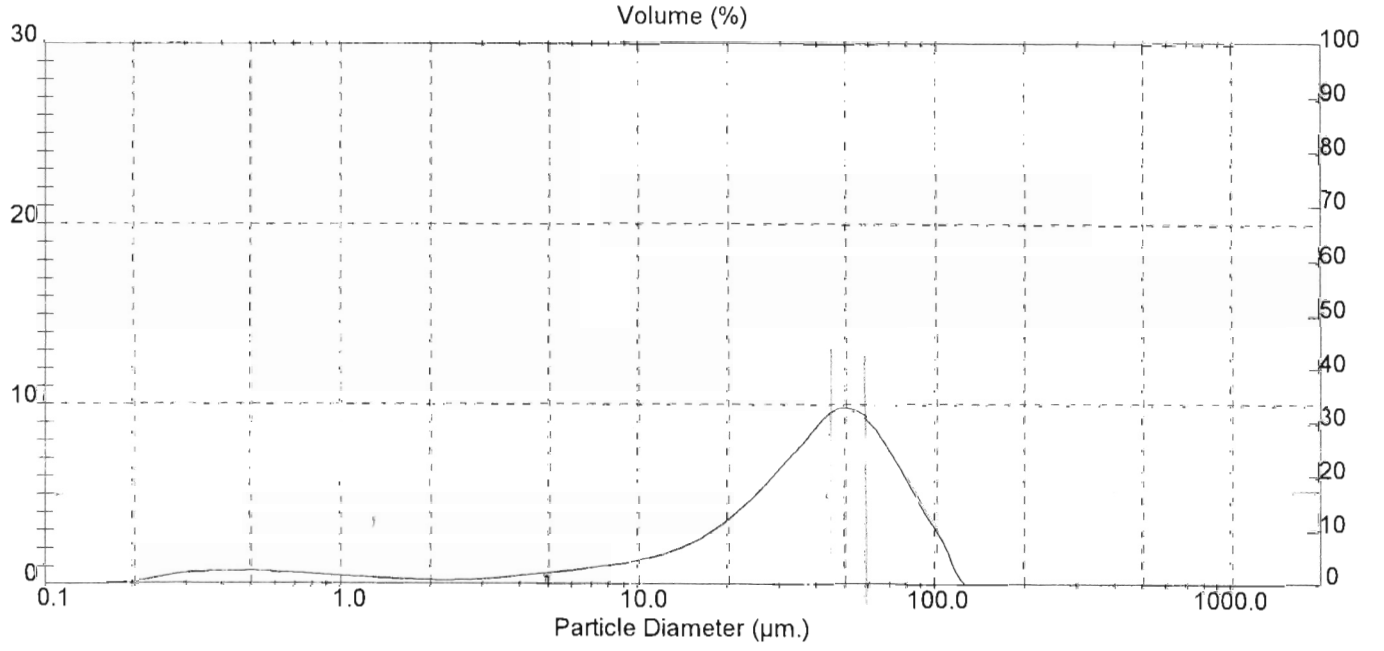

Result: Analysis Table

ID: Tebogo-90+63 Run No: 1 Measured: 7/11/05 11:35AM
File: HELEN Rec. No: 321 Analysed: 7/11/05 11:35AM
Path: C:\SIZERS\DATA\ Source: Analysed

Range: 300RF mm Beam: 2.40 mmSampler: MS17 Obs': 16.1 %
Presentation: 3OHD Analysis: Polydisperse Residual: 0.460 %
Modifications: None

Conc. = 0.0368 %Vol Density = 3.100 g/cm^3 S.S.A.= 0.2104 m^2/g
Distribution: Volume D[4, 3] = 74.50 um D[3, 2] = 9.20 um
D(v, 0.1) = 13.38 um D(v, 0.5) = 75.36 um D(v, 0.9) = 129.47 um
Span = 1.541E+00 Uniformity = 4.512E-01

Size (um)	Volume In %	Size (um)	Volume In %	Size (um)	Volume In %	Size (um)	Volume In %
0.05	0.00	0.58	0.46	6.63	0.54	76.32	12.53
0.06	0.00	0.67	0.39	7.72	0.65	88.91	12.34
0.07	0.00	0.78	0.31	9.00	0.78	103.58	10.37
0.08	0.00	0.91	0.25	10.48	0.92	120.67	7.47
0.09	0.00	1.06	0.22	12.21	1.05	140.58	4.60
0.11	0.00	1.24	0.21	14.22	1.15	163.77	1.73
0.13	0.00	1.44	0.18	16.57	1.23	190.80	0.00
0.15	0.00	1.68	0.15	19.31	1.33	222.28	0.00
0.17	0.00	1.95	0.14	22.49	1.49	258.95	0.00
0.20	0.03	2.28	0.14	26.20	1.80	301.68	0.00
0.23	0.11	2.65	0.16	30.53	2.30	351.46	0.00
0.27	0.27	3.09	0.19	35.56	3.06	409.45	0.00
0.31	0.42	3.60	0.25	41.43	4.18	477.01	0.00
0.36	0.47	4.19	0.30	48.27	5.76	555.71	0.00
0.42	0.51	4.88	0.37	56.23	7.89	647.41	0.00
0.49	0.54	5.69	0.44	65.51	10.33	754.23	0.00
0.58		6.63		76.32		878.67	

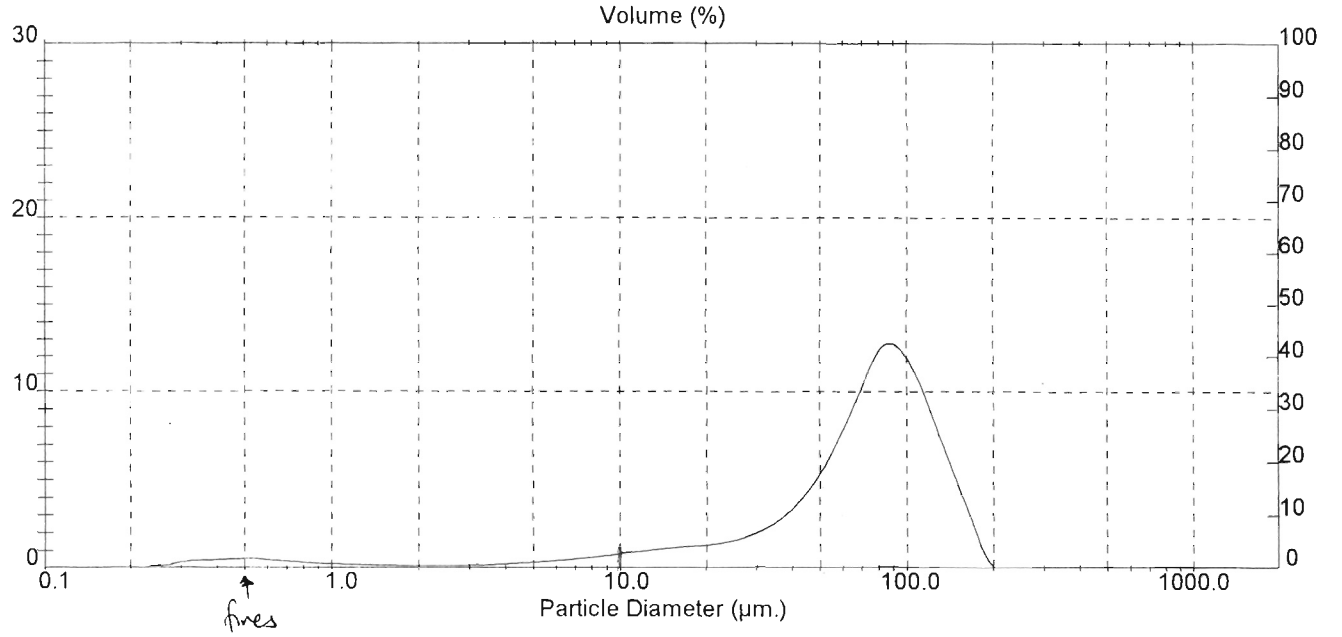

≈ 10µm = 0.92%

Result: Analysis Table

ID: Tebogo-106+90 Run No: 1 Measured: 7/11/05 11:46AM
File: HELEN Rec. No: 325 Analysed: 7/11/05 11:46AM
Path: C:\SIZERS\DATA\ Source: Analysed

Range: 300RF mm Beam: 2.40 mm Sampler: MS17 Obs: 20.8 %
Presentation: 3OHD Analysis: Polydisperse Residual: 0.563 %
Modifications: None

Conc = 0.0431 %Vol Density = 3.100 g/cm^3 S.S.A. = 0.2452 m^2/g
Distribution: Volume D[4, 3] = 87.86 um D[3, 2] = 7.89 um
D(v, 0.1) = 9.72 um D(v, 0.5) = 88.64 um D(v, 0.9) = 165.32 um
Span = 1.755E+00 Uniformity = 5.500E-01

Size (um)	Volume In %	Size (um)	Volume In %	Size (um)	Volume In %	Size (um)	Volume In %
0.05	0.00	0.58	0.50	6.63	0.72	76.32	7.41
0.06	0.00	0.67	0.44	7.72	0.87	88.91	9.52
0.07	0.00	0.78	0.36	9.00	1.06	103.58	11.18
0.08	0.00	0.91	0.31	10.48	1.29	120.67	10.51
0.09	0.00	1.06	0.27	12.21	1.53	140.58	8.22
0.11	0.00	1.24	0.25	14.22	1.76	163.77	5.54
0.13	0.00	1.44	0.21	16.57	1.94	190.80	3.26
0.15	0.00	1.68	0.18	19.31	2.03	222.28	1.61
0.17	0.01	1.95	0.17	22.49	2.02	258.95	0.00
0.20	0.05	2.28	0.18	26.20	1.98	301.68	0.00
0.23	0.16	2.65	0.21	30.53	1.99	351.46	0.00
0.27	0.35	3.09	0.26	35.56	2.15	409.45	0.00
0.31	0.49	3.60	0.33	41.43	2.53	477.01	0.00
0.36	0.53	4.19	0.41	48.27	3.19	555.71	0.00
0.42	0.56	4.88	0.49	56.23	4.20	647.41	0.00
0.49	0.58	5.69	0.59	65.51	5.60	754.23	0.00
0.58		6.63		76.32		878.67	

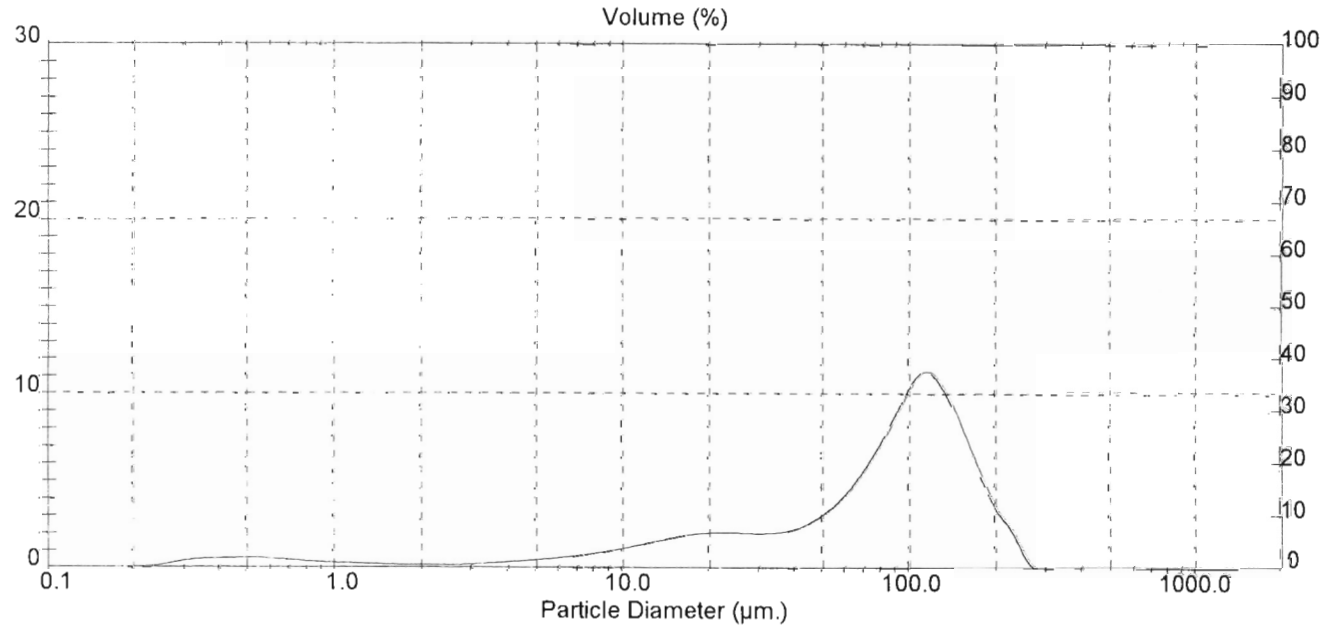

APPENDIX C1: DENSITY MEASUREMENTS FOR 38 - 63 μm, 63 – 90 μm, 90 - 106μm LCFeCr MILLED SAMPLES

LCFeCr
milled

AccuPyc 1330 V1.02
Serial Number: 10
Density and Volume Report

Sample ID: 08-07-05-03 -63+38μm
Number of Purges: 10
Cell Volume: 12.0441 cc

Sample Weight: 14.4748 g
Equilibration Rate: 0.0050 psig/min
Expansion Volume: 8.0267 cc

Run#	Volume cc	Deviation cc	Density g/cc	Deviation g/cc
1	4.6665	-0.0007	3.1019	0.0004
2	4.6661	-0.0010	3.1021	0.0007
3	4.6671	-0.0001	3.1015	0.0000
4	4.6677	0.0006	3.1010	-0.0004
5	4.6688	0.0017	3.1003	-0.0011
6	4.6675	0.0004	3.1012	-0.0002
7	4.6675	0.0003	3.1012	-0.0002
8	4.6673	0.0002	3.1013	-0.0001
9	4.6677	0.0006	3.1011	-0.0004
10	4.6652	-0.0020	3.1027	0.0013

Average Volume: 4.6671 cc
Average Density: 3.1014 g/cc

Standard Deviation: 0.0010 cc
Standard Deviation: 0.0007 g/cc

AccuPyc 1330 V1.02
Serial Number: 10
Density and Volume Report

Sample ID: 08-07-05-02 −90 +63μm
Number of Purges: 10
Cell Volume: 12.0441 cc

Sample Weight: 14.3202 g
Equilibration Rate: 0.0050 psig/min
Expansion Volume: 8.0267 cc

Run#	Volume cc	Deviation cc	Density g/cc	Deviation g/cc
1	4.6097	-0.0011	3.1065	0.0007
2	4.6109	0.0000	3.1057	-0.0000
3	4.6097	-0.0011	3.1065	0.0007
4	4.6116	0.0007	3.1053	-0.0005
5	4.6111	0.0003	3.1056	-0.0002
6	4.6109	0.0000	3.1058	-0.0000
7	4.6112	0.0004	3.1055	-0.0003
8	4.6110	0.0002	3.1057	-0.0001
9	4.6112	0.0004	3.1055	-0.0003
10	4.6109	0.0001	3.1057	-0.0001

Average Volume: 4.6108 cc
Average Density: 3.1058 g/cc

Standard Deviation: 0.0006 cc
Standard Deviation: 0.0004 g/cc

AccuPyc 1330 V1.02
Serial Number: 10
Density and Volume Report

Sample ID: 08-08-05-01 -100 +90µm
Number of Purges: 10
Cell Volume: 12.0441 cc

Sample Weight: 16.0746 g
Equilibration Rate: 0.0050 psig/min
Expansion Volume: 8.0267 cc

Run#	Volume cc	Deviation cc	Density g/cc	Deviation g/cc
1	5.1804	-0.0013	3.1029	0.0008
2	5.1811	-0.0007	3.1025	0.0004
3	5.1816	-0.0002	3.1023	0.0001
4	5.1813	-0.0005	3.1024	0.0003
5	5.1823	0.0005	3.1019	-0.0003
6	5.1820	0.0002	3.1020	-0.0001
7	5.1821	0.0003	3.1019	-0.0002
8	5.1819	0.0001	3.1021	-0.0001
9	5.1825	0.0007	3.1017	-0.0004
10	5.1827	0.0009	3.1016	-0.0005

Average Volume: 5.1818 cc
Average Density: 3.1021 g/cc

Standard Deviation: 0.0007 cc
Standard Deviation: 0.0004 g/cc

APPENDIX C2: DENSITY MEASUREMENTS FOR 38 - 63 μm, 63 – 90μm, 90 - 106μm UG2 MILLED SAMPLES

AccuPyc 1330 V1.02
Serial Number: 10
Density and Volume Report

Sample ID: 07-03-05-1
Number of Purges: 10
Cell Volume: 12.0491 cc

Sample Weight: 10.3066 g
Equilibration Rate: 0.0050 psig/min
Expansion Volume: 8.0239 cc

Run#	Volume cc	Deviation cc	Density g/cc	Deviation g/cc
1	3.5253	-0.0030	2.9236	0.0025
2	3.5266	-0.0017	2.9225	0.0014
3	3.5280	-0.0004	2.9214	0.0003
4	3.5278	-0.0005	2.9215	0.0004
5	3.5286	0.0003	2.9209	-0.0002
6	3.5288	0.0004	2.9207	-0.0004
7	3.5290	0.0007	2.9205	-0.0006
8	3.5294	0.0011	2.9202	-0.0009
9	3.5305	0.0022	2.9193	-0.0018
10	3.5292	0.0009	2.9204	-0.0007

Average Volume: 3.5283 cc
Average Density: 2.9211 g/cc

Standard Deviation: 0.0015 cc
Standard Deviation: 0.0012 g/cc

AccuPyc 1330 V1.02
Serial Number: 10

Density and Volume Report

Sample ID: 04-07-05-01
Number of Purges: 10
Cell Volume: 12.0441 cc

Sample Weight: 8.8851 g
Equilibration Rate: 0.0050 psig/min
Expansion Volume: 8.0267 cc

Run#	Volume cc	Deviation cc	Density g/cc	Deviation g/cc
1	2.9685	-0.0026	2.9931	0.0026
2	2.9720	0.0009	2.9897	-0.0009
3	2.9696	-0.0014	2.9920	0.0014
4	2.9716	0.0005	2.9900	-0.0005
5	2.9715	0.0004	2.9901	-0.0004
6	2.9712	0.0002	2.9904	-0.0002
7	2.9702	-0.0009	2.9914	0.0009
8	2.9716	0.0005	2.9901	-0.0005
9	2.9721	0.0010	2.9895	-0.0010
10	2.9725	0.0014	2.9891	-0.0014

Average Volume: 2.9711 cc
Average Density: 2.9905 g/cc

Standard Deviation: 0.0012 cc
Standard Deviation: 0.0013 g/cc

APPENDIX D1: XRPD PATTERNS FOR LCFeCr SLAG ORIGINAL SAMPLE

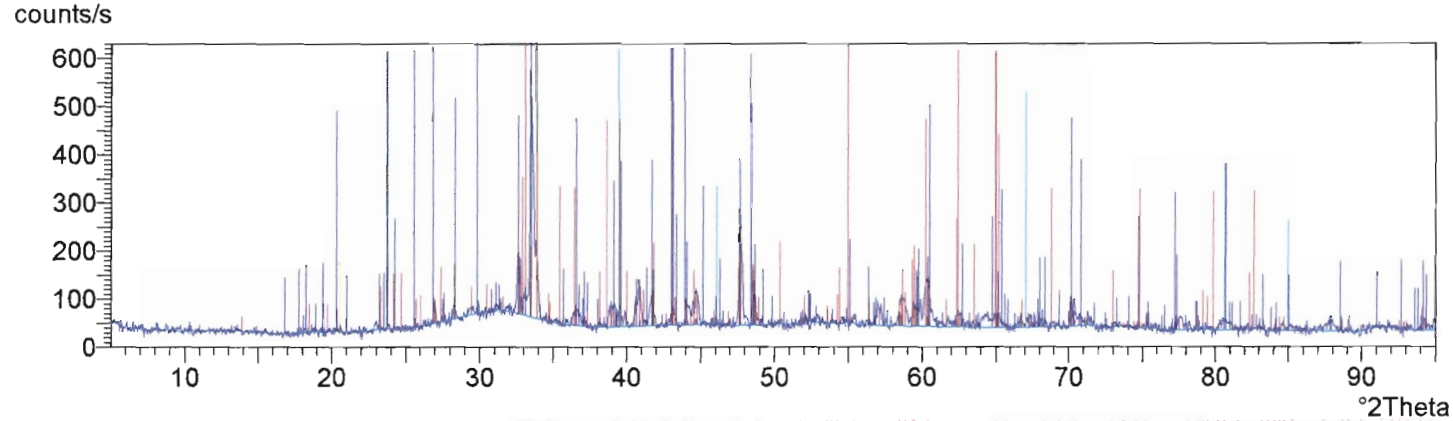

39-0262	Chromium Samarium Oxide	SmCrO3
45-0946	Periclase, syn	MgO
24-1069	Sodium Calcium Silicate	Na2CaSiO4
17-0912	Calcium Oxide	CaO
31-1236	Silver Carbonate	Ag2CO3
16-0335	Calcium Aluminum Oxide Sulfate	Ca4Al6O12SO4
05-0701	Chromium Niobium	Cr2Nb
33-0853	Magnesium Aluminum Oxide	MgAl2O4
03-0816	Sodium Calcium Silicate	Na2CaSiO4
20-1073	Sodium Aluminum Oxide	NaAlO2
35-0796	Magnesium Titanium Oxide	MgTi2O5
29-0448	Chromium Germanium	Cr3Ge
16-0440	Yeelimite, syn	Ca3Al6O12!CaSO4
39-1110	Rhenium Thorium Uranium	Th0.75U0.25Re2
27-1241	Lithium Germanium Oxide	Li8GeO6
32-0761	Potassium Chromium Oxide Hydro	K4Cr3(OH)5(CrO4)4!6H2O

X'Pert Graphics & Identify
Legend of graph: TS2

Description
Slag sample

Pattern	Description	Date & Time	Type	
TS2	Slag sample	2006/11/29 16:15	Scan: measured	1
TS2	Slag sample	2006/11/30 11:01	Peak list: searched	C
TS2	Slag sample	2006/11/30 11:01	Scan: background - calculated	B
Chromium Samarium Oxide	SmCrO3		Reference Pattern	C
Periclase, syn	MgO		Reference Pattern	D
Sodium Calcium Silicate	Na2CaSiO4		Reference Pattern	E
Calcium Oxide	CaO		Reference Pattern	1
Silver Carbonate	Ag2CO3		Reference Pattern	1
Calcium Aluminum Oxide Sulfat	Ca4Al6O12SO4		Reference Pattern	1
Chromium Niobium	Cr2Nb		Reference Pattern	1
Magnesium Aluminum Oxide	MgAl2O4		Reference Pattern	1
Sodium Calcium Silicate	Na2CaSiO4		Reference Pattern	1
Sodium Aluminum Oxide	NaAlO2		Reference Pattern	1
Magnesium Titanium Oxide	MgTi2O5		Reference Pattern	1
Chromium Germanium	Cr3Ge		Reference Pattern	1
Yeelimite, syn	Ca3Al6O12!CaSO4		Reference Pattern	1
Rhenium Thorium Uranium	Th0.75U0.25Re2		Reference Pattern	C
Lithium Germanium Oxide	Li8GeO6		Reference Pattern	B
Potassium Chromium Oxide Hyd	K4Cr3(OH)5(CrO4)4!6H2O		Reference Pattern	C